Characterisation of a novel model of optic atrophy

Malgorzata Piechota

A thesis submitted to Cardiff University in accordance with the requirements for the degree of Doctor of Philosophy in the disciplines of Cell and Molecular Biology

School of Optometry and Vision Sciences

Cardiff University

October 2009

ProQuest LLC
789 East Eisenhower Parkway
P.O. Box 1346
Ann Arbor, MI 48106-1346

DECLARATION

This work has not previously been accepted in substance for any degree and is not concurrently submitted in candidature for any degree.

Signed ..... (candidate) Date .....08.01.10.....

STATEMENT 1

This thesis is being submitted in partial fulfillment of the requirements for the degree of .....PhD.....(insert MCh, MD, MPhil, PhD etc, as appropriate)

Signed .....(candidate) Date .....08.01.10.....

STATEMENT 2

This thesis is the result of my own independent work/investigation, except where otherwise stated.
Other sources are acknowledged by explicit references.

Signed ..... (candidate) Date .....08.01.10.....

STATEMENT 3

I hereby give consent for my thesis, if accepted, to be available for photocopying and for inter-library loan, and for the title and summary to be made available to outside organisations.

Signed ..... (candidate) Date .....08.01.10.....

ACKNOWLEDGEMENTS

Many people have helped bring this thesis into being. Firstly, I must thank Marcela Votruba for giving me the opportunity of doing this PhD in her group, constant encouragement and the space for my own scientific development. I am also very grateful to Mike Boulton for his advice, guidance and his patience in answering my endless questions.

I would like to thank Kate Powell for her many helpful suggestions, understanding and support. Special thanks to Yadan Zhang who devoted her time to introduce me to the cell culture work and was always happy to help me. Thank you to Vanessa Davies for being helpful with work on animals and providing me with the images of H&E stained retinal sections. I would also like to thank James Morgan who was kind enough to show me the whole-mount retinal method and Andrew Hollins for the western blot protocol. Thank you to Malgorzata Rozanowska and Kinga Handzel for the help with the experiment on light-treated cells and Matthew Davies for providing me with the SF10PF medium. This work would not be possible without Martin Taylor's, Jennifer Davies' and Elaine Taylor's assistance with the animal work. Thank you to the Administrative and Supportive Staff, in particular to Sue Hobbs, Phil Booth, Robin O'Donovan, Stephen Morgan and John Speck. I must also thank other postgraduate students for their optimism and infectious enthusiasm.

Finally I would like to thank Izabela Katzer, whose younger sister I am fortunate to be and thank greatly John Moore for his support, consideration and many comments about my work.

ABSTRACT

Autosomal dominant optic atrophy (ADOA) is a slowly progressive ocular disorder associated with retinal ganglion cell loss and optic atrophy, manifesting with a variable reduction in visual acuity, colour vision defects and visual field loss. Genetic studies lead to the identification of mutations in the *OPA1* gene on chromosome 3q28-qter, which is the main ADOA-causing gene. OPA1 is an ubiquitously expressed, nuclear dynamin-related GTPase, targeted to the inner mitochondrial membrane, which plays a role in mitochondrial fusion and ultimately has a protective role against apoptosis.

In order to study the pathophysiology of ADOA, a new ENU-induced mutant mouse carrying a protein truncating nonsense mutation in Opa1 has been generated in our laboratory (B6;C3-Opa1^{Q285STOP}). The heterozygous mutation leads to approximately 50% reduction in Opa1 protein in mitochondria from retinal samples studied by Western blot. The homozygous mutation is embryonic lethal. The phenotype of heterozygous mutant mice is not associated with a severe neuro-degenerative process, in keeping with the variable and relatively mild phenotype observed in many patients with ADOA. Thus, visual phenotyping shows reduced visual function and electron microscopy reveals significant abnormalities in myelin bundles and increased autophagy with increasing age up to two years. Despite this, heterozygous adult mutants (up to 2 years of age) do not show age-dependent loss of retinal ganglion cell (RGC) bodies when studied on retinal sections stained with H&E and there is no visibly increased apoptosis in the retina (at 2 years of age) on TUNEL staining. In retinas from mice of 4-5 months of age proteolysis of Opa1 is normal and no statistically significant reduction in the average mitochondrial membrane potential is observed in the retina and brain. Quantitative RT-PCR on retinal samples does not indicate any differences in the expression of the six genes involved in the mitochondrial structure in mutant versus wild type mice. However, the observation of mitochondrial network in Mitotracker stained mouse embryonic fibroblasts (MEFs) at E13.5 demonstrates a higher incidence of fragmented mitochondria in MEFs taken from heterozygous mice, with a 15% increase in the number of opa1 +/- MEFs showing mitochondrial fragmentation (the average length of mitochondrial particles below 1μm), when compared to *Opa1* +/- MEFs. However, their growth and survival after oxidative stress (with H_2O_2 and blue light) was not significantly affected when compared to the wild type control in a MTT assay.

In conclusion, in *Opa1* +/- mice, a reduction in the mitochondrial level of Opa1 caused a mild defect in mitochondrial morphology without any significant decline in those cellular functions investigated.

ABBREVIATIONS

A	Adenine
ADOA	Autosomal Dominant Optic Atrophy
ADOAD	Autosomal Dominant Optic Atrophy and Deafness
ADP	Adenosine diphosphate
APS	Ammonium persulphate
ATP	Adenosine-5'-triphosphate
C	Cytosine
CCCP	Carbonyl cyanide *m*-chlorophenylhydrazone
cDNA	Complementary deoxyribonucleic acid
COX	Cytochrome oxidase
CPEO	Chronic progressive external ophthalmoplegia
DAPI	4'-6-Diamidino-2-phenylindole
dATP	2'-deoxyadenosine 5'-triphosphate
dCTP	2'-deoxycytidine 5'-triphosphate
dGTP	2'-deoxyguanosine 5'-triphosphate
dNTP	Deoxyribonucleotide triphosphate
dTTP	2'-deoxythymidine 5'-triphosphate
dUTP	2'-deoxyuridine 5'-triphosphate
DEPC	Diethyl pyrocarbonate
DMEM	Dulbecco's modified Eagle's medium
D-PBS	Dulbecco's phosphate-buffered saline
Dpc	Days post coitum
d-Rib	2-Deoxy-d-ribose
DTT	Dithiothreitol
E	Efficiency
EDTA	Ethylenediaminetetraacetic acid
EM	Embryonic stem cells
ENU	N-ethyl-N-nitrosourea
EST	Expressed sequence tag
FA	Formaldehyde agarose
FBS	Fetal bovine serum
G	Guanine

GED	GTPase effector domain
Gln	Glutamine
GO	Gene Ontology
GOI	Gene of interest
GTP	Guanosine-5'-triphosphate
H&E	Hematoxylin and eosin
HEPES	4-(2-hydroxyethyl)-1-piperazineethanesulfonic acid
HET	Heterozygote
H_2O_2	Hydrogen peroxide
HRM	High resolution melt
HRP	Horse Radish Peroxidase
IgG	Immunoglobulin G
IMM	Inner mitochondrial membrane
IMS	Intermembrane space
INL	Inner nuclear layer
IS	Inner segments
kb	Kilobase
LHON	Leber Hereditary Optic Neuropathy
MEFs	Mouse embryonic fibroblasts
MELAS	Mitochondrial myopathy, encephalomyopathy, lactic acidosis, and stroke-like episodes
MERRF	Myoclonic epilepsy associated with ragged-red fibers
MESA	MOPS-EDTA-sodium acetate
MGI	Mouse Genome Informatics
m*OPA1*	Mouse optic atrophy (gene)
MOPS	3-(N-Morpholino)propanesulfonic acid
mRNA	Messenger ribonucleic acid
MS	Mass spectrometry
mtDNA	Mitochondrial deoxyribonucleic acid
MTT	Thiazolyl Blue Tetrazolium Bromide
Mut	Mutant
NADPH	Nicotinamide adenine dinucleotide phosphate
NCBI	National Center for Biotechnology Information
NMD	Nonsense Mediated Decay

Nnt	nicotinamide nucleotide transhydrogenase
OCT	Optical Coherence Tomography
OE	Overexpression
OKN	Optokinetic nystagmus
OMIM	Online Mendelian Inheritance in Man
OMM	Outer mitochondrial membrane
ONL	Outer nuclear layer
O/N	Optic nerve
OPL	Outer plexiform layer
OXPHOS	Oxidative phosphorylation
PAGE	Polyacrylamide gel electrophoresis
PARL	Presenilin-associated rhomboid-like
PEG	Polyethylene glycol
PERG	Pattern Electroretinogram
PBS	Phosphate-buffered saline
PD	Population doubling
PTC	Premature termination codon
qRT-PCR	Quantitative reverse transcription polymerase chain reaction
RFL	Retinal fibre layer
RIPA	Radio-Immunoprecipitation Assay
RGC	Retinal ganglion cell
RNAi	RNA interference
ROS	Reactive oxygen species
RP	Retinitis pigmentosa
RT-PCR	Reverse transcription polymerase chain reaction
SD	Standard deviation
SDS	Sodium dodecyl sulphate
SEM	Standard error of the mean
SIMH	Stress-induced mitochondrial hyperfusion
SNP	Single nucleotide polymorphism
SOD2	Superoxide dismutase 2
T	Thymine
T_m	Melting temperature
TBE	Tris/Borate/EDTA

TBS	Tris-buffered saline
TdT	Terminal deoxynucleotidyl transferase
TE	Tris/EDTA
TUNEL	TdT-mediated dUTP nick end labeling
UV	Ultraviolet
VIS	Visible
WT	Wild type

CONTENTS:

LIST OF FIGURES

Chapter 1

Chapter 2

Chapter 3

Chapter 4

Chapter 5

Chapter 6

Chapter 7

LIST OF TABLES

1. INTRODUCTION

1. INTRODUCTION

1.1 Inherited optic neuropathies

Inherited optic neuropathies form a genetically heterogeneous group of disorders with various modes of inheritance (autosomal dominant or recessive, X-linked recessive or mitochondrial) that are characterized by dysfunction of the optic nerve (Votruba et al., 2004). As a result of genetic heterogeneity, there are considerable variations in the clinical presentation of optic atrophy diagnosed in these diseases. The general sign is a light, flat optic disc with well defined margins and a reduction in the numbers of the smaller diameter blood vessels supplying the disk. Nearly all of the inherited optic neuropathies eventually have symmetric, bilateral, central visual loss. In many of these disorders, the papillomacular nerve fibre bundle is affected, with resultant central or cecocentral scotomas. Optic nerve damage is usually permanent and, in many diseases, may be progressive (Newman, 2005).

The hereditary optic atrophies can be divided into two main groups. First, there are the primary optic atrophies, such as Leber hereditary optic neuropathy (LHON). In primary optic atrophy, the disease is linked to a specific genetic defect which results in degeneration of the retina and/or optic nerve fibres. Second, in secondary optic atrophy, the pathological changes affecting the optic disc are accompanied by many other symptoms in complex clinical syndromes, such as Wolfram and Behr's and the damage to the optic nerve may be secondary to other pathological changes that take place in the body.

The two most common inherited optic neuropathies are autosomal dominant optic atrophy (ADOA, Kjers' disease) and LHON. LHON (OMIM 535000) was described by Leber in 1871 and is now recognized as the most frequently occurring mitochondrial disease. The condition is inherited through the female line by maternal transmission of mtDNA. LHON has usually a sudden onset of visual loss in both eyes asynchronously and appears at the age of 18-35 years. Both disorders are the result of mitochondrial dysfunction. Mutations in LHON affect the respiratory chain complexes, whereas the ADOA main nuclear-encoded gene *OPA1* codes for inner mitochondrial membrane protein critical for proper mitochondrial structural plasticity, mtDNA maintenance and oxidative phosphorylation. The fundamental pathology of both diseases is a degeneration of retinal

ganglion cells (RGC) and atrophy of the optic nerve. However, other neurological defects and muscle abnormalities have also been reported in so-called "LHON plus" and "ADOA plus" syndromes (Jun et al., 1994; Amati-Bonneau et al., 2008). Both diseases are characterized by a variability in severity of visual dysfunction and an incomplete penetrance, which implies that additional genetic and/or environmental factors must modulate the phenotypic expression (Yu-Wai-Man et al., 2008). No current treatment is available for either disease.

1.1.1 Autosomal dominant optic atrophy: clinical features and histopathology

Autosomal dominant optic atrophy (ADOA) (OMIM 165500) is the most prevalent hereditary optic neuropathy with estimated disease prevalence ranging between 1:12,000 in Denmark, and 1:50,000 worldwide. ADOA is a progressive disorder with onset in the first decade of life that often leads to legal blindness. Clinically it is characterized by a loss of visual acuity, development of centrocoecal scotoma, bilateral temporal atrophy of the optic nerve and colour vision disturbances (Votruba et al., 2003). The peripheral fields are usually full. The appearance of the optic nerve ranges from complete atrophy through temporal pallor to subtle pallor (Fig.1.1).

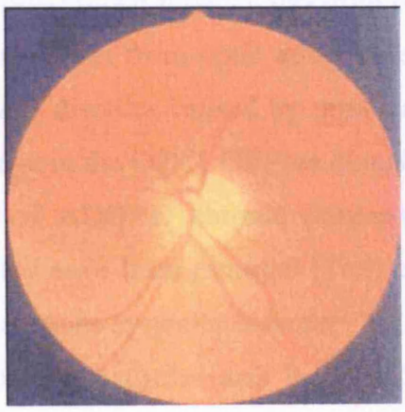

Fig.1.1 A left fundus photograph from a patient with ADOA, showing temporal pallor (from Votruba et al., 2003).

ADOA has incomplete penetrance. It varies from family to family and mutation to mutation. It has been reported as high as 100% with the IVS12+1g>t mutation resulting in *OPA1* exon 12 skipping (Thiselton et al., 2002) and as low as 43% with the 2708del (TTAG) mutation in *OPA1* exon 27 (Toomes et al., 2001) and in some families asymptomatic carriers have been observed. Post-mortem histopathological studies of two patients identified a selective loss of RGCs, primarily in the macula and in the papillo-macular bundle of the optic nerve and loss of myelin (Johnston et al., 1979; Kjer et al., 1983). Magnetic resonance imaging has also confirmed thinning of the optic nerve in ADOA patients (Votruba et al., 2000). Recent data from *in vivo* optical coherence tomography (OCT) have shown the thinning of the retinal layers, excluding outer layer with photoreceptors, in the macular area (Ito et al., 2007). On electrophysiology an absent or delayed pattern visual evoked potential has been observed showing that there is a conduction defect in the optic nerve. The pattern electroretinogram (PERG) shows reduced amplitude of the N95 waveform, suggesting RGC dysfunction (Berninger et al., 1991; Holder et al., 1998). The colour vision defect is often reported as an acquired blue-yellow loss, or tritanopia (Eliott et al., 1993), but mostly a generalized non-specific dyschromatopsia has been diagnosed.

1.1.2 Different ADOA phenotypes

Recent genetic studies identified much broader spectrum of clinical phenotypes linked to mutations in the *OPA1* gene. Apart from optic atrophy sensorineural deafness has been reported in so-called ADOAD disorder caused by missense mutation in exon 14, which leads to the amino acid change in the OPA1 GTPase domain (R445H) (Amati-Bonneau et al., 2003). In some cases of ADOAD chronic progressive external ophthalmoplegia (CPEO), ptosis and myopathy have been reported (Treft et al., 1984; Meire et al., 1985; Payne et al., 2004). Another multi-systemic disorder: "ADOA plus" has been described, which affects peripheral nerves, muscles and brain and is associated with missense mutations in the GTPase domain of *OPA1* gene and mtDNA instability (Amati-Bonneau et al., 2008, Liguori et al., 2008). Recently one case of reversible ADOA, where 23-year-old man partially recovered from bilateral optic neuropathy, has been reported (Cornille et al., 2008). The mutation in the alternative exon 5b was found to be responsible for this reverse effect.

This phenotypic variation in *OPA1* diseases mirrors the effect of mutation on cellular function. In classic ADOA disease *OPA1* mutations affect mitochondrial morphology and ultrastructure, mitochondrial fusion and oxidative phosphorylation (Zanna et al., 2008). In patients with a more complex phenotype (ADOAD and "ADOA plus" syndromes) defects in mitochondrial morphology and oxidative phosphorylation have been found to be more pronounced (Fig.1.2) (Amati-Bonneau et al., 2005; Chevrollier et al., 2008). Generally there are some reasons to believe that the pathomechanism depends on the type of *OPA1* mutation. Premature termination of translation that results in haploinsufficiency is mostly related to classic ADOA with affected RGC layer and optic nerve. Some mutations in GTPase domain may result in a dominant negative effect, in which dysfunctional OPA1 protein still exists in the cell and does more harm than good. This effect could underlie more severe disease presentations.

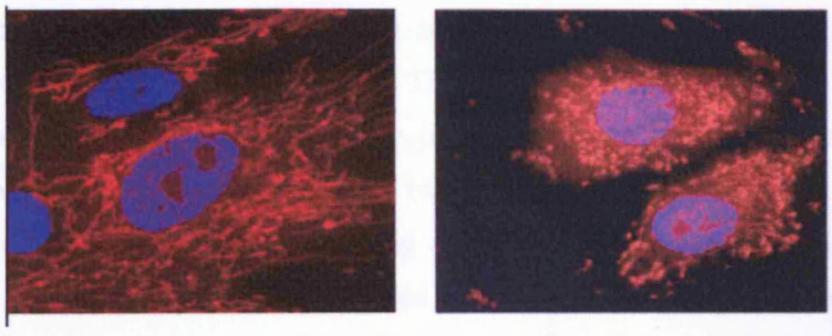

Fig. 1.2 Mitochondrial network morphology. Fibroblasts from a control subject (left) and ADOAD patient carrying the R445H mutation (right). Cells were labeled with Mitotracker. In control fibroblasts mitochondria form interconnected network. In contrast more than 90% of the cells from patients have fragmented mitochondria (from Amati-Bonneau et al., 2005).

1.1.3 Genetic mapping studies in human and mouse

The predominant locus for ADOA was mapped to chromosome 3q28-29 (Eiberg et al., 1994) and refined genetic mapping narrowed this region to 1.4 cM. (Jonasdottir et al., 1997; Stoilova et al., 1997; Votruba et al., 1997). The nuclear gene, *OPA1* that mapped within this candidate region was identified by two laboratories using either positional cloning and construction of a high-density PAC contig (Alexander et al., 2000) or by searching for a human Msp1/Mgm1p homologue in nucleotide databases and fluorescence in situ hybridization (Delettre et al., 2000).

About 60% of ADOA cases are now linked to mutations in the *OPA1* gene. Two further loci have been reported (OPA4 and OPA5), but the genes involved have not yet been identified (Kerrison et al., 1999; Barbet et al., 2005). Mouse *mOpa1* was isolated as a mouse ortholog of the large G protein previously cloned from salmon brain. Amino acid sequence of the salmon clone was used as a probe to carry out a search of a mouse EST database followed by screening of a mouse brain cDNA library (Misaka et al., 2002). Comparison of mouse and human OPA1 sequences revealed 88% and 97% identity at the nucleotide and amino acid levels, respectively.

1.1.4 Structure of *OPA1*

1.1.4.1 Splice variants

The h*OPA1* gene is composed of 31 exons that are distributed across ~ 100 kb of genomic DNA. The last exon is not coding, and exons 4, 4b, and 5b generate at least eight splicing isoforms (Delletre et al., 2001). The full open reading frame translates into a large predicted protein of 1015 amino acids. The isoform 1 without 4b and 5b exons produces a 960 amino acid protein. A recent study, published whilst the work in this thesis was being undertaken, showed that in mice only two alternative exons 4b and 5b (without exon 4) are involved in the alternative splicing and form four mRNA isoforms (Akepati et al., 2008). It is suggested that this complex posttranscriptional regulation of *OPA1* enables cells to produce discrete protein isoforms with distinct functions. One study has shown that isoforms containing exon 4 have an evolutionary conserved function in mitochondrial fusion and maintenance of mitochondrial membrane potential, whereas isoforms with exons 4b and 5b are vertebrate specific and involved in cytochrome c release and control of apoptotic process (Olichon et al., 2007a).

1.1.4.2 Transcript expression

Northern blot analyses of *OPA1* transcripts have shown the ubiquitous presence of *OPA1* RNA in almost all human tissues examined (Fig.1.3)

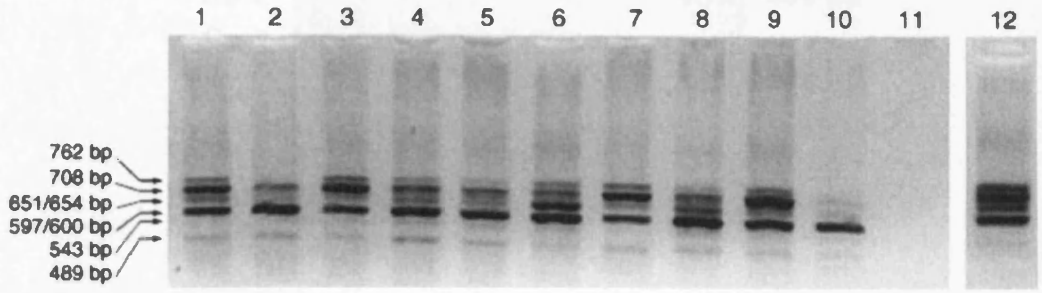

Fig.1.3 RT-PCR analysis. Alternatively spliced exons 4, 4b and 5b produce multiple *OPA1* transcripts in human tissues. Human thyroid (*lane 1*), retina (*lane 2*), kidney (*lane 3*), lung (*lane 4*), ovary (*lane 5*), skeletal muscle (*lane 6*), liver (*lane7*), heart (*lane 8*), colon (*lane 9*), fetal brain (*lane 10*), no RNA (*lane 11*) and leukocytes (*lane 12*) (from Delettre et al 2001).

Some splicing isoforms demonstrate different abundance in different human organs (Olichon et al., 2007a). The qRT-PCR analysis of different isoforms revealed that the Ex4-containing mRNAs are systematically abundant. In the liver, kidney and thymus, the presence of Ex5b predominated among all variants (e.g. splice variant 5) whereas in the brain, Ex4b was highly expressed (splice variant 7). Similarly to humans, expression of splice variants in mice showed a tissue-specific variability with the largest difference in the expression between neuronal tissue (brain) and other tissues studied (heart, kidney, liver) (Akepati et al., 2008). In brain tissue a splice variant 1 showed the highest abundance (Fig.1.4). These results suggest that selective alternate splicing of *OPA1* mRNA may be important in the regulation of mitochondrial function in different tissues.

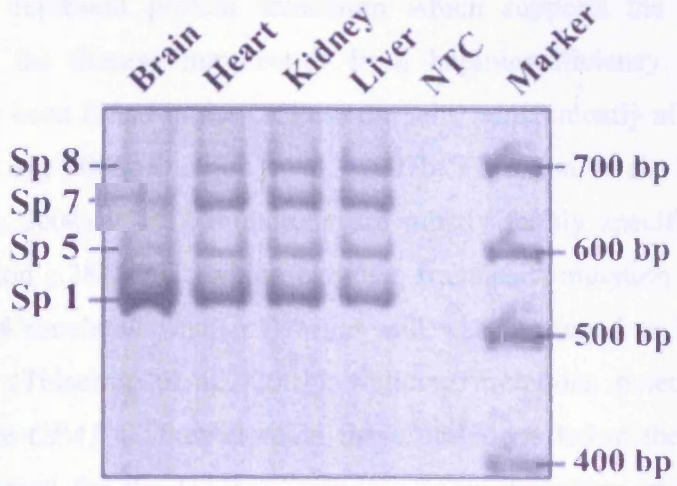

Fig.1.4 Silver stained 5% PAGE gel after RT-PCR of mouse OPA1 transcript. Four splice variants (Sp) generated by alternative splicing of exons 4b and 5b were found in the mouse tissues and their relative abundance was tissue-specific (from Akepati et al., 2008).

1.1.5 Mutation spectrum of *OPA1*

Screening of ADOA patients is still increasing the number of known pathogenic *OPA1* mutations. Currently (July 2009) there are 204 mutations registered in a specific eOPA1 database (http:lbbma.univ.angers.fr/eOPA1/). Different *OPA1* mutations have been reported in Caucasian, British, French, Belgian, German, Danish, Australian and Japanese families. The mutations are spread throughout the gene coding sequence, but the GTPase domain and the dynamin central region are more frequently affected (Fig.1.5)

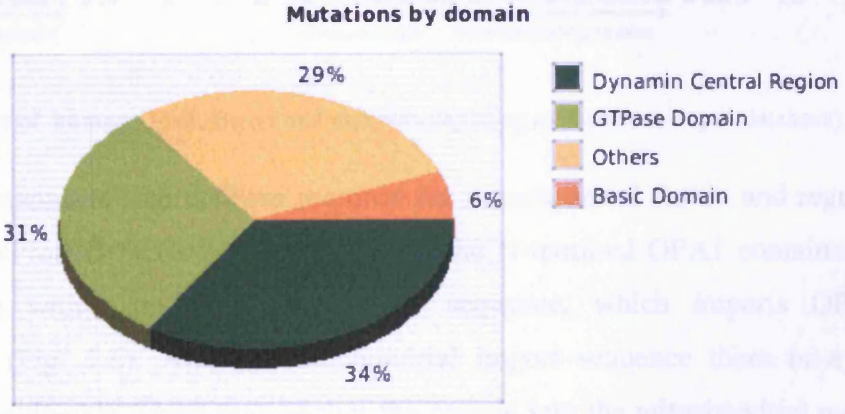

Fig.1.5 OPA1 mutation statistics (eOPA1 database). (Ferre et al., 2005)

At least 40% represent protein truncation which supports the view that dominant inheritance of the disease may result from haploinsufficiency of OPA1. Missense mutations have been found in the GTPase domain, which mostly affect conserved amino acids (Ferre et al., 2005; Olichon et al., 2007b; Thiselton et al., 2002; Toomes et al., 2001; Votruba, 2004). *OPA1* mutations are mostly family specific but one common deletion mutation c.2826delT, which causes a frameshift mutation in exon 28, has been identified in 14 unrelated Danish families and was presumed to be an evidence for a founder effect (Thiselton et al., 2001). Splicing mutations potentially result in exon skipping. In the *OPA1* GTPase domain these mutations led to the lack of amino acids presumably critical for the GTPase activity. Some mutations may be semi-dominant, because one compound heterozygote patient has been reported to have more severe symptoms than the patient's simple heterozygote parents and siblings (Pesch et al., 2001). In addition one 560-860 kb microdeletion on chromosome 3q28 that results in the complete loss of one copy of the *OPA1* gene was reported (Marchbank et al., 2002) and recently genomic aberrations at the *OPA1* gene locus have been shown in ADOA patients (Fuhrmann et al., 2009).

1.2 OPA1 protein

1.2.1 The Dynamin-related GTPase protein family

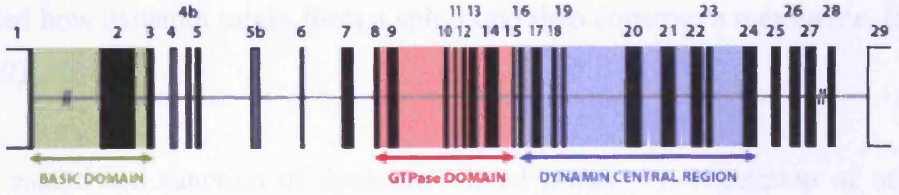

Fig.1.6 Structure of human Opa1. Boxes and numbers depicting exons (from Eopa1 database).

OPA1 is a dynamin-related GTPase required for mitochondrial fusion and regulation of apoptosis (UniProtKB/Swiss-Prot O60313). At the N-terminal OPA1 contains a highly basic domain with a mitochondrial leader sequence, which imports OPA1 into mitochondria (Fig. 1.6). After a mitochondrial import sequence there is a putative transmembrane domain which may anchor the protein into the mitochondrial membrane. There are two coiled coil domains, which may be involved in the formation of homodimers or polymers (Olichon et al., 2007a). The first coiled coil is located within

exons 5b to 7. The other predicted coiled coil is located at the extreme C-terminal and is thought to be GTPase effector domain (GED or assembly domain involved in the oligomerization and activation of dynamins). Crucial for OPA1 fusion activity is a GTPase domain. This domain is highly conserved between dynamin-related proteins. Mutations in this domain result in mitochondrial fragmentation in fibroblasts from ADOA patients (Olichon et al., 2007b). Next to GTPase there is a dynamin central domain of unknown function.
There is still much to discover about Opa1 self-assembly, detailed interactions with other molecules and the mechanism of GTP binding/hydrolysis. So far the evidence presented suggests that Opa1 physically interacts with different respiratory complexes subunits (Zanna et al., 2008).

Dynamins play an important role in membrane-associated cellular processes. They are large proteins characterized by their common structure and by conserved sequences in the GTP-binding domain. As mentioned above for Opa1, the GTPase domain is followed by a central domain and an assembly domain which typically has a propensity to form coiled coil. It is suggested that a common property of all these proteins is to self-assemble into higher ordered oligomers on specific templates (i.e. membranes) and to undergo a conformational change upon GTP binding or hydrolysis. The prototype for this family is dynamin, a protein involved in endocytosis (Danino and Hinshaw, 2001; van der Bliek, 1999). A series of binding interactions between its three domains have been proposed and suggested how dynamin might form a spiral and then constrict a membrane. (Smirnova et al., 1999).

A well established function of dynamin-related proteins is regulation of mitochondrial morphology and distribution (Rube and van der Bliek, 2004). Genetic studies in yeast, *Drosophila melanogaster* and *Caenorhabditis elegans* have identified several of these highly conserved proteins and their homologues have been found in humans and mice. In yeast mutations in Dnm1, and a homologous protein from *C. elegans*, called Drp1, block mitochondrial division (Bleazard et al., 1999; Otsuga et al., 1998). While overexpression of Drp-1 triggers mitochondrial fission in *C. elegans,* knockdown of Drp-1 by RNAi silencing has a converse effect and blocks mitochondrial outer-membrane scission. Immuno-electron microscopy and immunofluorescence show that Dnm1 and Drp1 co-localize with constrictions in mitochondria. A human dynamin related protein Drp1 is

most closely related to *C. elegans* Drp1 (62% amino acid identity) and is postulated to be responsible for proper distribution of mitochondria throughout the cell and mitochondrial division (Smirnova et al., 2001; Smirnova et al., 1998) Knock-down of Drp1 (Drp–RNAi) causes excessively elongated and interconnected mitochondria that often collapse into perinuclear aggregates (Chen et al., 2003).

Another dynamin-like protein discovered in *Saccharomyces cerevisiae*: Mgm1p is the OPA1 orthologue and like OPA1 has a mitochondrial leader sequence in its highly basic amino-terminal domain. Deletion of Mgm1p in yeast leads to extensive mitochondrial fragmentation, loss of mitochondrial DNA, deficits in respiration and abnormal cristae structure (Jones and Fangman, 1992; Sesaki et al., 2006; Wong et al., 2000).

1.2.2 OPA1 isoforms

In a Western blot analysis, human or mouse OPA1 is detected as six distinct bands between 100 and 80 kDa (Fig.1.7). In mice the identity of all the six bands was confirmed by electron spray ionization tandem MS/MS (mass spectroscopy) (Akepati et al., 2008). These bands (two long L-isoforms and three short S-isoforms) are the products of the translation of distinct mRNA isoforms and posttranslational proteolytic processing.

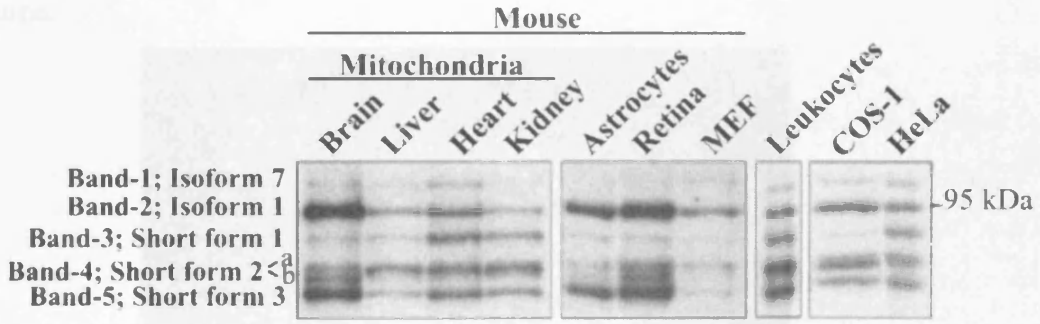

Fig.1.7 Six different protein isoforms are translated from four OPA1 splice variants and undergo proteolytic processing. Western blot analysis of mouse mitochondrial lysates from brain, liver, heart and kidney, total protein lysates from mouse astrocytes, retina and mouse embryonic fibroblasts (MEF); total protein lysates from human leukocytes, COS-1 cells and mitochondrial lysates from HeLa cells as detected by a-OPA1 monoclonal antibody show six different protein isoforms (from Akepati et al., 2008).

Both isoforms exist in yeast Mgm1 (OPA1 ortholog) and the small isoform (s-Mgm1) is produced after cleavage of the mature form by the mitochondrial rhomboid protease Pcp1/Rbd1/Mdm37/Ugo2- a homolog of serine protease Rhomboid (Herlan et al., 2003). The expression of both isoforms in yeast is essential for the maintenance of mitochondrial morphology and mtDNA. In PARL knockout mouse (PARL is the homolog of yeast Rbd1 in mammals and the so-called "presenilin- associated rhomboid-like") the reduction of a soluble, intermembrane space (IMS) form of OPA1 in Parl $^{-/-}$ cells has been observed indicating the importance of rhomboid protease in mouse OPA1 isoforms processing (Cipolat et al., 2006).

1.2.3 Opa1 protein localized to mitochondrial membrane

Mitochondria are double membrane organelles composed of outer (OMM) and inner (IMM) membranes. The large surface area of the inner membrane is shaped into numerous invaginations, or cristae (Fig.1.8). Cristae is highly specialized and contains the electron transport chain responsible for producing energy in the process of oxidative phosphorylation and ATP synthesis (Sesaki et al., 2006). The formation of cristae is supposed to facilitate ATP production by enabling more electron transport chain complexes to be packed into the mitochondrion. Crista are highly flexible, and undergo morphological changes in response to alteration of the metabolic state and/or matrix volume.

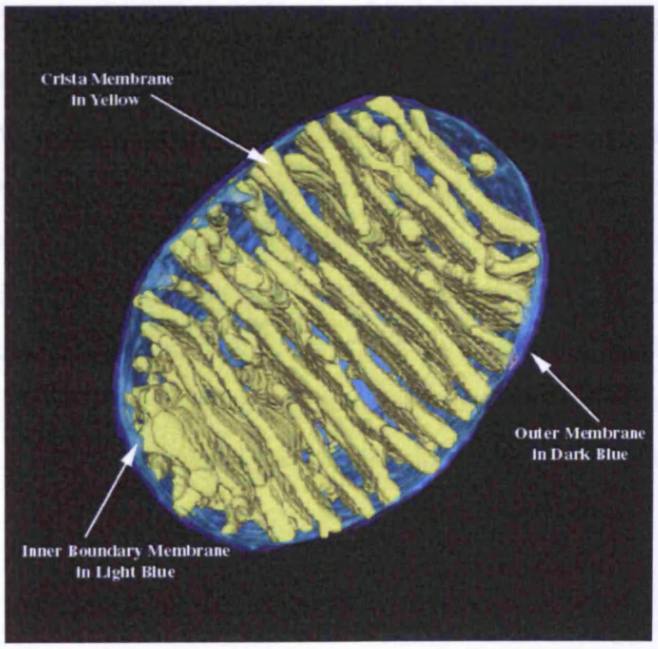

Fig.1.8 The tomogram of the mitochondrion (from http://www.sci.sdsu.edu/TFrey/MitoMovie.htm).

OPA1 localization to mitochondria has been experimentally confirmed by co-localization with Hsp60 in HeLa cells (Olichon et al., 2007a) and reporter gene analysis: fusion of the N-terminal 60 or 90 amino acids of mOPA1 with green fluorescent protein results in its mitochondrial targeting. Also subcellular distribution of mOPA1 overexpressed in COS-7 cells largely overlaps that of endogenous cytochrome c, a well known mitochondrial marker. Subcellular localization of mOPA1 has also been investigated in primary culture of dissociated rat cerebellar cells, where it shows labelling, distributed in a vesicular pattern in the somas of MAP-2-positive neurons and a weaker signal in the dendrites (Misaka et al., 2002).

OPA1 is closely associated with the inner membrane although it has been reported that different isoforms of OPA1 produced by the alternative splicing are sublocalized to the inner and outer mitochondrial membranes of HeLa cells (Olichon et al., 2002; Satoh et al., 2003). In proteolysis experiments OPA1 is digested together with the IMS marker Tim13. Analysis by electron microscopy using antibodies to OPA1 has shown most gold grains within mitochondria close to cristae and no labelling has occurred on the external border delimited by the OM. Labelling of the cristae by anti-OPA1 has been confirmed by the similar pattern of gold grain distribution obtained using antibodies to UCP, a cristae marker (Olichon et al., 2002).

OPA1 L- isoforms are anchored to the inner membrane and processed to soluble S-isoforms (Ishihara et al., 2006) (Fig.1.9). It appears that OPA1 specific processing and sublocalization of its isoforms in mitochondrial membrane compartments enable OPA1 to regulate cristae structure and thus perform its anti-apoptotic activity. It has been postulated that some OPA1 molecules localize to IMS and cristae matrix and contribute to the maintenance of cristae integrity. Other molecules, and currently it is believed that it could be an isoform containing exon 5b (Olichon et al., 2007a), form the cristae junctions which are the gates through which cytochrome c is released during apoptosis. By keeping these junctions tight, OPA1 could prevent (or delay) apoptotic events (see also 1.26).

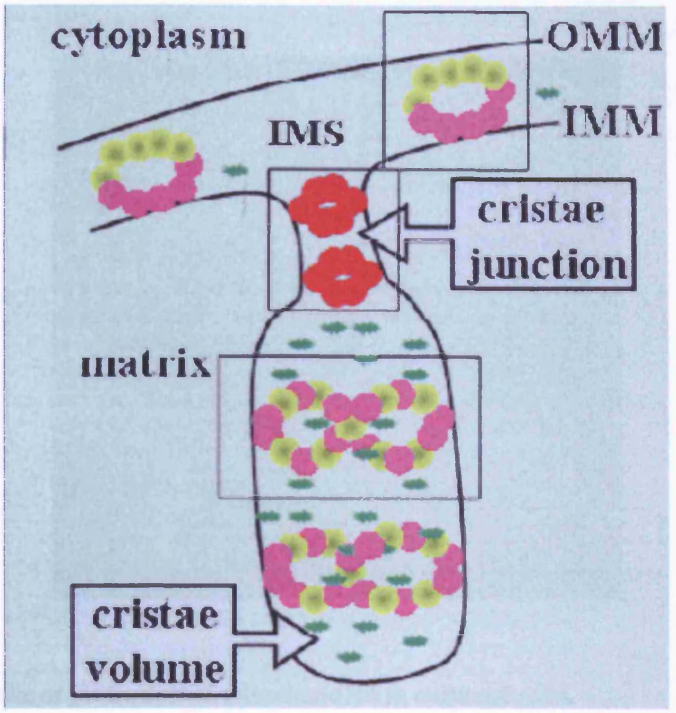

Fig.1.9 Schematic representation of OPA1 roles in structuring cristae, cristae junction and the interaction between outer and inner mitochondrial membranes.

Dots in pink represent OPA1 L-isoforms anchored to the membrane, dots in green represent OPA1 S-isoforms not interacting with the membrane, both being required for cristae structure and OMM to IMM bridging. Dots in red represent OPA1 isoforms forming the cristae junction. Cytochrome c, depicted as green stars, is mostly segregated in the cristae volume (from Lenaers et al., 2009); IMS- intermembrane space.

1.2.4 Opa1 responsible for mitochondrial fusion

Mitochondria are known to be motile and to undergo frequent divisions or to fuse with other mitochondria (Karbowski and Youle, 2003). Sometimes mitochondria exist as a single elaborate network and at other times they become fragmented, both events are physiological and in normal cells proceed smoothly and under the control of cellular mechanisms (Fig.1.10).

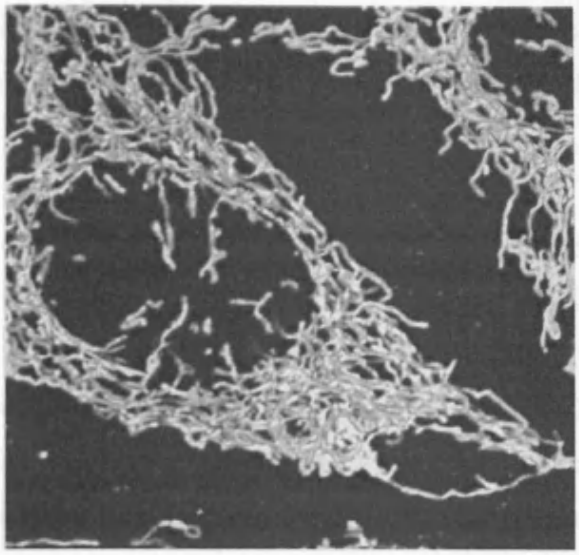

Fig.1.10 Network-like organization of mitochondria in cultured cells.
HeLa cells were stained with anti-cytochrome *c* antibodies and imaged using confocal microscopy (from Benard and Karbowski, 2009).

Mitochondrial fission is required in dividing cells to ensure inheritance of mitochondria by daughter cells but also occurs in postmitotic cells that are not able to divide, such as neurons. It is an important event during differentiation, in response to new energy demands and as a result of toxin exposure. Mitochondrial fission is balanced with mitochondrial fusion. The best known function of mitochondrial fusion is to maintain mitochondrial tubular morphology which exerts a protective effect on mitochondrial and cellular function. For example it can protect β-cells against nutrient-induced apoptosis (Molina et al., 2009). It can facilitate transfer of the mitochondrial membrane potential from oxygen-rich to oxygen-poor cellular regions. It can allow for an interaction of mtDNA gene products and prevent the stochastic depletion of materials, such as metabolic substrates and mtDNA. Cell hybrids between parental cells containing mutant mtDNA molecules result in restoration of respiratory activity indicating that complementation of mtDNA products can occur in fused mitochondria. In *Drosophila* mitochondrial fusion is a necessary event during development, and blocking mitochondrial fusion by mutation of the fuzzy onion (Fzo) gene (homologue of mammalian *MFN1* and *MFN2*) results in male sterility (Hales and Fuller, 1997). Fusion-defective cells have dramatically reduced growth rates, reduced respiration, an increase in reactive oxygen species (ROS) and a highly heterogeneous mitochondrial population

prone to loss of $\Delta\psi$ (mitochondrial membrane potential) and the mtDNA. Such cellular defects have been observed in OPA1-RNAi or Mfn-null (lack both of Mfn1 and Mfn2-) mammalian cells and were corrected upon restoration of mitochondrial fusion (Chen et al., 2003).

Different proteins control mitochondrial fusion and fission. Fusion is a multi-step process requiring the coordinated action of both the outer and inner membranes, ultimately resulting in mixing of matrix contents. Mitofusins (Mfn1 and Mfn2) are the proteins that act early and are essential for outer membrane fusion, whereas OPA1 is required for only inner membrane fusion (Song et al., 2009). This process requires the combined actions of S- and L-OPA1 isoforms (Song et al., 2007). Interesting results were obtained from overexpression of OPA1 protein (OPA1-OE) or its individual isoforms. Overexpression of wild type or mutant forms of Opa1 protein, in particular with Gln_{297} mutation affecting GTPase activity, caused mitochondria to fragment and accumulate to various extents in the cells near the nucleus (Misaka et al., 2002). However studies using PEG fusion assays showed that while OPA1-RNAi cells are devoid of any mitochondrial fusion even after 24hr. OPA1-OE cells were still able to fuse their mitochondria as efficiently as wild-type cells and the mitochondrial fragmentation observed in these cells was not due to the lack of fusion. Interestingly, mitochondrial fragmentation due to OPA1 overexpression was blocked when the fission molecule Drp1 was down-regulated by RNAi showing the balance between fusion and fission action in cells (Chen et al., 2003). The essential role of OPA1 in fusion was also shown in yeast cells where a strong loss of OPA1 orthologue-Mgm1 function caused mitochondria to be incapable of fusion, even when the mitochondrial fragmentation phenotype was suppressed by mutations in the yeast mitochondrial division protein Dnm1p (Sesaki et al., 2006). Moreover the Opa1p role in fusion depends on another mitochondria shaping protein: Mitofusin1 (Mfn1). In cells deficient in Mfn1, Opa1 could not promote mitochondrial fusion (Cipolat et al., 2004). Important results in relation to optic atrophy came from knockdown of Opa1 in retinal and cerebellar ganglion cells. Opa1 knockdown resulted in mitochondrial network aggregation in both cell cultures but occurred at a higher rate in retinal than cerebellar ganglion cells (Kamei et al., 2005).

1.2.5 OPA1 processing and mitochondrial membrane potential

Mitochondrial membrane potential is the electrochemical gradient that exists across the mitochondrial inner membrane and is maintained by the electron transport chain (Detmer et al., 2007). Mitochondrial membrane potential is an integral part of the respiratory process and reduced mitochondrial membrane potential may indicate dysfunction in energy production. Recent observations have shown that dissipation of mitochondrial membrane potential induces OPA1 proteolytic processing (Ishihara et al., 2006). Many apoptotic stimuli were also shown to exert this effect and this process has been linked to the decrease in the ATP level in mitochondria (Baricault et al., 2007).

OPA1 processing leading to accumulation of S-OPA1 isoforms was found in patients suffering from mitochondrial diseases marked by an impaired respiration (Duvezin-Caubet at al., 2006) (Fig.1.11). Moreover, it was shown on mouse embryonic fibroblasts derived from mice with homozygous knock-in of a variant of mtDNA polymerase γ. The reduction of larger Opa1 isoforms with the ultimate increase in the levels of the shorter forms was associated with severe mitochondrial dysfunction and was also accompanied by extensive fragmentation of the mitochondrial network (Fig.1.12).

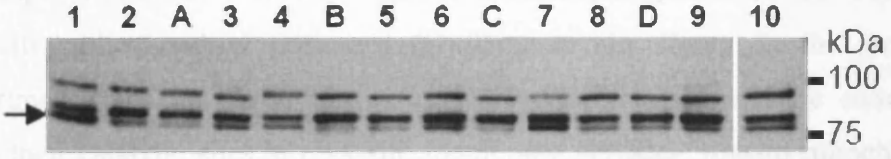

Fig.1.11 Patterns of OPA1 isoforms are altered in tissue samples exemplary of mitochondrial dysfunction. Homogenates from skeletal muscle biopsies from control individuals (A-D) and from patients suffering from respiratory disorders analyzed by western blotting for OPA1. The smallest form of OPA1 detected is indicated by an arrow (from Duvezin-Caubet et al., 2006).

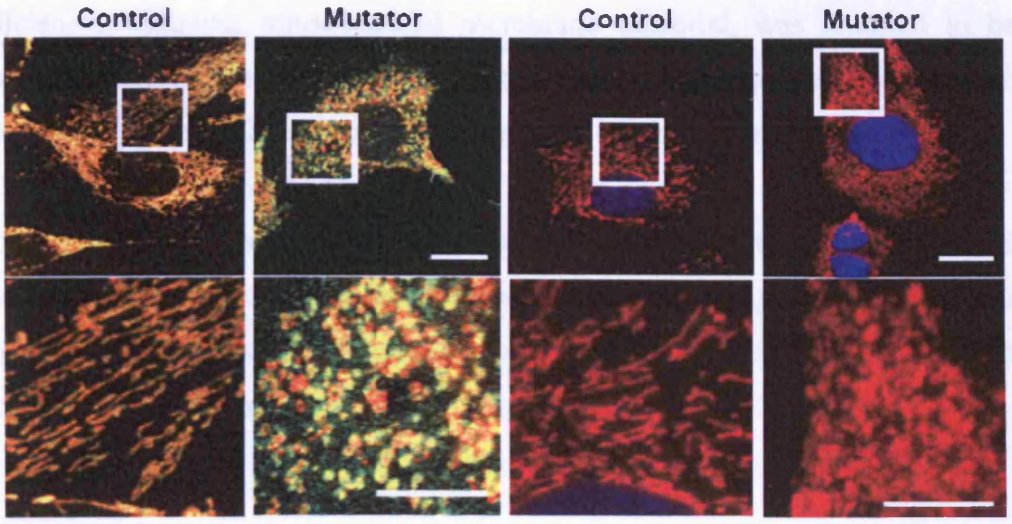

Fig.1.12 Mutator mouse embryonic fibroblasts show fragmentation of mitochondria. Immortalized mouse embryonic fibroblasts from two control mice and two mutator mice were cultured, stained with MitoTracker (red), fixed, and either immunostained against cytochrome *c* (green) or stained with DAPI (blue). Merged confocal fluorescence images are shown. Top, overview (scale bar 20 μm); bottom, indicated box, (scale bar 10 μm). Mitochondrial (from Duvezin-Caubet et al., 2006).

Degradation of OPA1 stimulated by dissipation of the mitochondrial membrane potential, for example with CCCP (carbonyl cyanide *m*-chlorophenylhydrazone), requires the action of specific mitochondrial proteases (Guillery et al., 2008). In the inner membrane compartment there are AAA proteases: ATP-dependent proteolytic complexes, which expose their catalytic sites at opposite membrane surfaces: toward mitochondrial matrix and intermembrane space (IMS) (Arnold and Langer, 2002). Studies showed the involvement of m-AAA proteases in OPA1 processing (Ishihara et al., 2006; Duvezin-Caubet et al., 2007). However, further experiments are required to point at the different activity of specific proteases in OPA1 processing in physiological (posttranslational modification of the protein) and pro-apoptotic conditions.

Mouse embryonic fibroblasts lacking Opa1 have defects in mitochondrial membrane potential and respiratory capacity (Chen et al., 2003). A decrease in the mitochondrial membrane potential was observed in fibroblasts from ADOAD patients harbouring the R445H mutation and suffering from optic atrophy and deafness (Amati-Bonneau et al., 2005). In addition, OPA1 mutations in ADOA fibroblasts have been shown to impair ATP synthesis driven by complex I under forced oxidative metabolism (fibroblast were

grown in galactose medium) (Zanna et al., 2008). However in another study, energetic efficiency, including mitochondrial membrane potential, was reported to be normal, despite prominent defects in mitochondrial morphology and distribution observed in fibroblasts and myotubes from ADOA patients (Spinazzi et al., 2008).

When defects in mitochondria accumulate mitochondria lose membrane potential, OPA1 and fusion capacity and are targeted to autophagy (Twig et al., 2008). Autophagic degradation separates defective mitochondria from the pool of healthy mitochondria, which continue fusion & fission cycle (Fig.1.13).

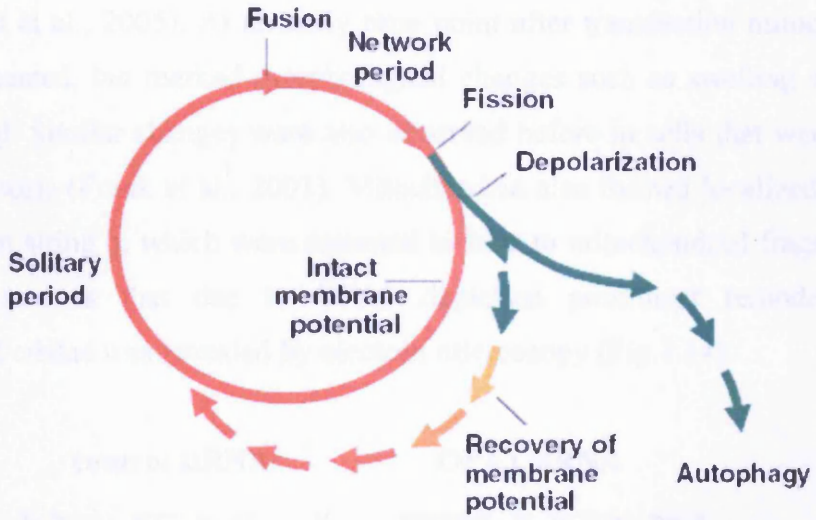

Fig.1.13 A model of the mitochondrion's life cycle that integrates mitochondrial dynamics and turnover. The mitochondrion cyclically shifts between a post fusion state (network) and a post fission state (solitary). Fusion is brief and triggers fission. Following a fission event, the daughter mitochondrion may either maintain intact membrane potential (red line) or depolarize (green line). If it depolarizes, it is unlikely to proceed to a subsequent fusion, unless it re-polarizes. After being depolarized and solitary for a few hours, the mitochondrion is removed by autophagy (from Twig et al., 2008).

1.2.6 Opa1 involvement in apoptosis and cellular response to stress

During apoptosis mitochondria undergo changes in mitochondrial architecture and permeability, which facilitate the apoptotic process (Green and Kroemer, 2004; Youle and Karbowski, 2005). Apoptosis is a complex process and numerous studies have focused on establishing the links between various events taking place during apoptosis. The release of cytochrome c and other pro-apoptotic factors, e.g. AIF, from mitochondria seems to be the key event. Several findings have recently pointed at the significant role of OPA1 in this process. It was shown that downregulation of OPA1 in HeLa cells by small interfering siRNA resulted in mitochondrial fragmentation, dissipation of the mitochondrial membrane potential and drastic disorganization of the cristae, which was followed by cytochrome c release and apoptosis (Olichon et al., 2003; Griparic et al., 2004; Arnoult et al., 2005). At an early time point after transfection mitochondria were not yet fragmented, but marked morphological changes such as swelling and stretching were observed. Similar changes were also observed before in cells that were at the early stage of apoptosis (Frank et al., 2001). Mitochondria also formed localized constrictions ("the beads on string"), which were assumed to lead to mitochondrial fragmentation. Of most importance is that due to OPA1 depletion prominent remodelling of the mitochondrial cristae was revealed by electron microscopy (Fig.1.14).

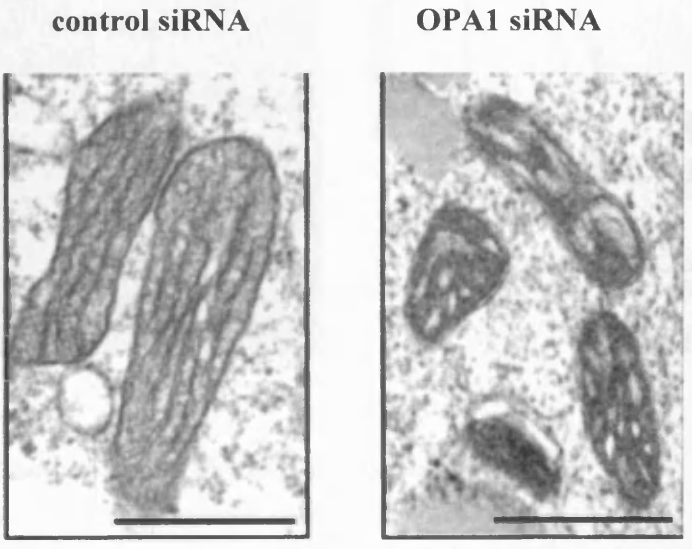

Fig.1.14 Mitochondrial ultrastucture. HeLa cells were transfected sequentially 3 times with control or OPA1 siRNA and mitochondrial ultrastructure was investigated by transmission electron microscopy. Bars represent 500nm (from Arnoult et al., 2005).

In one study the most striking abnormalities in the morphology of the cristae were observed in cells at the stage when the level of OPA1 protein was reduced by 86% (Griparic et al., 2004). OPA1 controls the shape of mitochondrial cristae by keeping their junctions tight, which is correlated with OPA1 oligomerization and prevents from mobilization of cytochrome c from the cristae stores during apoptosis. The proapoptotic BCL-2 family member BID, which widens cristae junctions, also disrupts Opa1 oligomers (Frezza et al., 2006). In one experiment the delay in release of cytochrome c induced by H_2O_2 was achieved by the expression of OPA1, whereas the expression of OPA1 mutant: ($OPA1^{K301A}$ with the mutation of conserved amino acid in the GTPase domain) failed to protect from H_2O_2 (Fig.1.15).

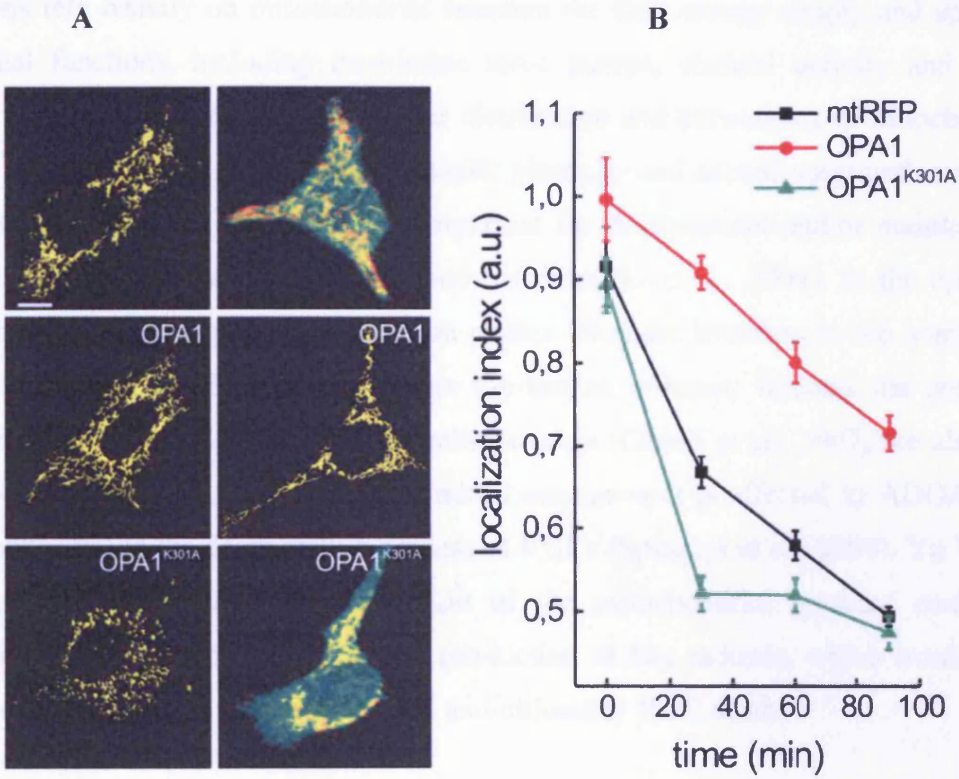

Fig. 1.15 OPA1 Delays Release of Cytochrome c during apoptosis.

A) Representative images of subcellular cytochrome c distribution. WT MEFs were cotransfected with mtRFP (red), and the indicated plasmids were left untreated or treated for 30 min with 1mM H_2O_2 fixed and immunostained for cytochrome c (green). Bar, 15μm. B) Localization index of cytochrome c. Experiments were performed as in A but cells were fixed at the indicated times (from Frezza et al., 2006)

OPA1 mutations in ADOA can lead to the increased vulnerability to apoptosis, as demonstrated in fibroblasts taken from ADOA patients and treated with staurosporine (Olichon et al., 2007b).

Interestingly, new mechanism that requires OPA1 activity and represents an adaptive pro-survival response against stress has been recently described. In cells exposed to selective stressful stimuli, e.g. UV light mitochondria hyperfuse and form a highly interconnected network. This stress-induced mitochondrial hyperfusion (SIMH) was shown to be dependent on L-OPA1 (but not S-OPA1) (Tondera et al., 2009).

1.3 Mitochondrial trafficking in neurons

Neurons rely heavily on mitochondrial function for their energy supply and specialized neuronal functions, including membrane ionic pumps, channel activity and synaptic transmission (Hollenbeck, 2005). Proper distribution and networking of mitochondria in axons and at synapses is critical for synaptic plasticity and axonal outgrowth since it has been shown that Opa1 and Drp1 are important for development and/or maintenance of spines and synapses in hippocampal neuron culture (Li et al., 2004). In the optic nerve mitochondria show a specific distribution pattern: they are abundant in the unmyelinated initial portion of the RGC axons before the lamina cribrosa, whereas the postlaminar optic nerve is myelinated and has less mitochondria (Carelli et al., 2007; see also 1.3.1). It is possible that this specific mitochondrial arrangement is affected in ADOA disease and contributes to the degenerative process of RGCs (Spinazzi et al., 2008). Yu Wai Man et al., (2005) postulated that disruption of the mitochondrial gradient could cause profound ATP depletion and increased production of free radicals, which would disturb conduction through the optic nerve head and ultimately RGC death.

Recently *in vivo* imaging of the mouse retina showed that mitochondria in RGC and optic nerve are short, punctuated and often form clusters, while non-neuronal cells exhibit longer, highly interconnected mitochondrial network (Uo et al., 2009). This difference may be taken into account when addressing the issue of particular vulnerability of RGC in ADOA disease.

1.3.1 Optic nerve physiology

All 1.2 million fibers of the optic nerve derive from the RGC of the inner retina (Carelli et al., 2004). Each RGC axon travels into the nerve fibre layer (NFL) and then toward the optic nerve head. These unmyelinated NFL axons form varicosities rich in mitochondria and desmosome- and hemidesmosomelike junctions with other axons or glial cells. At the optic nerve head axons turn posteriorly and pierce the many collagen plates that form the lamina cribrosa. Posterior to the lamina cribrosa, the axons become myelinated by oligodendroglia and build the optic nerve where a sharp decrease in mitochondrial numbers is observed (as shown by decreased COX staining (Fig.1.16). This reflects the differences in functional requirements of unmyelinated versus myelinated section of the nerve. Unmyelinated RGC axons are bioenergetically weak, have much slower conduction velocities and require more energy to restore the electrical potential, as compared to the posterior myelinated portion of these same axons which use saltatory conduction.

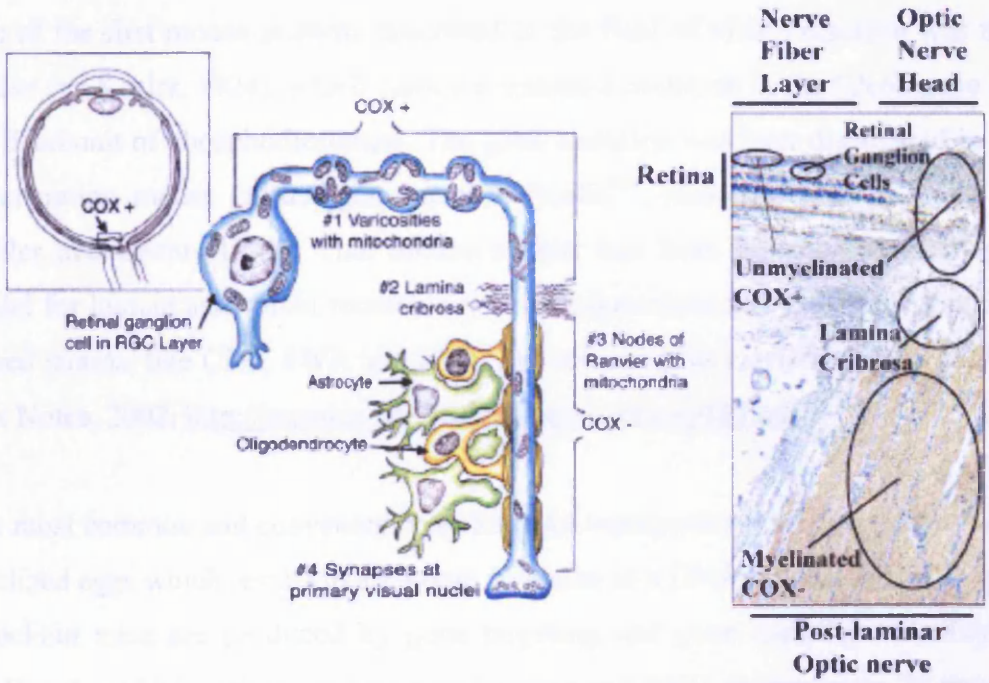

Fig.1.16 RGC system: diagrammatic view of pattern for staining of COX.

Cytochrome c oxidase (COX) accumulates at the sites of greatest oxidative phosphorylation (OXPHOS). Intense COX staining characterizes the NFL and the prelaminar RGC axons. This staining suddenly decreases posteriorly in concert with the appearance of myelin posterior to the lamina. On the left side is a sagittal view of the human eye. The boxed part is enlarged. There is a drastic decrease in mitochondrial

numbers within the retrolaminar portion (COX-). Mitochondria, in this part of the RGC axon, are mostly located under the unmyelinated nodes of Ranvier. On the right side is illustrated a histological sagittal section of a normal human eye showing a parallel transition from the retina to the optic nerve head, the lamina cribrosa and a portion of the myelinated retrolaminar optic nerve. The ocular tissue was stained by a method using immunoperoxidase for myelin basic protein, (from Carelli et al 2004).

1.4 Animal models of ADOA

1.4.1 Mouse models- natural mutants, chemical mutagenesis and technology of knockout and transgenic animals

Mouse models provide a valuable tool for investigating the genetic basis and the pathophysiology of human diseases, and to evaluate therapeutic treatments. At present, 197 genes are known to be involved in the formation of retinal diseases in humans (RetNet, http://www.sph.uth.tmc.edu/Retnet), but mouse models are available for only a few of them (Dalke and Graw, 2005).

One of the first mouse mutants described in the field of vision research was the *rodless* mouse (*r*); Keeler, 1924), which carries a nonsense mutation in the Pde6b gene coding for the β-subunit of phosphodiesterase. The gene mutation was later discovered in the retinal degeneration mouse (actual gene symbol Pde6b^{rd1}, formerly referred to as *rd1* or *rd* (Pittler and Baehr, 1991). This mouse mutant has been the most extensively studied model for human autosomal recessive retinitis pigmentosa (RP). Several common mouse inbred strains, like C3H, SWR and FVB, are homozygous carriers of the *Pde6brd1* allele (Jax Notes, 2002, http://jaxmice.jax.org/jaxnotes/archive/485.pdf.)

The most common and convenient way to make transgenic mice is pronuclear injection of fertilized eggs which results in a random insertion of a DNA sequence into the genome. Knockout mice are produced by gene targeting and gene trapping in embryonic stem (EM) cells, which are vector-based techniques and ENU mutagenesis. In the year 2004 published knockouts exist for about 10% of mouse genes (Austin et al., 2004).

A big collection of the spontaneous mouse mutant lines is maintained and characterized in the Jackson Laboratory. The limitation of this approach is the low frequency at which spontaneous mouse mutants occur. One of the spontaneous mutants is *(nr) nervous* mouse

in which retinal degeneration combined with the loss of cerebellar Purkinje cells is observed (De Jager et al., 1998).

N-ethyl-N-nitrosurea (ENU) is currently the most powerful mutagen for the generation of large numbers of new mutants including allelic series of single genes.
ENU targets premeiotic spermatogonial stem cells inducing discrete lesions, specifically point mutations, through alkylation of nucleic acids. The most common mutations induced by ENU are A/T → T/A transversions and A/T → G/C transitions.

By contrast other efficient germline chemicals such as chlorambucil or radiation usually cause large deletions or inversions that often involve more than one gene. ENU mutagenesis has been carried out for systematic phenotype-driven studies of mammalian gene function which can model human disease but can also be used for a gene-driven identification of new mutations. Genome-wide screens for both recessive and dominant mutations can be carried out and phenotypes not evident in recessive screens, including dominant, gain-of-function mutations, dominant-negative mutations, and mutations arising from haploinsuffiency can be revealed (Hatten and Heintz, 2005; Justice et al., 1999).

1.4.2 B6;C3-*Opa1*^{Q285STOP} mouse model of ADOA

In order to study the mechanism of ADOA disease, a new mouse targeted *Opa1* mutant has been generated in our laboratory by ENU mutagenesis (Davies et al., 2007). 10,000 DNA samples from ENU-treated C3H male strain mice (Ingenium) were screened. Exons 1, 8, 9, 10, 12, 28 of *OPA1* were amplified by PCR following heteroduplex analysis by temperature gradient capillary electrophoresis (TGCE: SpectuMedix). 5 SNPs were found in *OPA1*. One nonsense mutation 1051C→T in *OPA1* was selected for IVF (in vitro fertilisation), as it appeared to be highly likely to represent a functional allele. This mutation inserts a STOP signal instead of glutamine amino acid (Q285X) in exon 8 and causes premature protein truncation.

Western blot for Opa1 on different mutant mouse tissues showed the reduction of Opa1 (Fig.1.17).

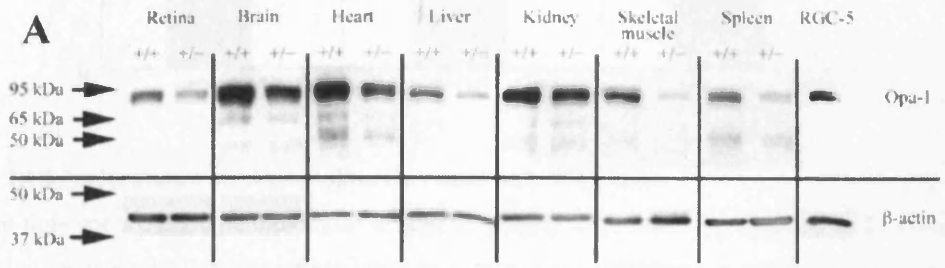

Fig.1.17 Western blot showing expression of the OPA1 protein in a panel of tissues taken from *Opa1*+/- and *Opa1*++ mouse. Protein extracts from retina, brain, heart and liver, kidney, skeletal muscle, spleen and RGC-5 cells. Equal loading was assessed by β-actin expression, and RGC-5 cells were used as an internal control for Opa1 (from Davies et al. 2007).

Homozygous mutant mice die at the embryonic stage, while heterozygous mutant mice develop relatively mild symptoms of optic neuropathy without any gross abnormalities affecting other organs. However, in a SHIRPA neurological assessment, which allows observational assessment of 37 different general health and neurological measures, reduced locomotor activity in the 6 month old *Opa1* +/- mice was found, which may reflect early changes in neurological function. Visual function in heterozygous mice was tested with the optokinetic drum (OKN) and the circadian running wheel. Both tests showed the functional reduction in visual function in 12 month old *Opa1* +/- mice. In contrast to WT mice, *Opa1*+/- mice continued their running wheel activity during the presentation of the light at night, indicating that they had not seen or detected the light. On OKN drum mutant mice could track all gratings, as WT mice, however did it less often than littermate controls (Fig. 1.18).

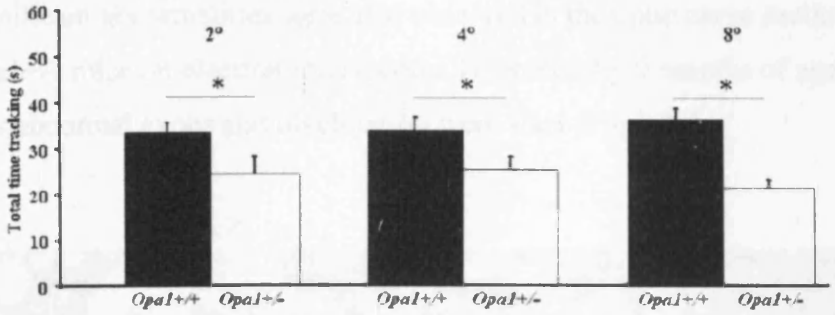

Fig. 1.18 Performance on the optokinetic visual screening test.

Mean time spent tracking a moving 2° 4° and 8° grating on the optokinetic drum at 12 months of age. The *Opa1*+/- mice track all three gratings less often compared to littermate controls (from Davies et al., 2007).

In 3 month old heterozygous mice an apparent alteration in mitochondrial morphology, with an increase in mitochondrial fragmentation was demonstrated by fluorescent microscopy in muscle explants. Retinal morphology appeared normal in the 6-month-old *Opa1*+/– mice and there was no RGC loss on H&E stained retinal sections at this age (Fig.1.19).

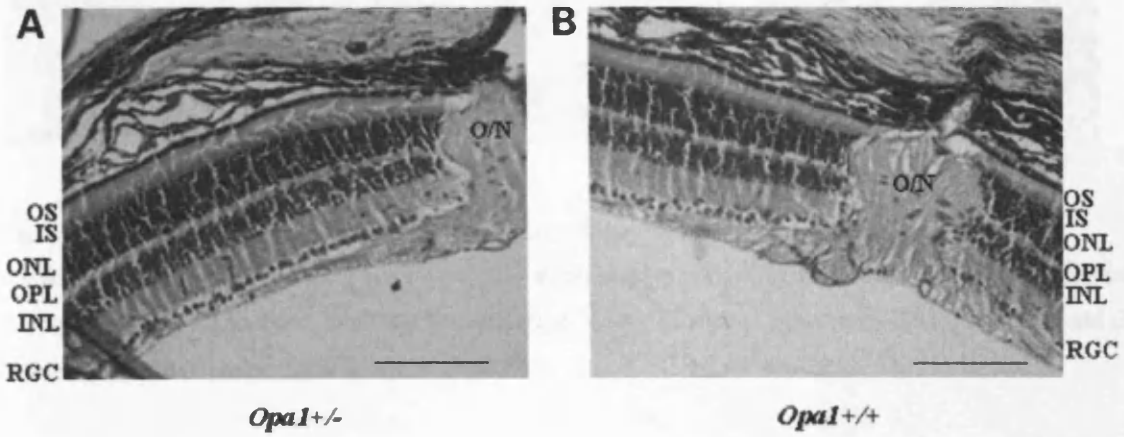

Fig. 1.19 Analysis of the RGC layer of *Opa1* +/- mutant compared with *Opa1* +/+ control.

(A) Representative H&E retinal section from an Opa1+/- (A) and *Opa1* +/+ mouse (B). The Opa1 +/- mice display equivalent RGC counts compared with littermate controls. O/N, optic nerve; OS, outer segments; IS, inner segments; ONL, outer nuclear layer; OPL, outer plexiform layer; INL, inner nuclear layer; RGC, retinal ganglion cell layer. Bar 100μm.

No significant abnormalities were also observed in the optic nerve sections from 6-month-old opa1+/– mice on electron microscopy. However, by 9 months of age and at 18 and 24 months abnormal axons and myelination were seen (Fig.1.20).

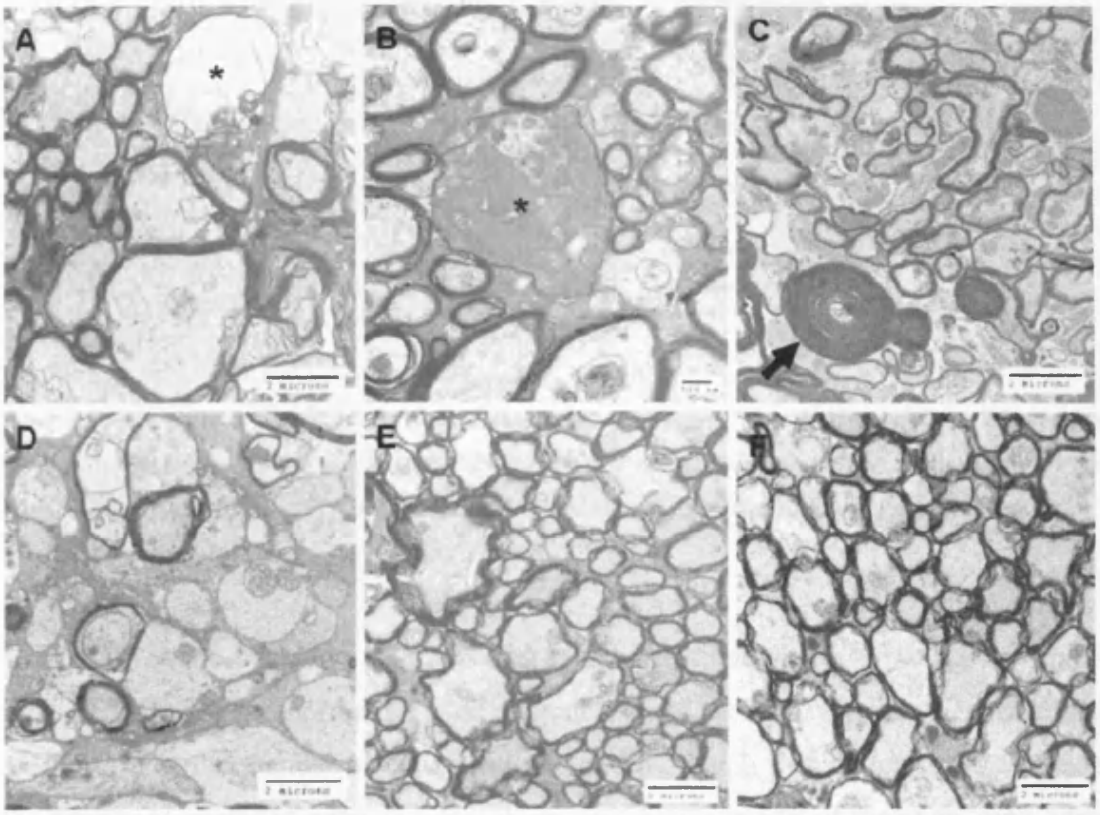

Fig.1.20 Electron micrographs of optic nerve axons from 24-month-old mice.
Axon abnormalities were classified as (**A**) watery degeneration (*asterisk*), (**B**) dark degeneration (*asterisk*), (**C**) myelin clumping (*arrow*), and (**D**) demyelination. Areas of normal optic nerve from 24-month-old (**E**) and 6-month-old (**F**) mice (from White et al., 2009).

Opa1 +/- mice demonstrated age- related axon loss from the optic nerve. There was also an increase in the number of autophagosomes in the RGC layer in 24 month old heterozygous mutants, which suggested the increase in the number of dysfunctional, depolarized mitochondria that were targeted to degradation (White et al., 2009) (Fig.1.21).

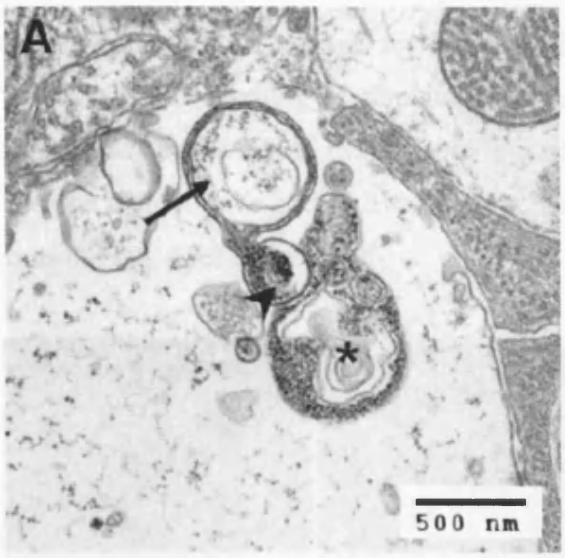

Fig.1.21 Electron micrograph of early- and late-stage autophagy in retinal ganglion cell layer from a 24-month-old mouse. In the earlier stage, the doublemembrane bound structure (*arrow*) is fusing with a lysosome (*arrowhead*). At the later stage (*asterisk*), fusion with the lysosome has taken place, and the structure is undergoing proteolysis (from White et al., 2009).

It was also found that some mitochondria in the optic nerves of 24-month-old *Opa1* +/- mice had structural abnormalities and vesiculation of the inner membranes. In addition, an increase in the number of opaque mitochondria, which may represent an increase in the density of cristae in order to fulfill the energy requirements of the axon, were seen by electron microscopy by 6 months of age. However, 11 month old *Opa1* +/- mice did not show cytochrome c oxidase deficiency or accumulate secondary mtDNA defects in their RGC layer (Yu Wai Man et al., 2009).

In conclusion *OPA1* heterozygous mutant mice show slow and age-related degeneration of the optic nerve associated with mitochondrial morphological abnormalities and increased autophagy.

1.4.3 Other models of ADOA

Another mouse model has been recently published (Alavi et al., 2007). The mutant mouse has a splicing mutation in *OPA1*, which induces skipping of exon 10 during transcript processing and leads to the deletion of 27 amino acids in the GTPase domain. Like B6;C3-*Opa1*^{Q285STOP}, homozygous mouse mutants are lethal at the early embryonic stage,

whereas heterozygous mutant mice showed an age-dependent degeneration of the optic nerve. Electron microscopy micrographs of axial section through the optic nerve showed significant reduction of axons and swelling of remaining axons. Mitochondria in these axons had disorganized cristae. In the retina progressive loss of RGCs was observed so that at the age of 13 months mutant mice had on average less than 50/% of the number of RGCs compared to controls (Fig. 1.22).

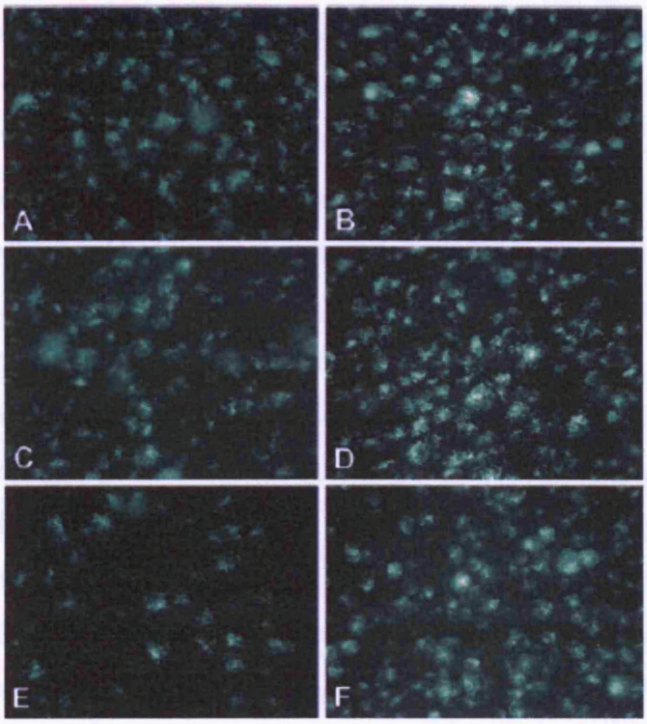

Fig.1.22 Age-dependent loss of retinal ganglion cells in *Opa1*$^{enu/+}$ mice.
(A-F) Whole mount retina preparation of *Opa1*$^{enu/+}$ and control mice following injection of hydroxystilbamidine into the superior colliculus that enables the specific labelling of retinal ganglion cells. *Opa1*$^{enu/+}$ mice (A,C, E) show a reduced number of labeled cells in comparison with age-matched wild-type littermates (B, D, F) that progresses with age (A, B: 2 months; C, D: 9 months; E, F: 13 months) (from Alavi et al., 2007).

In invertebrate models of ADOA: *Caenorhabditis elegans* and *Drosophila melanogaster,* the prominent feature was the high oxidative stress, which could be counteracted by anti-oxidant treatment (Kanazawa et al., 2008; Yarosh et al., 2008). These two models suggest that over production of reactive oxygen species (ROS) may contribute to the pathogenesis of ADOA and that anti-oxidant treatment may be beneficial to patients.

1.5 Summary

Dominant optic atrophy (ADOA) is the most prevalent inherited optic neuropathy characterized by a loss of visual acuity, development of centrocoecal scotoma and bilateral temporal atrophy of the optic nerve. Post-mortem histopathological studies of two patients identified a selective loss of retinal ganglion cells and loss of myelin. About 60% of ADOA cases are now linked to mutations in the *OPA1* gene, which encodes a dynamin-related GTPase involved in mitochondrial morphology, cristae organization and apoptosis. OPA1 controls inner membrane fusion, which by counteracting fission maintains the morphology of mitochondrial network in dynamic balance. Loss of OPA1 function is induced by dissipation of the mitochondrial membrane potential and the pro-apoptotic process and can result in the increased autophagy of defective mitochondria.

However, the link between *OPA1* dysfunction and the clinical manifestations of ADOA has not been fully explained yet. It still remains unclear why the disease in its classic form is restricted to the apparent ocular phenotype.

In order to help with these unanswered questions, a new mouse targeted *Opa1* mutant has been produced, which carries a nonsense mutation in exon 8 causing a reduction in the cellular Opa1 level. Homozygous mutant mice die at the embryonic stage, while heterozygous mutant mice develop late and slowly progressive optic neuropathy with the reduction in visual function. Of most importance is that by 24 months of age loss of axons in the optic nerve is accompanied by abnormalities in mitochondrial ultrastructure and increased autophagy.

1.6 Project objectives (Fig.1.23)

The main aim of this PhD project was to study the magnitude of mitochondrial dysfunction and cellular response to the reduction in Opa1 level in *Opa1* mutant mice. Cell growth and susceptibility to oxidative stress, morphology of mitochondrial network, cristae and mitochondrial membrane potential were studied. In addition, histological evaluation of RGC loss and apoptotic staining in aging animals was performed. The purpose of these experiments was to give possible insight into the impaired cellular mechanisms which lead to visual defects and an optic atrophy in *Opa1* mutant mice.

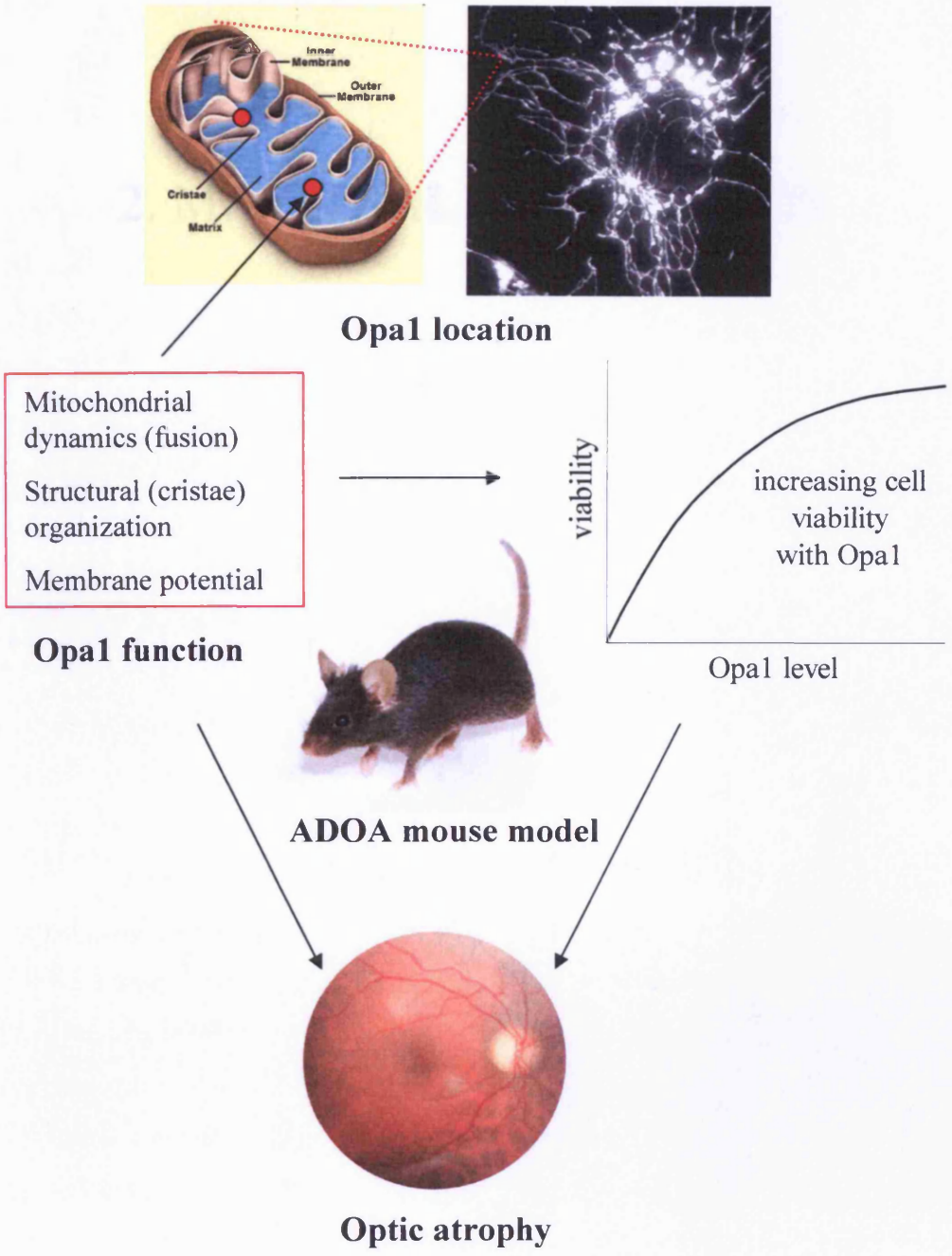

Fig. 1.23 PhD project. ADOA mouse model with Opa1 deficiency has been used to study mitochondrial and cellular dysfunctions, which could lead to visual defect and an optic atrophy in mutant mice.

2. MATERIALS & METHODS

2. MATERIALS AND METHODS

2.1 Breeding strategy

*Opa*1+/- "founder" mice were crossed with C57Bl/6JCrl mice (Charles River, UK) to move the mutation to a C57Bl/6JCrl background. This was continued at F2 to F5. For embryo generation matings were assumed to take place at midnight, and the day of plug detection was designated 0.5 days post coitum (dpc). Embryos were dissected daily from pregnant dams at 13.5 dpc. The number of animals maintained in the *Opa1* colony was approximately 100-150 at any one time. Animals were on a normal controlled 12hr-12hr light-dark cycle. 3-4 week old animals were weaned and genotyped. Breeding, maintenance and sacrifice were in compliance with the *ARVO Statement for the Use of Animals in Ophthalmic and Vision Research.*

2.2 DNA extraction and quantification

DNA was extracted from mouse tail (Wizard SV Genomic DNA Purification System, Promega, UK) according to the manufacturer's protocol. Tails of approximately 0.3-0.5 mm long were lysed in 275µl Digestion Solution Master Mix (see Appendix 1) containing Proteinase K 20mg/ml (Bioline, UK) at 55°C in the oven overnight. Next digested tissues were centrifuged and the supernatants were taken to the subsequent procedures. 250µl of Wizard SV Lysis Buffer was added to each sample. Warm lysates were loaded onto the columns and centrifuged 1550g for 3min, the flow-through was discarded. Columns were washed with ethanol four times and bound DNA was eluted with 500µl of sterile and distilled water. 2µl of DNA were added to PCR (polymerase chain reaction) mix (Bioline, UK) for genotyping. For some samples DNA was quantified by UV spectrophotometry (U- 2800 Spectrophotometer, UV Solutions software, Hitachi, Japan). 1:20 dilutions were prepared and samples absorbance measured at 260nm and 280nm. DNA concentration was calculated by the formula: $C = A_{260}$ x dilution x 50µg/ml. Purity of the total DNA was assessed by spectrophotometric ratio A260/A280 (1.9–2.1).

Alternatively mouse tails were lysed in 200µl DirectPCR Lysis Reagent (Tail) (Viagen Biotech, US) with 0.4mg/ml Proteinase K (Bioline, UK) at 55°C for 5hr to overnight until no tissue clumps were observed. Crude lysates were incubated in the water bath at 85°C for 45min and stored at 4°C for PCR genotyping. For PCR 1µl of lysate was used. For embryo genotyping DNA from mouse embryos was extracted by DirectPCR Lysis Reagent (Ear) (Viagen Biotech, US).

2.3 *Opa1* and *Nnt* genotyping

2.3.1 *Opa1* allele-specific genotyping

For genotyping of *Opa1* mutant animals two reactions were carried out with two sets of primers. The forward primer 5'-TCTCTTCATGTATCTGTGGTCTTTG-3' was identical for both reactions amplifying wild-type and mutant allele. Reverse primers: 5'-TTACCCGTGGTAGGTGATCATG-3', 5'-TTACCCGTGGTAGGTGATCATA-3' were designed to bind specifically to the WT and a mutant allele, respectively. Primers were designed with Primer3 software (Whitehead Institute for Biomedical Research, US). PCR reactions were run on TC-512 Techne Thermal Cycler (Techne Inc., US) For each reaction 2µl of DNA template from individual animal were used. DNA was amplified with 1pmol/µl primers in 25µl reaction PCR mix (BioMix Red; Bioline, UK). Additionally, a control reaction without DNA template for each assay was carried out. PCR was performed with initial denaturation for 5 minutes at 94°C followed by 35 cycles of denaturation (1 minute at 94°C), annealing (1 minute at 55°C) and elongation (1 minute 72°C) after which the final elongation was carried out for 10 minutes at 72°C. PCR products were separated by 2% agarose gel electrophoresis in TBE buffer (Tris-borate-EDTA (Materials and Methods 2.4 and Appendix 1). 5µl of 100bp DNA ladder (Invitrogen) were loaded into the well for size determination.

2.3.2 *Nnt* genotyping

Mice were genotyped by PCR of missing exons 7 and 11 of *Nnt* gene. Primer sequences were taken from Freeman et al., 2006 and were for *Nnt* exon 7:

Nnt7 forward 5'- GTGCATTGAACCCTCAAAGG-3'

Nnt7 reverse 5'-CAGGTAAGAAAGCTCCTGTTTT-3';

for *Nnt* exon 11:

Nnt11 forward 5'-TCCTGCTATTCCTCCTCCTG-3'

Nnt11 reverse 5'- GCTGCCTTGACTTTGGATATT-3'.

Primers 6L4 and 12L1 (taken from Ting-Ting Huang et al., 2006) flanked the deletion in *Nnt* gene. Their sequence was for 6L4: 5'- TCCCCTCCCTTCCATTTAGT-3' and 12L1: 5'- GTAGGGCCAACTGTTTCTGC-3'. Primers were used at the concentration 1pmol/µl. PCR was performed on TC-512 Techne Thermal Cycler (Techne Inc., US) in 25 µl reaction mix (BioMix Red; Bioline, UK). PCR products were separated by 2% agarose gel electrophoresis (see Materials and Methods 2.4).

2.4 Agarose gel electrophoresis

Agarose (Invitrogen) was dissolved in 100ml TBE buffer in a microwave oven. After cooling the solution to about 60°C ethidium bromide was added to the final concentration 0.5 μg/ml and the solution was poured to the casting tray containing a sample comb and was allowed to solidify at the room temperature for 1hr. 12μl of PCR samples were loaded into the wells. Electrophoresis was run in the electrophoresis chamber with the gel completely covered with TBE buffer for about 1hour at 75-120V. DNA fragments were visualized by UV light (UVITECH transilluminator).

2.5 Denaturing agarose gel electrophoresis

To check the integrity of extracted RNA samples, 5μl of the samples were heated in 10μl RNA sample loading buffer (Sigma) at 65°C for 10min, chilled on ice and loaded onto the 1.2% denaturing (formaldehyde) agarose gel (see Appendix 1). Electrophoresis was run at 5V/cm in formaldehyde MESA buffer (MOPS-EDTA-sodium acetate; see Appendix 1). RNA bands were observed under UV light.

2.6 Primer design and specificity

Primers were designed using Primer3 software. A transcript sequences in FASTA format were retrieved from NCBI database (National Center for Biotechnology Information, http://www.ncbi.nlm.nih.gov/) and the default settings for primer design were used: an optimal primer size 20bp, an optimal melting temperature 60°C. Primers were stored at -20°C at the concentration 100μM diluted in TE buffer (Tris- EDTA; see Appendix 1) or in MilliQ H_2O.

2.6.1 Primer design for qRT-PCR (quantitative reverse transcription PCR)

Each set of primers targeted a coding region of mRNA sequences that were obtained from NCBI database (Table 2.1).

Primers	**Sequence 5'-3'**
Mus musculus Mfn2 Forward	ATGCAGACGGAGAAGCAGTT
Mus musculus Mfn2 Reverse	GGCAGACACGAAGAAGATCC
Mus musculus Spg7 Forward	CACCTCAAGGATGAAGCAGA
Mus musculus Spg7 Reverse	AGGAAATACTGCCCCCACTT
Mus musculus Bik Forward	GAAGGAGCCTGTGAGAGACG
Mus musculus Bik Reverse	GTTTTCCCTGAGGTTGGTGA
Mus musculus Dnm1l Forward	TTTGCTCGTGTGAAGACTGG
Mus musculus Dnm1l Reverse	TGGAGCTTCCTTTCTGAGGA
Mus musculus Slc25a4 Forward	GATCGAGAGGGTCAAACTGC
Mus musculus Slc25a4 Reverse	GAAGTTCAGGGCTTGAGTGG
Mus musculus Atp5k Forward	CGGTTCAGGTCTCTCCACTC
Mus musculus Atp5k Reverse	CGCCAGTTCTCTCTCAATCC
Mus musculus Hprt1 Forward	AGCTACTGTAATGATCAGTCAACG
Mus musculus Hprt1 Reverse	AGAGGTCCTTTTCACCAGCA

Table 2.1 Primer sequences for qRT-PCR analysis.

2.6.2 Melting curve analysis

To check the specificity of the primers, cDNA samples were prepared in serial dilutions and SYBR Green based real time RT-PCR was performed using conditions that were experimentally optimized for each set of primers (see 2.8.3). PCR was followed by a melting step with default conditions (the temperature range 50°C -99°C). A melting curve was obtained by plotting the derivative of the fluorescence with respect to temperature (*dF/dT)* (Rotor-Gene™ 6000 instrument, Melt Report).

2.7 RNA preparation

2.7.1 Isolation of RNA

Tissues (retina, kidney, liver, spleen) were dissected from WT and heterozygote animals and RNA was extracted using Rneasy Mini Kit (Qiagen). Two retinas were pooled into one sample. Tissues were placed in RNA *later* (Sigma) and stored at -20°C until extraction was performed. On the day of extraction tissue was transferred to 600µl of Buffer RLT and homogenized immediately until the sample was uniformly homogeneous (20-40s). Homogenate was centrifuged at 15000g for 3min and supernatant was transferred to a new 1.7ml tube by pipetting. 600µl of 70% ethanol was added to the lysate and mixed by pipetting. A 700µl sample was applied to an RNeasy mini column placed in a 2ml collection tube and the sample was centrifuged for 15s at 9000g. Flow-through was discarded. The step was repeated with the rest of the sample. Next each column was washed with 350µl buffer RW1, centrifuged for 15s at 9000g and the flow-through was discarded. To avoid DNA contamination samples were treated with DNase. For each sample 10µl DNase I stock solution (Qiagen) was added to 70µl Buffer RDD (Qiagen) and mixed by gently inverting the tube. The Dnase I mix was pipetted directly onto a silica-gel membrane and placed on the benchtop (20-30°C) for 15min. Afterwards the columns were transferred onto new collection tubes, 500µl Buffer RPE was pipetted onto the column followed by centrifugation for 15s at 9000g to wash the column. The flow-through was discarded. Another 500µl Buffer RPE was added to the column and centrifuged for 2min at 9000g to dry the silica-gel membrane. For RNA elution the column was transferred to 1.7ml collection tube and 40µl TE was added directly onto the silica-gel membrane and centrifuged for 1min at 9000g.

2.7.2 Measurement of RNA quantity and quality

2.7.2.1 RNA quantification by spectrophotometry

For RNA quantification 1:20 dilutions were prepared and the samples' absorbance was measured at 260nm and 280nm using Spectrophotometer U- 2800 equipped with UV Solutions software. Purity of the RNA was assessed by spectrophotometric ratio A260/A280 (1.9–2.1). RNA concentration was calculated by the formula:

$C = A_{260} \times 20 \times 40\mu g/ml$

2.7.2.2 RNA quantification using RiboGreen

RNA concentration was measured using the fluorescent reagent RiboGreen (Molecular Probes, Inc., Eugene, Oregon, US). A standard curve was prepared with the ribosomal RNA (16S and 23S rRNA): 100µg/ml was diluted in TE to make the 2µg/ml stock solution and stored at -20°C. On the day of the experiment, the RiboGreen reagent was diluted 200-fold in TE and 10µl was added to 10µl of RNA standard different dilutions to obtain the final RNA concentrations: 1µg/ml, 750ng/ml, 500ng/ml, 250ng/ml and blank (no RNA added). Samples were mixed and incubated for 5min at room temperature, protected from light. The experimental RNA samples were diluted 50 fold in TE to a final volume of 10µl and 10µl of RiboGreen reagent was added to each sample.

Samples were mixed well and incubated at room temperature for 5min, protected from light. All samples were prepared in duplicate. The fluorescence of the samples in the final volume of 20µl was measured and the standard curve was generated using Corbett Rotor-Gene 6000 (software version Rotor-Gene 1.7.34, Concentration Measurements).

The program default setting was:

Hold 50°C - 2min

Cycling 10 repeats- 50°C hold 5s

Fluorescence was acquired to the Green Channel with the fluorescein excitation and emission wavelengths: ~480nm and 520nm, respectively. The instrument's gain was automatically set according to the concentration of the reference sample on the first position in the rotor: the RNA standard at the highest concentration. The value of the reagent blank was subtracted from that of each sample and obtained concentrations were multiplied by the dilution factor 50 (Appendix 2).

2.8 Reverse transcription (RT) and PCR

2.8.1 First strand cDNA synthesis

For cDNA synthesis (for qRT-PCR) 200ng of total RNA was mixed with 1µl (270ng) oligo $(dT)_{18}$ primers and 1µl dNTP mix: dATP, dGTP, dCTP, dTTP, 10mM each (Bioline, UK) in the total volume of 13µl. Next, the mixture was heated to 65°C for 5min and incubated on ice for 1min. Afterwards 4µl 5x First Strand Buffer (Invitrogen),

1µl 0.1M DTT (Invitrogen), 1µl RNase Inhibitor 10U/µl (Bioline) and

1µl SuperScript III RT 200 U/µl (Invitrogen) were added to each tube followed by 1hr incubation at 50°C. The enzyme was inactivated by heating at 70°C for 15min.

2.8.2 RT- PCR of Opa1 transcript isoforms

For RT-PCR of Opa1 transcript isoforms cDNA was synthesized on the template of 1μg of RNA. PCR amplification was performed on TC-512 Techne Thermal Cycler (Techne Inc., US) in 25μl reaction mixture containing 2μl cDNA, 1μM primers forward and reverse, 12.5μl 2x BioMixRed (Bioline, UK).

The PCR conditions were identical for all designed primers:

Initial denaturation 5min 94°C

35 cycles:

1. Denaturation 30s 94°C
2. Annealing 1min 54°C
3. Elongation 1min 72°C

Final elongation 10min 72°C

2.8.3 Quantitative PCR amplification of cDNA- $\Delta\Delta C_t$ method

The relative expression of genes was calculated on the basis of $\Delta\Delta C_t$ values (Livak and Schmittgen, 2001). The method assumes an optimal doubling of the target DNA during each performed real time PCR cycle. The C_t is determined for each sample to compare the distinct cycle differences between samples at the selected level of fluorescence.

Real time PCR was performed on a Rotor-Gene™ 6000 instrument (Corbett Research) in SYBR Green JumpStart Taq Mix (Sigma) containing 200nM primers and 2μl cDNA sample. The PCR conditions were as follows:

Hold 2min 95°C

Cycling (40 cycles):

1. Denaturation 15s 95°C
2. Annealing 20s 58°C
3. Elongation 20s 72°C

Hold 2min 72°C

For each run standard curves were prepared for both GOI (gene of interest) and reference gene (housekeeping gene) with four dilutions and the blank (negative control). All samples were run in duplicate. The $\Delta\Delta C_t$ method relies on "identical" efficiency of amplification (E) between GOI and the reference gene. The E was automatically calculated and the differences in efficiencies were estimated. The C_t threshold was automatically set in the exponential phase and C_t values for all samples were calculated.

The expression of GOI was normalized to the expression of the reference gene and the results were calibrated to those of the first WT sample.

2.9 Mitochondrial isolation from mouse tissue

Mitochondria were isolated using a Mitochondria Isolation Kit (Sigma). All steps were performed on ice; samples were centrifuged at 4°C. Freshly excised mouse tissue (120mg brain, 6 retinas and optic nerves) was washed twice in ice-cold Extraction Buffer (10mM HEPES, pH 7.5, 200mM mannitol, 70mM sucrose, 1mM EGTA). Next tissue cut into small pieces was homogenized on ice with 1.5ml Extraction Buffer containing 2mg/ml albumin in a precooled 3ml volume glass homogenizer by moving the pestle up and down 25 times. Homogenate was transferred to 2ml Eppendorf tube and centrifuged at 600g for 5min. Supernatant was recovered and centrifuged at 11000g for 10min. For brain samples the resulting pellet was resuspended in 1.5ml Extraction Buffer and two centrifugation steps were repeated. Mitochondria in the pellet were suspended in 80µl (mitochondria isolated from brain) or 10µl (retina) Storage Buffer (10mM HEPES, pH 7.4, 250mM sucrose, 1mM ATP, 0.08mM ADP, 5mM sodium succinate, 2mM K_2HPO_4, 1mM DTT). Mitochondrial protein concentration was quantified using absorption spectroscopy methods: colorimetric DC Protein Assay (Bio-Rad) or UV spectrophotometric assay (Picodrop) (see 2.10) Mitochondria were aliquoted and stored in -80°C.

2.10 Protein quantification

2.10.1 *DC* protein assay (Bio-Rad) - colorimetric method

Mitochondrial suspension and the gamma globulin standard were diluted in 2% SDS. For the standard fresh dilutions: 0, 0.05, 0.1, 0.15, 0.2, 0.29, 0.5 mg/ml in triplicate were prepared. 5µl of standards and samples were pipetted into wells of a 96-well plate. 25µl of reagent A containing reagent S were added into each well followed by 200µl of reagent B. After 15min the plate was placed in a plate reader and was shaken for 5s at medium speed. The absorbance was measured at 750nm (Multiskan *Ascent*, Labsystems, Finland). The concentration of the samples was extrapolated from the standard curve (Fig.2.1).

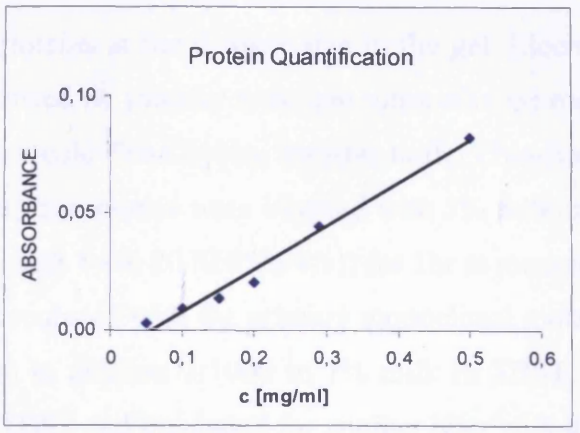

Fig.2.1 A standard curve for protein quantification assay

2.10.2 UV spectrophotometric assay

Mitochondrial concentration was calculated from the absorbance values at 280nm using Picodrop UV/VIS spectrophotometer (Picodrop Limited, UK). The absorbance of 3µl of mitochondrial suspension was measured in disposable pipette tips provided by the company. The IgG (immunoglobulin G) was used as an internal reference protein. The average of three readings was taken (Appendix 2).

2.11 Protein extraction from mouse embryonic fibroblasts (MEFs)

For the whole cell extraction cells were culturing in T25 flasks (Triple Red, UK). The cell medium was removed and cells were rinsed with ice cold PBS buffer (phosphate buffered saline, see Appendix 1). To lyse cells 0.8ml of ice cold RIPA (Radio-Immunoprecipitation Assay; Sigma) buffer containing a complete protease inhibitor cocktail (tablets, Roche) was added and cells were gently rocked on ice for 15min. Next the cells were scraped and transferred into microcentrifuge tubes on ice. Cells were further disrupted by passing the lysate 5 times through a 21-gauge needle. The protein supernatant was collected after centrifugation at 8000g for 10min at 4°C. Protein extract aliquots were stored at -80°C. Care was taken to avoid freeze-thaw cycles.

2.12 Western blotting

Protein samples were boiled for 5min at 95°C in a sample loading buffer (Appendix 1). 20µg of protein extracts were separated by 8% SDS-PAGE (sodium dodecyl sulphate-polyacrylamide gel electrophoresis) in Tris/Glycine/SDS running buffer (Bio-Rad).
The composition of the resolving (8%) and stacking (5%) gels is described in Appendix1. The Precision Plus Protein Standard (Bio-Rad) was loaded in a volume of 10µl/ lane to

show the location of proteins at the distinct size in the gel. Electrophoresis was run for 1hr15min at 100V followed by transfer to 0.2μm nitrocellulose membrane (Bio-Rad) for 1hr15min at 250mA in a cold Tris/Glycine transfer buffer (Bio-Rad) with 20% methanol (v/v). After the transfer, membranes were blocked with 5% milk in TBST (Tris-Buffered Saline (tablets, Sigma) with Twin 20 (0.05% v/v)) for 1hr at room temperature.
The membranes were incubated with the primary monoclonal mouse Opa1 antibody (250 μg/ml BD Biosciences) in dilution 1:1000 in 1% milk in TBST. The membranes were washed three times in TBST and incubated for another hour with the secondary goat anti-mouse antibody conjugated with HRP, diluted by 1:10000 in 1% milk in TBST. After three washing in TBST blots were subjected to chemiluminescent detection with Pierce ECL Western Blotting Substrate (Pierce) for 1min and exposed to blue sensitive radiographic film (Kodak). Immunoblot for Hsp60 was done on the same blot as for opa1 protein. The blot was cut in a way that these two proteins were separated and could be incubated with their specific antibodies. The primary antibody for Hsp60 was diluted by 1:1000 followed by incubation with the goat anti-mouse secondary antibody (1:10000). The cytochrome c mouse antibody (BD Pharmingen) was used in dilution 1:1000.

2.13 Analysis of the cell number in RGC layer and the retinal thickness

10 retinal cross sections of 24-month old *Opa1* +/+ and *Opa1* +/- mice (n=5) were mounted and stained with haematoxylin and eosin (H&E). These sections were collected from 5 areas that were 20 sections apart. Images of the whole retina were obtained using a Leica DMRA2 microscope equipped with a DC500 camera (Leica) and QWinV3 software.
The mounting, staining with H&E and imaging was carried out by Vanessa Davies.
Counts of cells in retinal sections were done manually by counting all nuclei in the RGC layer. The mean retinal thickness in retinal cross sections was obtained by taking the measurements across the thickest region of the retina in 5 areas as above.

2.14 Apoptotic assay on the mouse retina

Retinal sections from 2 year old animals (3 WT and 3 heterozygote) which had been embedded in wax were used for apoptosis assay-TUNEL assay using Apoptag Fluorescein In Situ Apoptosis Kit (Chemicon). Six sections per genotype were analyzed. For positive control sections were pre-treated with 1μg/μl Dnase (Qiagen). Sections where the TdT enzyme was omitted were negative control.

All sections were deparaffinized with xylene three times for 5min and then washed in decreasing concentrations of ethanol: 100% twice for 5min, 95% for 3min and 70% for 3min.

Dewaxed sections were washed in PBS for 5min, incubated in 0.1% TritonX-100 for 15min followed by two washes in PBS for 2min. Then for positive control, sections were incubated in 1μg/μl Dnase for 30min and rinsed in dH_2O 5 times for 3min each wash. Equilibration buffer was applied to all sections for 5min at room temperature followed by 1hr incubation at 37°C with 30μl TdT enzyme for each section. After incubation Stop/WASH Buffer was applied for 10min and then rinsed with 3 changes of PBS for 1min. 30μl of warmed Anti-Digoxigenin antibody conjugated with fluorescein was applied to the sections and incubated in a humidified chamber for 30min at room temperature. The chamber was covered with aluminium foil to protect from light. The sections were rinsed in PBS 4 times for 2min, counterstained with Hoescht 33342 (Invitrogen) and mounted with Hydromount (National Diagnostics) under glass coverslips. The slides were stored at 4°C. Pictures were taken with a DM6000B microscope equipped with CFC350FX camera and LAS AF6000 software under DAPI and fluorescein filters (Leica, Germany).

2.15 Mitochondrial membrane potential measurement

Membrane potential was measured in isolated mitochondria by JC-1 staining and analysis of JC-1 dye fluorescence at 595nm in an F-4500 fluorescence spectrophotometer (Hitachi High-Technologies, Tokyo, Japan). The excitation wavelength was set at 490nm. Assay was performed in a quartz cuvette with a 10mm optical pathway. 50μg of mitochondrial proteins suspended in a Storage Buffer (Sigma) were added to 1.9ml JC-1 Assay Buffer (Sigma) to total volume of 2ml. After addition of 2μl JC-1 Stain (Sigma), the sample was mixed by inversion and left at room temperature in the dark (covered with aluminium foil) for 7min to allow complete uptake of JC-1 dye into the mitochondria. The blank fluorescence measured in a cuvette with Assay Buffer lacking mitochondrial fraction was subtracted from the fluorescence of each sample.

2.16 Isolation of mouse embryonic fibroblasts (MEFs)

Two pregnant females were sacrificed at day 13.5 post coitum (assuming 0.5 day is the first day the plug is observed) by cervical dislocation and uterine horns were placed in DMEM (Dulbecco's modified Eagle's medium; Invitrogen) on ice. Each embryo was

placed into a petri dish containing PBS, and then separated from the placenta and surrounding membranes using a Leica MZ10F dissecting microscope (Leica, Germany). Tissue (head) was collected for *Opa1* genotyping and internal organs were cut away. The embryonic tissue was minced with a sterile razor blade in minimal amount of DMEM followed by 10min incubation in 0.25% trypsin/EDTA (Invitrogen) in a waterbath at 37°C. After neutralization of trypsin by suspension of cells in DMEM supplemented with 10% fetal bovine serum (FBS; Biosera, UK) the cells were transferred to T75 flasks (Triple Red, UK) with 15ml DMEM with 10% FBS and Antibiotic-Antimycotic solution (Invitrogen) and left for two days to attach to the dish.

2.17 Mitochondrial staining with Mitotracker

MEFs were grown on coverslips (Agar Scientific) in a 24-well plate (Triple Red, UK) in DMEM medium with 10% FBS. The DMEM medium was then removed and replaced by a medium containing 150nM Mitotracker Red (Mitotracker Red CMX-Ros; Molecular Probes) and 5μg/ml Hoescht 33342 (Invitrogen). After 30min incubation at 37°C, the cells were fixed at 4% paraformaldehyde (Sigma) in PBS for 15min at 37°C, rinsed in D-PBS (Dulbecco's phosphate-buffered saline; Invitrogen) three times and incubated in 0.1% Triton X-100 in PBS for 5min at room temperature. After three washes in D-PBS for 5min cells were mounted in non-fluorescing hydromount (National Diagnostics, UK). Pictures were taken with a DM6000B microscope equipped with CFC350FX camera and LAS AF6000 software under rhodopsin and DAPI filters (Leica, Germany).

2.18 Mitochondrial morphometry

Morphometric evaluations were performed using ImageJ (freely available image processing program, http://rsb.info.nih.gov/ij). The scale was calculated and the length of mitochondrial particles (perimeter) was measured manually according to the scale: 1μm=10.8 pixels. At least 25-50 measurements in each cell were recorded. Based on the obtained results mitochondrial morphology was classified into three categories: tubular, intermediate, fragmented and each cell was assigned to one of these categories.

2.19 Assessment of cell proliferation

MEFs were cultured in DMEM with 10% FBS in 6-well plates. MEFs were seeded at the density ~ $2x10^5$ cells in each well. Every third day MEFs were collected by trypsinization and counted in a haemocytometer. Counting was carried out on two wells from each

culture. Afterwards cells were seeded at the same density ~ $2x10^5$. Population doubling (PD) was calculated according to the equation: PD= (logY- logX)/log2, Y=final cell count, X= inoculation cell count.

2.20 Light treatment protocol

MEFs were seeded onto a 96-well plate at the density ~ $2x10^4$ cells in each well and incubated at 37°C. Before the day of the experiment the medium was replaced with the fresh DMEM with 2% FBS. Next day cells were exposed to the blue-filtered light (Lee filters) in SF10PF medium (a modified Ham's F10 without photosensitizers, such as phenol red, tryptophan, tyrosine, riboflavin, and folic acid; Schütt et al., 2000, Appendix 1) for max. 24 hours at the irradiance of 2.3 mW/cm^2. Fig.2.2 presents the spectrum of the light used. The temperature was maintained at 30°C. For control the plate was protected from light by wrapping it with black paper.

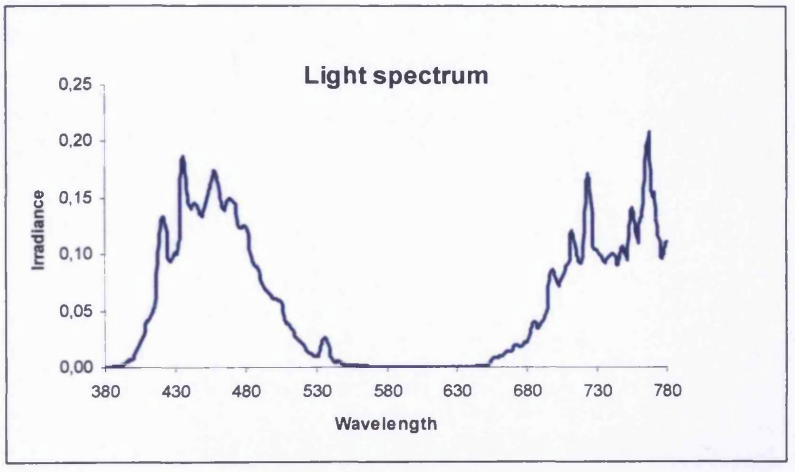

Fig.2.2 The spectrum of light used for irradiation of MEFs

After irradiation the cells were washed twice in D-PBS followed by a survival test (MTT assay, see 2.22) in DMEM supplemented with 10% FBS.

2.21 Hydrogen peroxide (H_2O_2) treatment protocol

MEFs were treated with one single dose of H_2O_2. MEFs cultured in DMEM with 2% FBS overnight in 96-well plates were rinsed once with D-PBS and treated with different concentrations of H_2O_2 in DMEM: 0.1, 0.2, 0.5, 0.8, 1mM for 1 and 2hr. For the control, cells were incubated with DMEM without H_2O_2. Afterwards the cells were rinsed twice in

D-PBS and DMEM with 10% FBS was added to each well. Cell viability was measured in MTT assay (2.22).

2.22 Measurement of cellular viability

MEFs were subjected to the appropriate treatments (2.20 and 2.21) in 96-well plates and then MTT (Thiazolyl Blue Tetrazolium Bromide; Sigma) was added to the wells at a final concentration of 1mg/ml for 2.5 hours at 37°C. Afterwards the medium was removed and reduced MTT was solubilized by adding 100µl of acidified (0.06N HCl) isopropanol. Absorbance was measured at 590nm and 690 nm (reference wavelength) on the 96-well plate reader (BioTek Instruments, US).

3. BREEDING STRATEGY & GENOTYPING OF *OPA1* +/- MOUSE MODEL

3. BREEDING STRATEGY AND GENOTYPING OF *OPA1* +/- MOUSE MODEL

3.1 Introduction

An *Opa1* mouse model for Autosomal Dominant Optic Atrophy has been generated by ENU-mutagenesis (see 1.4.2). The putative disease-causing nonsense mutation in exon 8 coding for a C to T transition at 1051bp of *Opa1* gene was predicted to cause protein truncation (Gln285 to Stop: Q285X).

All animals in the colony were bred on a mixed C57BL/C3H background (F1) and the experiments were performed on mice bred at generations F2 to F5 (Materials and Methods 2.1). The paternal line C3H/HeJ is homozygous for the retinal degeneration 1 mutation (*rd1*) in the phosphodiesterase 6B gene ($Pde6b^{rd1}$, ID: MGI: 1856373 Mouse Genome Informatics). This mutation causes blindness by weaning age and was gradually removed from animals by crossing them with the C57BL strain, genotyping for *rd1* and only breeding selectively to eliminate the mutant *rd* allele. Thus none of our experimental animals were affected by retinal degeneration.

C57BL/6J is the most widely used inbred strain and was used for outcrossing in our line. During the course of this work it was found that this strain has a spontaneous deletion in nicotinamide nucleotide transhydrogenase gene ($Nnt^{C57BL/6J}$, ID: MGI: 3626282 Mouse Genome Informatics), which causes glucose intolerance and impaired insulin secretion (Toye et al., 2005). This strain was used for outcrossing with the C3H strain and producing consecutive generations of *Opa1* mice on an increasing C57BL background.
The number of animals maintained in the *Opa1* colony was approximately 100-150 at any one time. Animals were on a normal controlled 12hr-12hr light-dark cycle. 3-4 week old animals were weaned and genotyped (Materials and Methods 2.2).

The objective of this Chapter is to present two strategies that were used for *Opa1* mice genotyping and the method for breeding out an unwanted mutation in the *Nnt* gene, which was inherited from C57BL/6J strain.

3.2 Genotyping of *Opa1* +/- mouse by allele-specific PCR

3.2.1 Allele-specific PCR amplification of DNA samples

This method was the primary method for *Opa1* genotyping. Details about DNA extraction, primers sequences and PCR conditions are described in Materials and Methods 2.2; 2.3.1.

The method required two separate reactions to be carried out with two sets of primers. The forward primer was identical for both reactions amplifying wild-type and mutant allele. Reverse primers were designed to bind specifically to a sequence with or without mutation to allow amplification of mutant and wild-type alleles respectively in separate reactions. The product size did not vary from wild type allele to mutant allele. Fig. 3.1 presents a 2% agarose gel of PCR-amplified *Opa1* gene fragments 150bp long. Top row: mutant allele, bottom row: WT allele. Samples that were run from top and bottom wells in the same line represent one animal. Samples 2, 3, 8, 11, 12 are wild type *Opa1* mice because in these samples the mutant allele was not PCR-amplified.

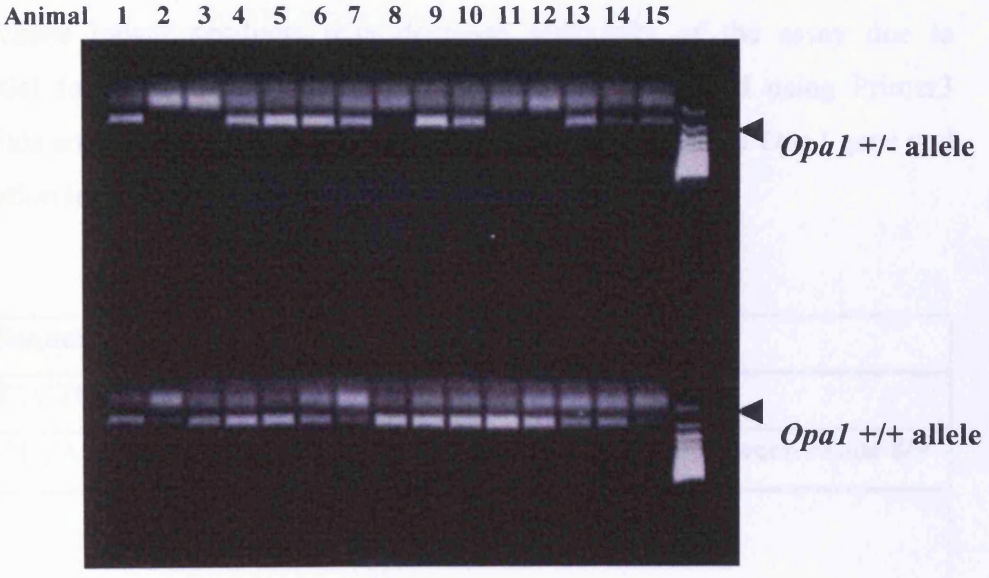

Fig.3.1 *Opa1* mouse model genotyping by allele-specific PCR.

PCR amplification of DNA samples was followed by 2% agarose gel electrophoresis. 12µl of PCR products were usually loaded onto gel wells. DNA samples were labelled

with Ethidium Bromide, which was added to the agarose gel before electrophoresis (Materials and Methods 2.4). Fluorescence of the samples was observed under UV light.

3.3 Designing of a new method for *Opa1* genotyping

3.3.1 High Resolution Melt Analysis- Introduction

A new protocol was designed for *Opa1* mouse genotyping based on High Resolution Melt (HRM) Analysis performed on a Rotor-Gene™ 6000 instrument (Corbett Research).

High Resolution Melt is a post-PCR analysis that can be used to differentiate between different PCR sequences due to their different thermal denaturation properties. Mutations are detected as either a shift in the melting temperature (T_m) or a change in the shape of the melting curve measured as a change in the level of fluorescence of DNA intercalating dye. For DNA genotyping, first DNA is amplified by PCR followed by denaturation of DNA duplex during HRM programme and data analysis.

3.3.2 Primers design

The assay design criteria found in the High Resolution Melt Assay Design and Analysis booklet (Corbett Research) recommended using primers that will amplify short products (100-250bp) because longer products may decrease sensitivity of the assay due to increased potential for multiple melt domains. Primers were designed using Primer3 software (Materials and Methods 2.6). They amplified 100bp fragment of *Opa1* gene and flanked the mutation inserted into this gene (Table 3.1)

Primer	Sequence	Location
forward	TTCTGAAGTTCTTGATGTTCTTTCTG	Exon 8
reverse	CTGACAGCAGGTCCTGGTCTAT	Intron between exons 8/9

PCR amplified *OPA1* fragment

5′ **TTCTGAAGTTCTTGATGTTCTTTCTG**ATTATGATGCCAGTTACAAT
ACA**C/T**AAGATCACCTACCACGGGTAAGGGGAAA**ATAGACCAGGACCTGCTGTCAG** 3′

Table 3.1 Primer sequences and *Opa1* fragment amplified in PCR reaction.
Primers (red) amplified 100bp fragment which flanked *Opa1* mutation (blue)

3.3.3 PCR and HRM protocol

High Resolution Melt Analysis (HRM) was performed using Corbett Research Instrument and Rotor-Gene 6000 Series Software. The reaction mix was prepared as shown in Table 3.2.

Reaction mix per 25 µl	
dH_2O	15.1 µl
10x PCR buffer (Qiagen)	2.5 µl
10mM dNTP mix	2 µl
4µM F Opa1 100bp	1.7 µl
4µM R Opa1 100bp	1.7 µl
50 µM SYTO dye (Invitrogen)	0.75 µl
Hot Star Taq 5U/µl (Qiagen)	0.25 µl

Table 3.2 Reaction mix for *OPA1* genotyping by High Resolution Melt Analysis.
The reaction mix was prepared for n samples and a 1µl mouse genomic DNA template was added to each tube to the final volume 25µl.

Genomic DNA template was obtained either from mouse tail or from embryonic tissue at E13.5 (Materials and Methods 2.2) and 1µl was taken to the reaction. The reaction was run in a 96-well carousel in 0.1 ml tubes. Total volume for each sample was 25µl. Each run had a control sample without DNA template and positive control samples from *Opa1* +/+ and *Opa1* +/- animals. For PCR amplification primers were used at the concentration of 270nM, Taq polymerase at 0.05 U/µl and SYTO dye at the concentration 1.5µM, which intercalated into DNA at the saturating level.
DNA samples were PCR amplified in 40 cycles followed by HRM. HRM was performed at a of 70-90°C. Denaturation was monitored every 0.1°C as progressive decrease in fluorescence caused by the release of SYTO dye from unfolding DNA double helix. Table 3.3 presents setup for PCR and HRM reactions.

Condition		Temperature	Time
Hold		95°C	15min
Cycling (40cycles)	Denaturation	95°C	15s
	Annealling	57°C	30s
	Extension	72°C	30s
HRM		70-90°C rising by 0.1°C each step	

Table 3.3 Setup for PCR & HRM protocol for *OPA1* genotyping using Corbett Research–Rotor Gene 6000.

3.3.4 Data analysis

Data analysis was performed using the Rotor-Gene™ 6000 instrument HRM Software. The raw melting curves were fluorescence-normalized so that all curves had the same starting and ending fluorescent signal level. Results show two different denaturation curves of *Opa1* DNA fragments obtained from *Opa1* +/+ (red) and *Opa1* +/- animals (blue) (Fig.3.2). The results were confirmed by allele-specific PCR method (Fig.3.3).

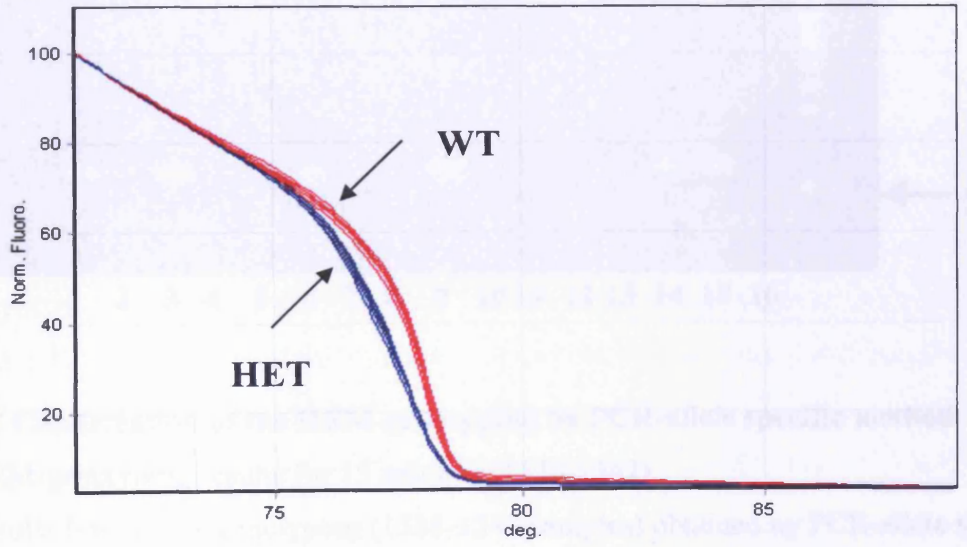

Fig.3.2 Genotyping results obtained by High Resolution Melt Analysis. Results from HRM genotyping for *Opa1* +/+ (WT) and *Opa1* +/- (HET) animals. The graph shows results from the genotyping of 15 animals (DNA samples: 1528-1542).

A)

No.	Sample (colour on HRM)	Genotype	No.	Sample (colour on HRM)	Genotype
1	**1528**	HET	9	**1536**	HET
2	**1529**	WT	10	**1537**	WT
3	**1530**	HET	11	**1538**	WT
4	**1531**	WT	12	**1539**	WT
5	**1532**	WT	13	**1540**	WT
6	**1533**	HET	14	**1541**	HET
7	**1534**	WT	15	**1542**	HET
8	**1535**	WT	16	No template control	

B)

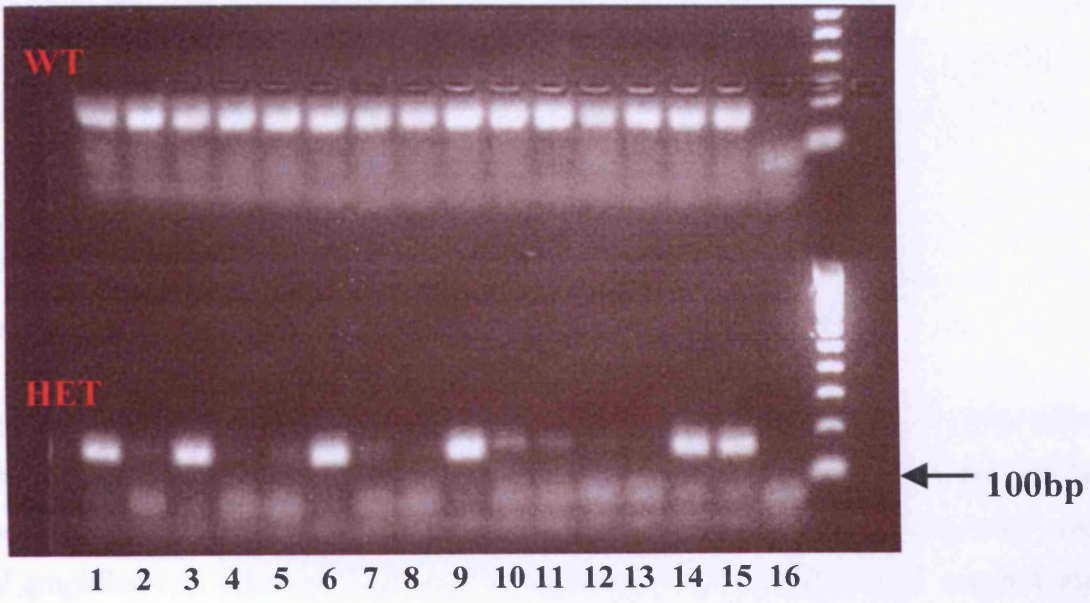

Fig.3.3 Confirmation of the HRM genotyping by PCR-allele specific method

A). HRM-genotyping results for 15 animals (1528-1542).

B). Results from *Opa1* genotyping (1528-1542 samples) obtained by PCR-allele specific method (Materials and Methods 2.3.1; Chapter 3.2). WT (top row) and mutant (bottom row) gene fragments 150bp long were stained with Ethidium Bromide on 2% agarose gel. The arrow shows the 100bp band in the ladder.

3.4 Inheritance of *Nnt* mutation from C57BL mouse and breeding out the mutation in *Opa1* mouse

Nicotinamide nucleotide transhydrogenase (*NNT*) is a nuclear-encoded mitochondrial inner membrane protein involved in detoxification of reactive oxygen species (ROS), couples the generation of NADPH to proton transport and provides NADPH for the regeneration of two important antioxidant compounds, glutathione and thioredoxin, in the mitochondria (Huang TT et al., 2006). Mutation in the *Nnt* gene has been reported in inbred C57BL/6J mice and underlies the glucose intolerance and impaired β cell function (JAX® Mice Database, Stock Number 000664, Jackson Laboratory). Mutation causes deletion of 17,814 bp region between exons 6 and 12 which results in missing of exons 7-11 in *Nnt* transcript. Mature protein is not detected in these mutants (Huang TT et al., 2006).

Opa1 mice inherited the *Nnt* mutant allele from some C57BL/6J animals – the parental inbred strain that was consecutively used for backcrossing. The *Nnt* allele was identified in *Opa1* animals of the generation F5 but all generations F1-F5 had to be genotyped because it was not possible to find out which of the C57BL/6J animals used for mating were *Nnt* deficient. Because of the role of Nnt in mitochondria there was a possibility that Nnt may be a genetic modifier that is capable of modulating the degree of potential mitochondrial changes caused by the Opa1 deficiency. Genotyping for *Nnt* allowed us to select *Nnt* mutation-free mice and breed them for the experiments.

The genotyping strategy consisted of three separate PCR reactions. PCR products were separated by 2% agarose gel electrophoresis (Materials and Methods 2.4). Sequences of the primers were already published (Materials and Methods 2.3.2). Primers *Nnt7* and *Nnt11* amplified two different fragments 250bp long in exon7 and exon11 respectively which were deleted in *Nnt* mutants. (Fig.3.4) These PCRs could select *Nnt* -/- mutants. Primers: Exon6L4 and Exon12L1 bound to DNA sequences that flank the deleted *NNT* region at opposite ends and produced 547bp fragment only in *Nnt* mutants. There were no products in animals with two wild type *Nnt* alleles (Fig 3.5).

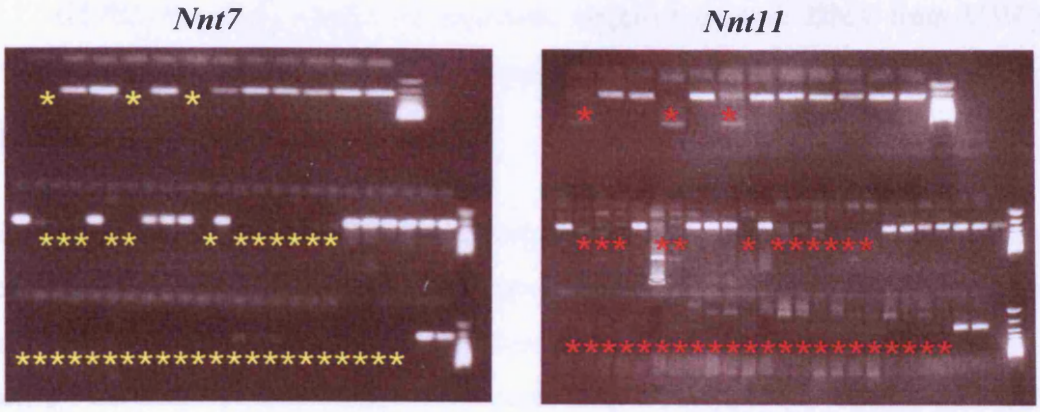

Fig.3.4 Results of *Nnt* genotyping of 60 *Opa1* mice by both *Nnt7* and *Nnt11* primers. PCR products were separated by 2% agarose gel electrophoresis and stained with Ethidium Bromide. Lack of products (labelled by *) selected *Nnt* -/- animals.

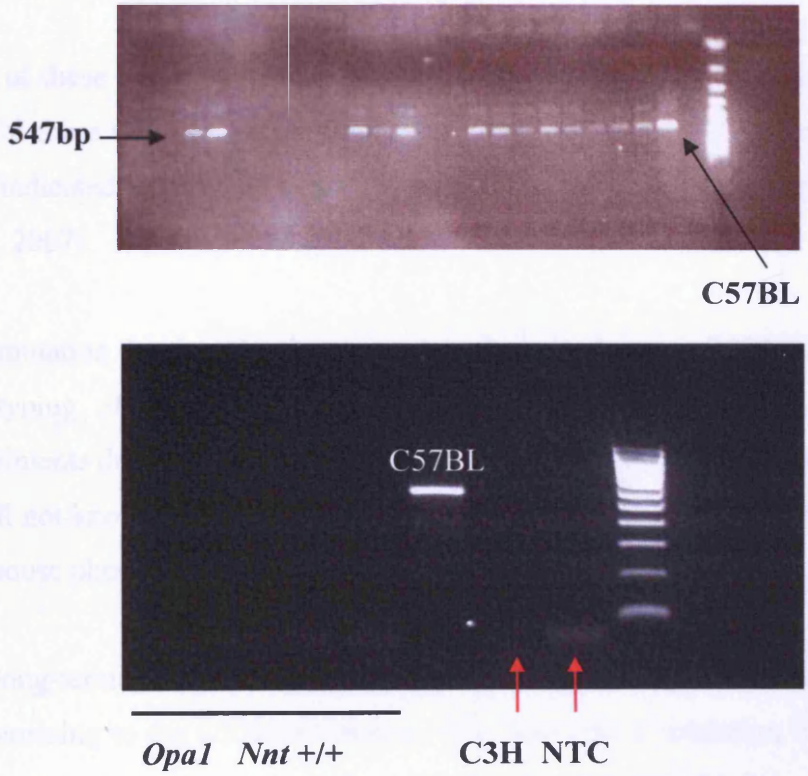

Fig.3.5 Results of *Nnt* genotyping by PCR with 6L4 and 12L1 primers.

A.) The presence of 547bp bands on 2% agarose gel reveals mutation in at least one *Nnt* allele in *Opa1* animals. No products indicated their *Nnt* +/+ status.

B.) Confirmation of *Nnt* +/+ genotype of 4 opa1 animals from different litters after selection of *Nnt*+/+ females and males for breeding. Positive control: DNA from a

C57BL/6J mouse with *Nnt* mutation, negative control: DNA from C3H mouse without *Nnt* mutation, NTC: no template control

3.5 Discussion

One of the aims of this chapter was to present two strategies used for genotyping *Opa1* mice. There is no doubt that the genotyping procedure needed to be reliable because it was the key to the interpretation of a *Opa1* mouse model. Both methods (the allele-specific PCR and HRM analysis) were interchangeable. HRM is a faster method and as opposed to the allele-specific PCR method HRM analysis did not need two primers sets for the assay. One reaction for each sample was carried out to obtain genotyping results. HRM analysis used real-time PCR amplification of DNA samples. This allowed for the estimation of the quality of DNA templates taken to the reaction and prevented the inclusion of false results.

Both of these two methods were applied for genotyping adult mice and embryos at 13.5 dpc. In these two groups the homozygous mutant *Opa1* -/- genotype was not observed. This indicated lethality of *Opa1* -/- embryos at the earlier stages of development (Davies et al., 2007).

Nnt mutation in the *Opa1* colony was inherited from C57Bl/6J parental strain. *Nnt* genotyping of the whole *Opa1* colony had some impact on the progress of the experiments due to the priority need to first select animals that were *Nnt* mutation-free. It is still not known if this mutation (especially when homozygous) could modify the *Opa1* +/- mouse phenotype, for example, the sensitivity to oxidative stress.

The long-term aim associated with *Opa1* mouse breeding is to develop a congenic line by backcrossing to the C57Bl/6J mouse. This will take a minimum of 10 generations (~2.5 years). So far, during this study, animals of generation F5 have been bred, which are estimated to be approximately 94% congenic. The production of a congenic line may significantly influence the *Opa1* mouse phenotype. It may smooth out the variability between animals and make the expression of the *Opa1* mutation more obvious: the phenotype may become more or less severe.

4. ANALYSIS OF MOUSE *OPA1* TRANSCRIPTS

4. ANALYSIS OF MOUSE *OPA1* TRANSCRIPTS

4.1 Introduction

The human *OPA1* gene is composed of 31 exons of which 3 exons: 4, 4b and 5b are involved in alternative splicing. Alternative splicing results in the formation of 8 different *OPA1* mRNA isoforms, which are ubiquitously expressed and show levels of expression specific to different tissues (Delletre et al., 2001; Olichon et al., 2007a; Introduction 1.1.4.1) Interestingly, only one mutation has been reported so far in *OPA1* alternative exons and this mutation is associated with partial recovery of visual loss (Cornille at al., 2008; Introduction 1.1.2).

The aim of this chapter was to characterize *Opa1* transcription and alternative splicing in the mouse. The transcript profile was compared between retina and other tissues and was studied in the *Opa1* heterozygous mutant and WT mice. Different *Opa1* splice variants were amplified by RT-PCR using 3 primer pairs and their relative abundance in the retina was shown.

4.2 Characterization of mouse *OPA1* mRNA isoforms

Mouse *Opa1* mRNA isoforms were studied by RT-PCR. RNA was isolated from *Opa1* +/+ and *Opa1* +/- mouse tissues (retina, kidney, liver and spleen) and subjected to RT-PCR (Materials and Methods 2.8.2). PCR products were separated by electrophoresis on 3.0-3.5% ethidium bromide stained agarose gel (Materials and Methods 2.4).

4.2.1 Primers design

To identify splice variants expressed in mouse tissues 3 different primer pairs were designed to full mouse *OPA1* transcript (*mOPA1*) (Materials and Methods 2.6). The m*Opa1* transcript variant containing 5b exon was taken from the Ensembl database (http://www.ensembl.org/Mus_musculus) Gene: Opa1 (ENSMUSG00000038084). To identify exon 4b encoded by m*Opa1*, human exon 4b was aligned to the genomic sequence of the m*Opa1* gene and a BLAST search was used to confirm the presence of

this sequence in the mouse cDNA library. Fig. 4.1 shows the primer sequences and their location in *mOpa1* transcript (exons 1-9 are shown). The forward primer was identical for all three pairs.

Primer pair		Sequence (5'-3')	Location
3F/8R	forward	AAGTGGATTGTGCCTGACTTT	exon 3
	reverse	CAACCCGTGGTAGGTGATCT	exon 8/9
3F/5R	forward	AAGTGGATTGTGCCTGACTTT	exon 3
	reverse	GCTCGAAATGCTGTTTCTCC	exon 5
3F/5bR	forward	AAGTGGATTGTGCCTGACTTT	exon 3
	reverse	GCTTCTGTTGGGCATAGCTC	exon 5b

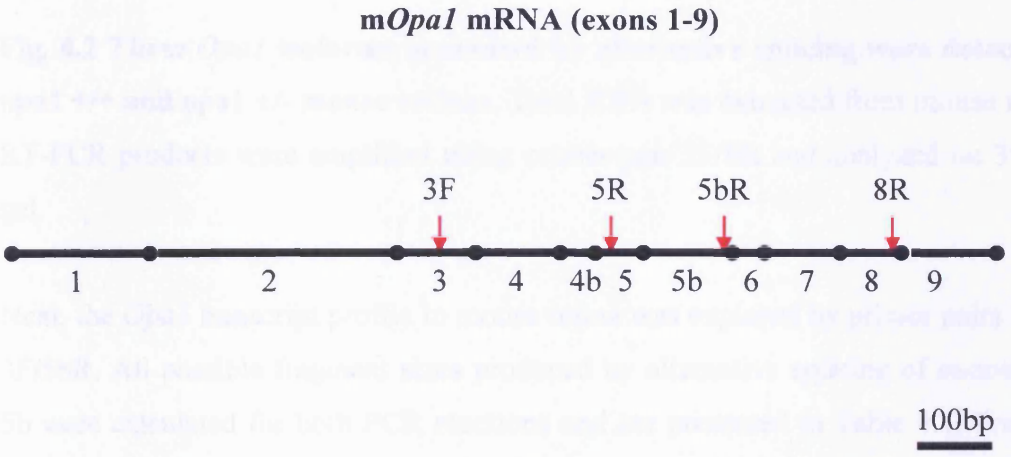

Fig. 4.1 Primer sequences for m*Opa1* transcript and schematic representation of an *Opa1* mRNA fragment (1-9 exons) with marked primer binding sites (arrows). Numbers below represent exons.

4.2.2 Identification of m*Opa1* splicing variants in the retina

RT-PCR with a primer pair 3F/8R resulted in an amplification of 3 *Opa1* fragments from retinal *Opa1* +/+ and *Opa1* +/- mouse samples. These fragments were postulated to be isoform 1 (478bp), isoform 7 (589bp) and isoform 8 (643bp), as described by Delettre et al (2001). Fig.4.2 depicts the relative abundance of these isoforms detected by ethidium bromide staining in a 3% agarose gel. Isoform 1 (without exons 4b and 5b) predominated. The longest isoform 8 was the full transcript containing all alternative exons: 4, 4b and 5b. Isoform 7 was also detected corresponding to the fragment at the position of 589bp.

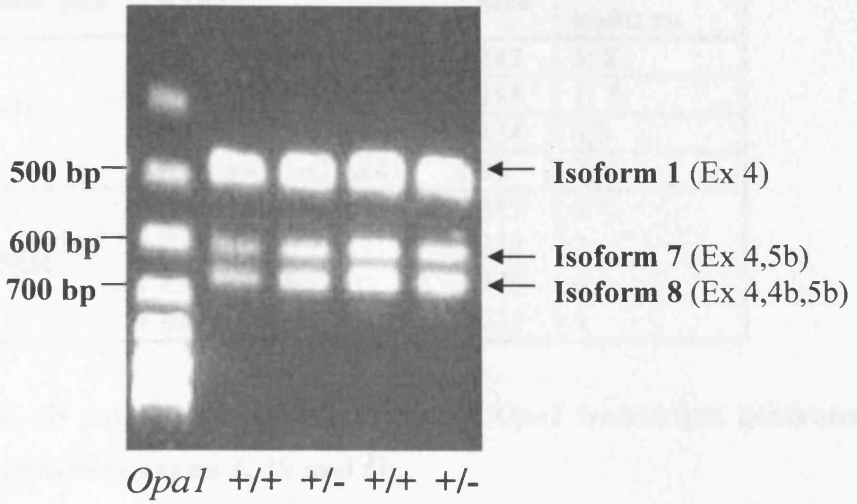

Fig. 4.2 Three *Opa1* isoforms generated by alternative splicing were detected in the opa1 +/+ and opa1 +/- mouse retinas. Total RNA was extracted from mouse retinas and RT-PCR products were amplified using primer pair 3F/8R and analyzed on 3% agarose gel.

Next, the *Opa1* transcript profile in mouse retina was explored by primer pairs 3F/5R and 3F/5bR. All possible fragment sizes produced by alternative splicing of exons 4, 4b and 5b were calculated for both PCR reactions and are presented in Table 4.1. Fragments of isoforms which did not contain exon 4 (279bp, 225bp, 134bp, 80bp) were not detected by RT-PCR and ethidium bromide staining in agarose gel (Fig. 4.3). In addition, the primer pair 3F/5R did not amplify an isoform containing exons 4 and 4b. With the primer pair 3F/5bR it was possible to produce one band corresponding to the fragment of isoform 7 (Ex4+Ex5b) or isoform 8 (Ex4+Ex4b+Ex5b).

Primer pair	Exons	Size	Possible isoforms
3F/5R	Ex4+Ex4b	242	5; 8
	Ex4	188	1; 7
	Ex4b	134	3;6
	No Ex4b and Ex4	80	2;4
3F/5bR	Ex4+Ex4b+Ex5b	387	8
	Ex4+Ex5b	333	7
	Ex4b+Ex5b	279	6
	Ex5b	225	4

Table 4.1 Sizes of all possible fragments of mouse *Opa1* transcripts generated by alternative splicing between exon 4, 4b and 5b.

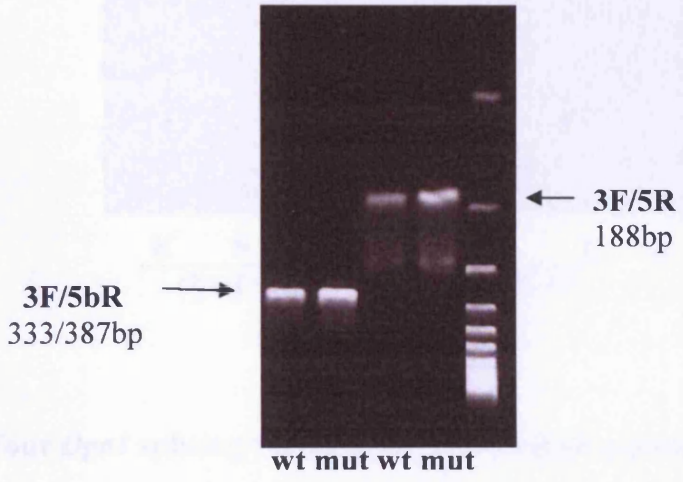

Fig.4.3. *Opa1* isoforms lacking exon 4 were not detected by RT-PCR in *Opa1* +/+ and *Opa1* +/- mouse retinas. Total RNA was extracted from mouse retinas and RT-PCR products amplified using primer pairs 3F/5R and 3F/5bR were analyzed on 3.5% agarose gel. Bands of the size 279bp, 225bp, 134bp and 80bp representing isoforms lacking exon 4 were not detected. Also a band at the position 242bp, being the fragment amplified with exons: Ex4 and Ex4b, was not detected.

4.2.3 Transcription of m*Opa1* in other mouse tissues

The *Opa1* transcript profile was compared between retina and three other mouse tissues (kidney, spleen and liver). RT-PCR with a primer pair 3F/8R resulted in the identification of three isoforms in the retinal samples. In other tissues one additional isoform (isoform 5: Ex4, 4b), which was not found in the retina, was also detected on Ethidium Bromide

stained 3.5% agarose gel as a band in length of 532bp (Fig.4.4). The results indicate tissue-specific regulation of *Opa1* transcription.

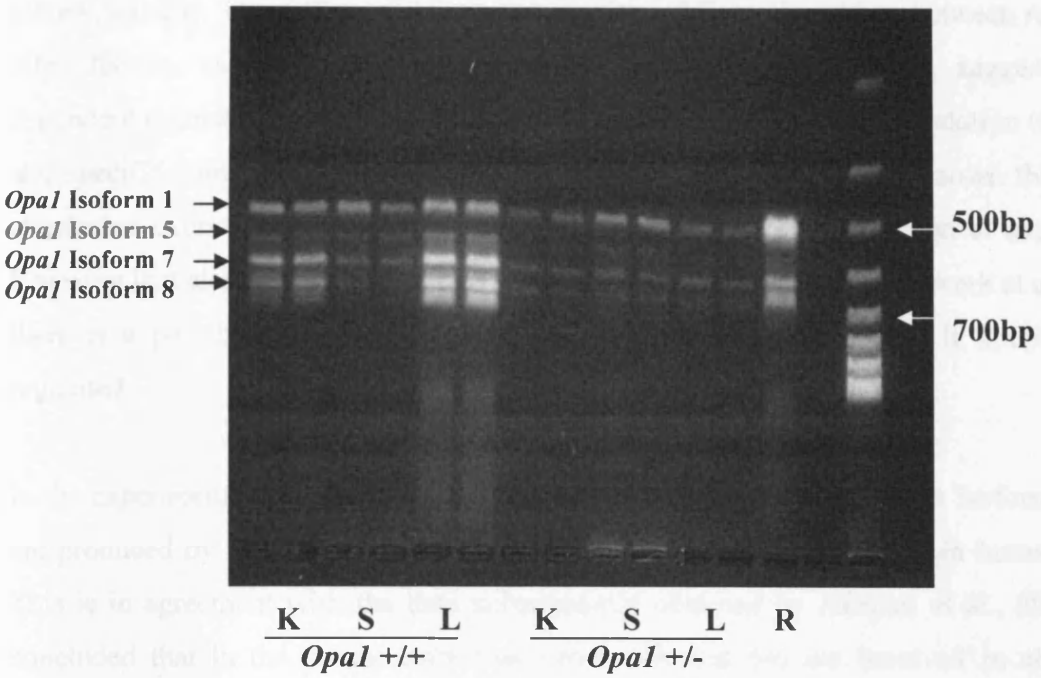

Fig. 4.4 Four *Opa1* splicing variants can be detected in mouse tissues.
RNA was isolated from kidney (K), spleen (S) and liver (L) of wild type and mutant mice at the age of 18 months. RT-PCR products amplified using primer pair 3F/8R were analyzed on 3.5% agarose gel. Samples were loaded in duplicate. R - *Opa1* isoforms from the retina of 6 month old opa1 heterozygote.

4.3 Discussion

This work studied *Opa1* transcription and alternative splicing in mouse tissues. In the retina of wild type and mutant mice three isoforms could be detected. The shortest isoform, which does not contain 4b and 5b alternative exons (isoform 1), is dominant, similarly to findings in the human retina (Delettre et al., 2001). Protein encoded by this variant was also found to be the most highly expressed isoform in the nervous tissue including retina (Akepati et al., 2008).

We believe that two other isoforms found in the retina are isoform 7 (Ex4, 5b) and isoform 8 (Ex4, Ex4b, Ex5b). Such a profile has also been reported in HELA cells by Satoh et al., 2003. In order to verify this result DNA could be analyzed by sequencing. The presence of additional isoform 5 (Ex4, 4b) was detected in other mouse tissues (liver, kidney, spleen). The differences in the expression of *Opa1* transcripts between retina and other tissues, especially the dominance of isoform 1 in the retina, suggest tissue-dependent regulation of *Opa1* transcription. This needs further study in relation to ADOA and specific vulnerability of RGCs in this disease. Furthermore it is known that *OPA1* alternative exons 4b and 5b are involved in apoptotic process (Olichon et al., 2007a). Knowing that alternative splicing can be modified during apoptosis (Schwerk et al., 2005) there is a possibility worth studying that *OPA1* alternative splicing is apoptotically-regulated.

In the experiments described in mouse tissues we were not able to detect isoforms which are produced by the alternative splicing of exon 4 and which are seen in human retina. This is in agreement with the data subsequently obtained by Akepati et al., 2008, who concluded that in the mouse only two exons (4b and 5b) are involved in alternative splicing. Interestingly, in invertebrates as in lower eukaryotes, no alternate splicing has been reported for *OPA1* orthologe genes (Olichon et al., 2007a). This is clearly an example of how the genome evolved with increasing complexity to ensure more sophisticated regulation of cellular processes.

Recently it has been shown that the majority of *OPA1* mutations that lead to a premature termination codon (PTC) results in reduction of *OPA1* transcript level in the cell by the mechanism known as nonsense-mediated mRNA decay (NMD) (Schimpf et al., 2008). NMD is the process triggered by ribosome to degrade aberrant mRNAs (Amrani et al., 2006). The *Opa1* mouse mutation causes the premature termination of translation (Introduction 1.4.2) and therefore it is likely to stimulate NMD pathway. Our qualitative RT-PCR analysis showed that the three *Opa1* isoforms found in wild type mouse retina were also expressed in mutant mice. Performing quantitative RT-PCR in the future would determine the level of their expression.

5. RETINAL DEGENERATION IN *OPA1* +/- MOUSE MODEL

5. RETINAL DEGENERATION IN *OPA1* +/- MOUSE MODEL

5.1 Introduction

The ADOA disease phenotype is characterized by RGC death and optic nerve degeneration (Johnston et al. 1979; Kjer et al., 1983; Introduction 1.1.1). Johnson et al. and Kjer et al. both reported that there was a significant reduction in RGCs in aged ADOA patients on retinal histology. In addition, we see evidence for RGC loss in patients with ADOA as evidenced by reduced PERG on electrophysiology (Berninger et al., 1991; Holder et al., 1998). The generation of *Opa1* mouse models allows the study of the mechanism of cell death in ADOA. At the young age of 6 months *Opa1* heterozygous mice do not lose cells in their retinal ganglion cell layer when assessed by counting nuclei in retinal sections (Davies et al., 2007; Introduction 1.4.2). However, in another *Opa1* mouse model with a splice site mutation that causes a skipping of exon 10 RGC loss has been observed and the cell loss was time-dependent. The experiments were done on whole mount retinal preparations with retrograde labelled RGCs from mice at the age of 2 to 13 months (Alavi et al., 2007; Introduction 1.4.3).

In this chapter RGC loss was studied in aging mice. RGCs were quantified in retinal sections from 24-month old heterozygous and WT mice. Additionally TUNEL assay was used to test whether an increase in apoptosis could be detected.

5.2 Quantification of RGCs and the retinal thickness in aged animals

Retinal cross sections of 24-month old *Opa1* +/+ and *Opa1* +/- mice (n=5) were mounted and stained with H&E (by Vanessa Davies). Counts of cells in retinal sections were carried out manually by counting all nuclei in the RGC layer (Materials and Methods 2.13). The results do not show a significant reduction in the number of cells in the RGC layer in mutant mice (Table 5.1). Overall retinal thickness was compared between wild type and heterozygote mice (n=5) in the same retinal cross sections with the measurements taken across the thickest region of the retina (Materials and Methods 2.13). No difference was found between the two genotypes (Table 5.1).

Genotype	mean of total score ± SEM	mean of retinal thickness ± SEM [μm]
Opa1 +/+	4831±552	277±26.4
Opa1 +/-	5513±664	287.6±14.9

Table 5.1 Mean total score of cell counts in RGC layers and retinal thickness of 24-month old opa1 +/+ and *Opa1* +/- mice. Data are presented as means of total score ±SEM of 5 animals for each genotype. The difference in the cell number and retinal thickness between groups was analyzed using unpaired Student's *t*-test and was not statistically significant.

However, there are a number of methodological problems with the original data set that may preclude further, meaningful and statistically significant analysis. Firstly, it needs to be emphasized that the raw data obtained showed a high distribution, which suggests that if there was any difference in the retinal thickness between wild type and mutant mice, it could be difficult to demonstrate. The most significant error in the measurements was derived from the comparison of the retinal thicknesses averaged from five different regions in each eye. This error is important due to the fact that the retinal thickness is not constant and varies with retinal eccentricity. Secondly, the eyes were fixed and embedded in a number of orientations, and hence sectioning is not consistently on the same axis. This makes comparison between eyes difficult. Thirdly, it is not possible to identify the optic nerve for orientation in the sections, to enable a positional 'like for like' approach.

Due to the lack of available animal resources the experiment could not be repeated with a new protocol. There are very few aged animals in the colony and it is not feasible to wait another 12 months for ageing of subjects. Were it to be possible, new histological sections of the retinas would be collected and equivalent sections of the retinas would be compared: all the eyes would be sectioned in the same plane and the retina would be measured in the same region marked by the presence of the optic nerve.

5.3 Apoptosis is not observed in the *Opa1* +/- RGC layer in old animals

Apoptosis was studied in the retinal sections of 24 month old animals (3 heterozygotes and 3 controls) by TUNEL assay (Materials and Methods 2.14). No TUNEL-positive cells were seen in the mutant RGC layers, or in the WT (Fig.5.1) but staining was observed in the positive control.

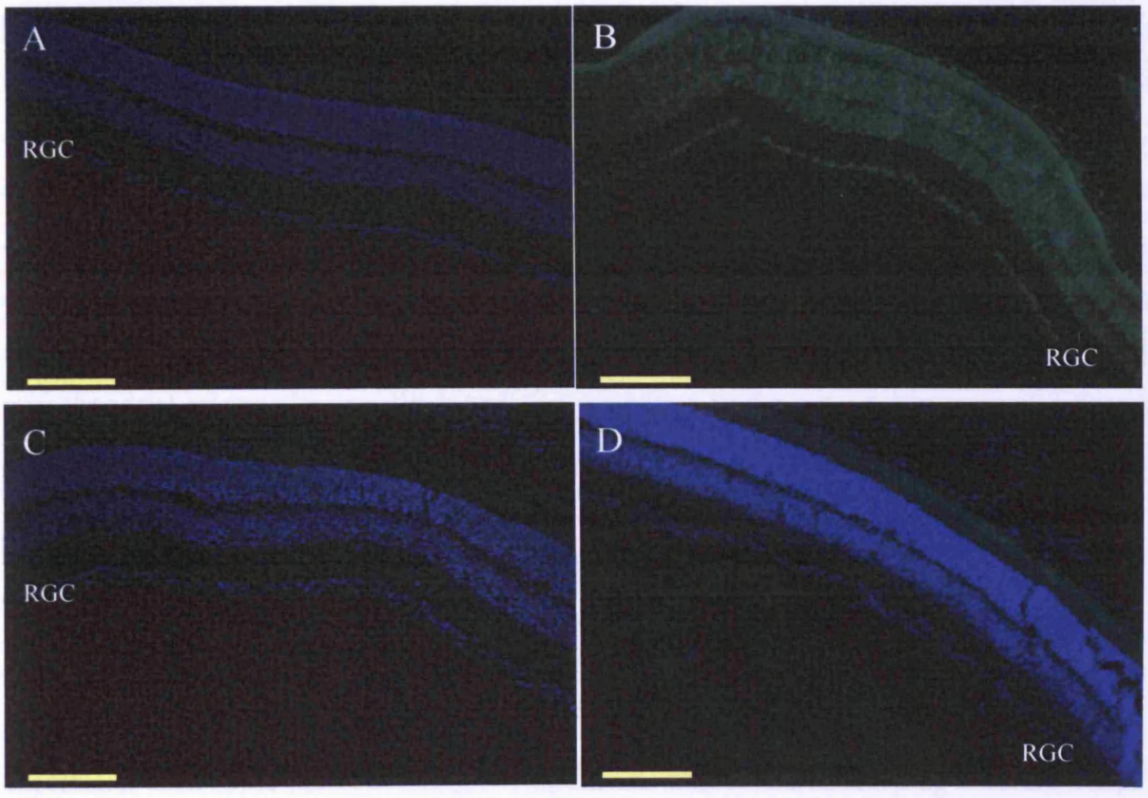

Fig.5.1 Representative retinal sections from 2 year old animals labelled for TUNEL

(A) Negative control sections without incubation with TdT enzyme

(B) Positive control section treated with DNase to induce DNA cleavage (for better presentation of fluorescein signal nuclei staining is omitted)

(C) Wild type and (D) mutant retinal sections demonstrate negative-labelling for TUNEL (fluorescein labelling) in the RGC layer (RGC). Nuclei were stained with Hoechst 33342. Pictures were taken with Leica DM6000B microscope equipped with CFC350FX camera and LAS AF6000 software under fluorescein and DAPI filters. Bar=100μm

5.4 Discussion

Degeneration in the *Opa1* +/- mouse model

In *Opa1* +/- aging mice we were unable to find an increased rate of cell death and detect apoptosis in the RGC layer. The images showed similar density of cells in the RGC layer in mutant and control mice and the number of cells counted was not significantly different. Although cell loss and active evidence of apoptosis was not detected other research using electron microscopy identified prominent degenerative changes in our mutant mouse line RGCs and optic nerves. In particular, an increased autophagy was observed in 24 month old mutant mice and it is postulated that it could be one mechanism contributing to RGC loss in ADOA (White et al., 2009). An increased autophagy in the *Opa1* mouse model could be primarily caused by impaired mitochondrial fusion, which could result in accumulation of defective mitochondria (Vicencio et al., 2008, White et al., 2009). Apart from the presence of more autophagosomes in mutant mice mitochondrial cristae abnormalities and demyelination of the optic nerve were also found (see also Introduction 1.4.2).

Mouse model of human disease

How well does the *Opa1* mouse model represent ADOA disease? The cell loss in the retinal ganglion cell layer, which is the major feature of ADOA disease, was not observed in mutant mice. However ADOA disease is characterized by its high variability of clinical expression with some patients being asymptomatic and others developing a severe visual impairment over time (Votruba et al., 2003). Performing the study on a larger number of mice could possibly reveal more affected animals.

There is evidence that visual function can be impaired in *Opa1* heterozygous mice (Davies et al., 2007). In the mutant *Opa1*+/- mice aged 12 months a significant reduction in OKN responses was reported suggesting that there must be some compromise to RGC or optic nerve functions. Furthermore it has been demonstrated with electron microscopy that morphological abnormalities were visible by 9 months of age in RGC axons and along the nerve fibre bundles in mutant mice (Davies et al., 2007). Therefore it is possible that we observe primarily axonal pathology occurring before RGC loss. A similar mechanism of degeneration has been also described in the DBA/2 mouse model of glaucoma (Buckingham et al., 2008).

A limitation of the current method was that the RGC count was performed on retinal sections. In addition to RGCs, the RGC layer is comprised of approximately equal numbers of displaced amacrine cells (Jeon et al., 1998). This made the observation of decrease in the number of RGCs alone difficult to detect. Supposing that the cell death proceeds in *Opa1* +/- mutant mice at the slow rate, it would still be very unlikely that we could capture some cells undergoing apoptosis at the same time in retinal sections. Therefore the fact that we could not see apoptosis does not argue against the possibility of the slow cell death. It is also important to bear in mind that mice lack macula, the area which is primarily affected in ADOA disease, and we do not know how this difference can be significant in our study.

To summarize retinal histological analysis in 24 month old mutant *Opa1* +/- mice did not show any significant reduction in the cell count in retinal sections. The process of RGC degeneration could be further studied using other techniques such as: optic nerve axon counts, quantification of immunolabelled (or retrograde labelled) RGC on whole mount retinas or the analysis of expression of RGC-specific genes.

6. OPA1 PROTEOLYSIS IN MITOCHONDRIA AND MITOCHONDRIAL MEMBRANE POTENTIAL IN *OPA1* +/- MOUSE MODEL

6. OPA1 PROTEOLYSIS IN MITOCHONDRIA AND MITOCHONDRIAL MEMBRANE POTENTIAL IN *OPA1* +/- MOUSE MODEL

6.1 Introduction

Although a role for OPA1 protein in mitochondria has been proposed (see Introduction 1.2.4-1.2.6) the pathological mechanism developing in ADOA disease is still unknown. Amongst possible causal factors considered are: bioenergetic failure, mitochondrial network and distribution abnormalities and increased apoptosis (Lodi et al., 2004; Amati-Bonneau et al., 2005; Spinazzi et al., 2008; Zanna et al., 2008).

In this chapter *Opa1* +/- mice have been used for the study of correlation between the level of Opa1 in the mitochondria and the polarization of the mitochondrial inner membrane. Many studies have highlighted the link between Opa1 function and the mitochondrial membrane potential. Firstly, Opa1 contributes to the formation of the mitochondrial network in a cell by controlling mitochondrial fusion, which strictly depends on the intact mitochondrial membrane potential (Meeusen et al., 2004). Secondly, Opa1 knockdown by siRNA has been shown to cause a dramatic drop in the mitochondrial membrane potential in cells (Olichon et al., 2002; Olichon et al., 2007a). Thirdly, Opa1 is known to be an antiapoptotic protein and the role of Opa1 protein in reducing the loss of mitochondrial membrane potential during apoptosis has been proposed (Frezza et al., 2006). Here, the experiment was performed to confirm a diminished mitochondrial level of Opa1 in *Opa1* +/- mutant mice followed by the measurement of an average mitochondrial membrane potential in the retina.

Human and mouse Opa1 protein exists in several isoforms of different length that have been categorized as long and short isoforms (Introduction 1.2.2). It has been demonstrated that dissipation of the mitochondrial membrane potential stimulates proteolysis of long isoforms culminating in the accumulation of short isoforms (Ishihara et al., 2006; Griparic et al., 2007; Guillery et al., 2008). Opa1 processing has been reported in some mitochondrial diseases and in mouse models where mitochondrial dysfunction has resulted in bioenergetic crisis (Duvezin-Caubet et al., 2006). To shed more light on mitochondrial dysfunction in ADOA disease Opa1 processing has been studied in *Opa1* +/- mice by analysis of the relative expression of long versus short Opa1 isoforms.

To summarise, these experiments centre on proteolysis of Opa1 in mitochondria and mitochondrial membrane potential and it is proposed that this can indirectly indicate a bioenergetic competence of mitochondria in heterozygous *Opa1* mice.

6.2 Opa1 deficient mouse (*Opa1* +/-) has a reduced level of Opa1 protein isoforms in mitochondria.

Comparison of Opa1 isoform expression in mitochondria of *Opa1* +/- mice to *Opa1* +/+ mice was made by western blot (Materials and Methods 2.12). Mitochondria were isolated from the retina and proximal part of the optic nerve of 9 animals of each genotype (Materials and Methods 2.9) and tissue samples from 3 animals were pooled. For data normalization cytochrome c was selected initially (6.2.1), but was later replaced by Hsp60 (6.2.2).

6.2.1 Western blot for cytochrome c on mitochondria isolated from mouse brain.

Originally for Opa1 quantification on the blot, cytochrome c was selected to control for variation in mitochondrial protein. The Western blot for cytochrome c was optimized on mitochondria isolated from brain tissue from two different *Opa1*+/+ mice and the representative blot from these two mitochondrial samples (mit1 and mit2 in Fig.6.1) shows bands specific to cytochrome c.

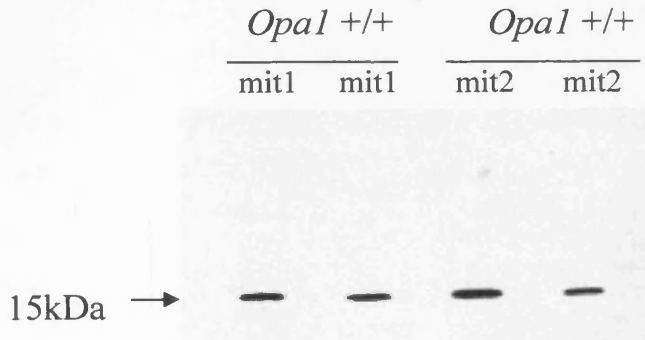

Fig.6.1 Western blot for cytochrome c (15kDa) on isolated mitochondria from brain. Mitochondria were isolated from *Opa1* +/+ mouse brain (Materials and Methods 2.9).

Fig.6.1 (continued) Mitochondrial proteins from two animals were loaded in duplicate onto SDS-polyacrylamide gel. SDS-PAGE electrophoresis was followed by blotting to nitrocellulose and cytochrome c antibody binding. The cytochrome c bands show the position of approximately 15kDa in the mitochondrial fraction.

Later cytochrome c was replaced by the mitochondrial molecular chaperone Hsp60 because of its larger molecular weight (~60kDa). In order to achieve better resolution of Opa1 various isoforms on the blot, SDS-polyacrylamide electrophoresis was extended until protein marker approximately 50kDa reached the bottom of the gel. Proteins of lower molecular weight including cytochrome c were lost from the gel.

6.2.2 Western blot for Opa1 on mitochondrial proteins from the retina and optic nerve. Calculation of relative expression of long versus short opa1 isoforms

Opa1 immunoblot revealed a reduction of Opa1 protein isoforms in mitochondria of *Opa1* +/- mice as compared to control group (*Opa1* +/+ mice) (Fig.6.2). This reduction was similar for both long and short isoforms, because the mean ratio: expression of long versus short isoforms was comparable in both genotypes (0.83 and 0.87 for *Opa1* +/+ and *Opa1* +/- respectively) (Fig.6.3).

The results showed that the mitochondrial Opa1 level was significantly reduced in *Opa1* +/- mice. However an increased proteolysis of long Opa1 isoforms, which could be triggered by the loss of mitochondrial membrane potential, was not observed in mutant mice.

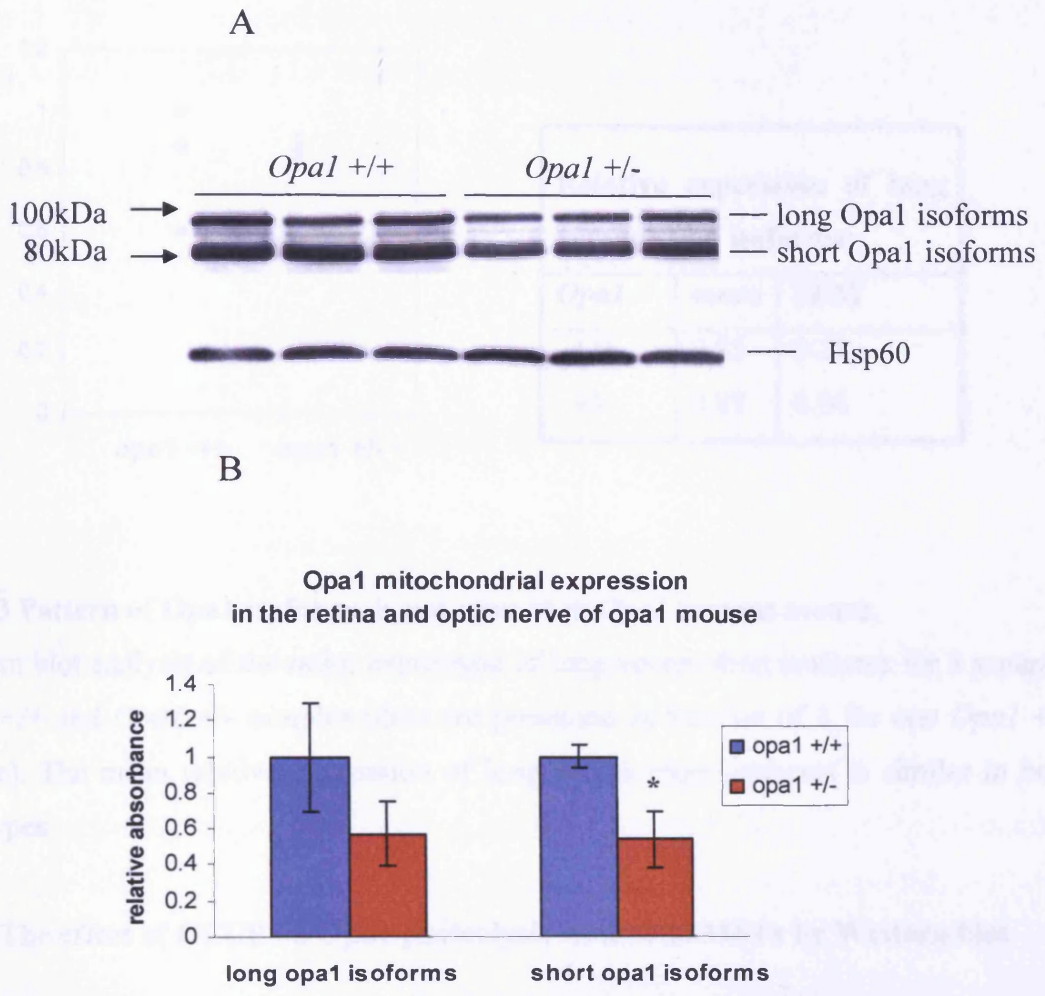

Fig.6.2 Western blot for Opa1 on isolated mitochondria from retina and proximal part of optic nerve.

A. Mitochondria were isolated from the retina and optic nerve of nine animals (3 animals per pool) and Western for Opa1 was performed. 20 μg of mitochondrial protein extract was separated in 8% SDS-PAGE followed by blotting to nitrocellulose and antibody binding. B. Opa1 expression in *Opa1* +/+ and *Opa1* +/- mice was measured by densitometry analysis of Opa1 bands. Opa1 band intensities were normalized to the Hsp60 signal from the same mitochondrial samples. The results are presented as mean ± SD of 3 independent samples and are expressed as fraction of the *Opa1* +/+ control.

Asterisk indicates statistical significance ($p < 0.05$) versus the respective *Opa1* +/+ group (two-tailed unpaired *t* test) obtained for short isoforms.

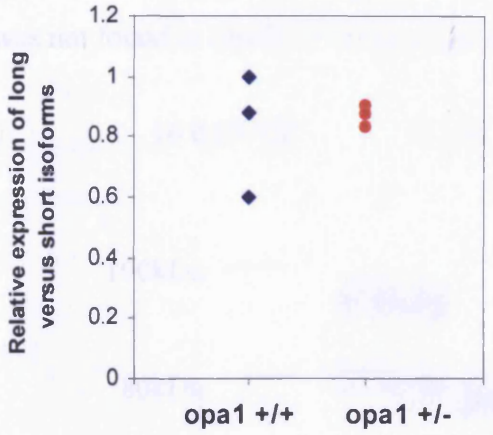

Relative expression of long versus short isoforms		
Opa1	**mean**	**SEM**
+/+	0.83	0.21
+/-	0.87	0.04

Fig.6.3 Pattern of Opa1 isoforms is not altered in *Opa1* mutant mouse.
Western blot analysis of the ratio: expression of long versus short isoforms for 3 separate *Opa1* +/+ and *Opa1* +/- samples (data are presented as fraction of 1 for one *Opa1* +/+ sample). The mean relative expression of long versus short isoforms is similar in both genotypes

6.2.3. The effect of CCCP on Opa1 proteolysis studied in MEFs by Western blot

To rule out the possibility that the lack of Opa1 proteolysis found in the mitochondria of mutant mice was due to the limitations of the method, Western blot was performed on MEFs isolated from *Opa1* +/+ 13.5 days post coitum (dpc) embryos (Materials and Methods 2.11) treated with carbonylcyanide *m*-chlorophenyl hydrazone (CCCP). CCCP is an uncoupling agent that disperses the mitochondrial membrane potential and has been recently shown to enhance the processing of Opa1, leading to the accumulation of short isoforms (Duvezin-Caubet et al., 2006; Ishihara et al., 2006). *Opa1* +/+ MEFs were treated with CCCP at two doses 10 and 20 μM for 16 hours and Western blot for Opa1 was performed on cells treated with CCCP and the control cells (not treated with CCCP) (Fig.6.4) (Materials and Methods 2.12). The blot showed the expression of five Opa1 isoforms in control cells. These isoforms are the products of translation of mRNA spliced isoforms and their posttranslational proteolytic processing at the S1 and S2 sites (Song et

al., 2007). The blot also shows CCCP-induced degradation of the long Opa1 isoforms (~100kDa MW) and accumulation of the short isoforms (~80kDa MW). Therefore, by using CCCP to induce dissipation of the mitochondrial membrane potential it was possible to observe Opa1 proteolysis on the immunoblot. The fact that Opa1 proteolysis was not found in *Opa1* +/- mice could not be to due to the limitations of the method.

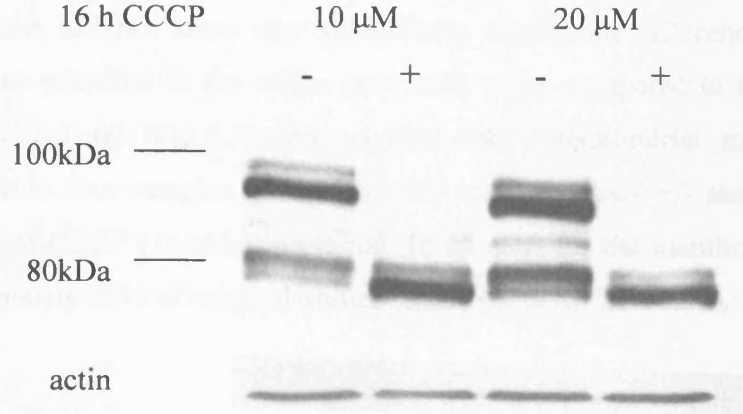

Fig.6.4 Western blot on *Opa1* +/+ MEFs showing accumulation of short Opa1 isoforms after 16 hours treatment with CCCP.

MEFs were treated with CCCP at concentrations of 10 and 20 μM for 16 hours. Both doses caused proteolysis of two Opa1 long isoforms that resulted in the lack of detectable Opa1 bands at the position of MW~100kDa. In the control samples five Opa1 isoforms including these degraded in CCCP-treated MEFs were observed. CCCP treatment in both doses induced the accumulation of the shortest isoforms at the position of MW~80kDa. Actin was used as a loading control.

6.3 Mitochondrial membrane potential in retina and brain of Opa1 +/- mouse is not changed

6.3.1 Δψ assessment in retina and brain using JC-1 dye

JC-1 fluorescence is sensitive to changes in mitochondrial membrane potential (Δψ).
In healthy polarized mitochondria the dye forms red fluorescent aggregates in mitochondria (fluorescence at 595nm), and the dissipation of membrane potential reduces red fluorescence proportionally to the change in (Δψ) (and increases green fluorescence of JC-1 monomers causing a shift in the emission spectrum from red to green colour).

To investigate if there is a difference in the average mitochondrial membrane potential between *Opa1* +/+ and *Opa1* +/- animals, mitochondria were isolated from retina and brain tissue (Materials and Methods 2.9) and membrane potential was assessed in isolated mitochondria by spectrofluorimeter analysis of JC-1 red fluorescence (Materials and Methods 2.15). The same concentration of mitochondria 25 μg/ml was used for the assay. The results did not show any statistically significant difference in *Opa1* +/- average membrane potential in the retina and brain when compared to *Opa1* +/+ mice ($p>0.05$, unpaired T-Test) (Fig.6.5). For control the mitochondrial membrane potential was measured in four samples (two *Opa1* +/+ and two *Opa1* +/- samples) two minutes after addition of CCCP (1nMMg^{-1}proteins). In all samples the membrane potential dropped to approximately 30% of original values (mean=33.875, SD=4.66).

A

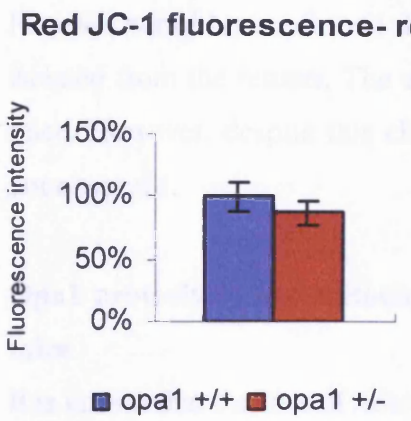

B

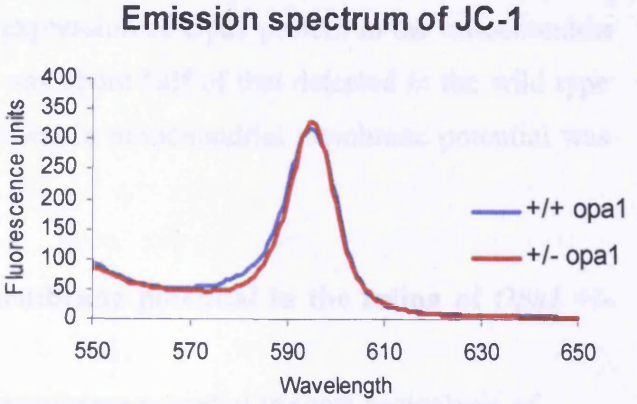

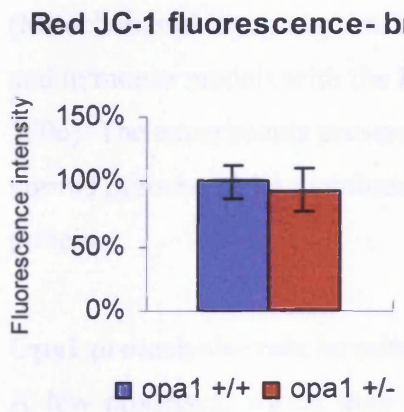

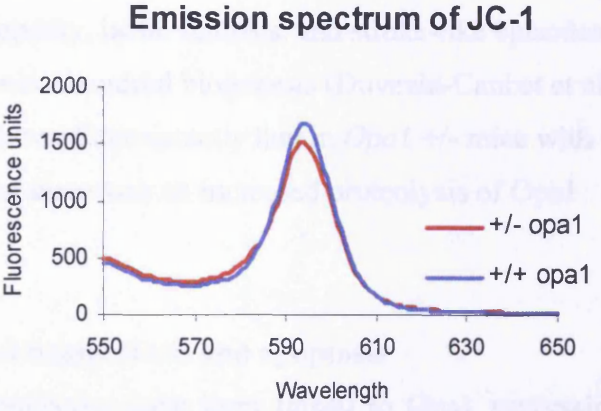

Fig.6.5 Mitochondrial membrane potential in the retina and brain of *Opa1* +/- mouse is not changed. (A) Mitochondria were isolated from the retina (n=3, 6 retinas per sample) and brain (n=3) of *Opa1* +/+ and *Opa1* +/- animals. Mitochondrial membrane potential was measured in *Opa1* +/+ and *Opa1* +/- samples by spectrofluorimeter analysis of JC-1 dye fluorescence at 595nm. The excitation wavelength was set at 490nm. The difference in JC1 fluorescence was not statistically significant in the *Opa1* +/- animals as compared to *Opa1* +/+ mice ($p>0.05$, T-test) in both brain and retina samples. (Data represent mean ± SD of 3 different samples and are expressed as % of *Opa1* +/+).
(B) Respective spectra of JC1 fluorescence in the retina and brain show the peak of the fluorescence at the approximately 590nm.

6.4 Discussion

The main aim of this chapter was to evaluate mitochondrial membrane potential in the retinas from *Opa1* +/- mutant mice.

First Western blot confirmed diminished expression of Opa1 protein in the mitochondria isolated from the retinas. The expression was about half of that detected in the wild type mice. However, despite this change reduction in mitochondrial membrane potential was not observed.

Opa1 proteolysis and mitochondrial membrane potential in the retina of *Opa1* +/- mice

It is known that the loss of mitochondrial membrane potential triggers proteolysis of Opa1 in the inner membrane. This has been reported in some mitochondrial diseases such as MERRF (Myoclonic epilepsy associated with ragged-red fibers) and MELAS (Mitochondrial myopathy, encephalomyopathy, lactic acidosis, and stroke-like episodes) and in mouse models with the impaired mitochondrial biogenesis (Duvezin-Caubet et al., 2006). The experiments presented here showed consistently that in *Opa1* +/- mice with normal mitochondrial membrane potential there was no increased proteolysis of Opa1 protein.

Opa1 proteolysis- role in mitochondrial homeostasis and apoptosis

A few proteases, which may act cooperatively, have been linked to Opa1 processing. Opa1 processing has been shown to be stimulated by ATP- dependent mAAA proteases, Yme1 and PARL (Cipolat et al., 2006; Duvezin- Caubet et al., 2006; Frezza et al., 2006; Ishihara et al., 2006; Song et al 2007). There is a distinction between a constitutive cleavage and an inducible cleavage of Opa1 with different proteases suspected to be implicated in these processes (Griparic et al., 2007). The constitutive cleavage is the physiological process that enables Opa1 protein to perform fusion, whereas inducible cleavage is triggered by the dissipation of mitochondrial membrane potential and probably inactivates Opa1 protein. The molecular mechanism for Opa1 inducible cleavage has not been fully described yet. Recently theory has developed that presents it as a mechanism which supports mitochondrial homeostasis. According to this proteolysis of long Opa1 isoforms is associated with mitochondrial fragmentation. As a result of this dysfunctional and energetically compromised mitochondria become segregated from the

intact tubular network, which reduces further propagation of the damage (Duvezin-Caubet et al., 2006).

Interestingly, a study on Opa1 protein isoforms in mice showed that the Opa1 band pattern is identical in neuronal tissues, like brain, retina and astrocytes but differed from the pattern expressed in other tissues (Akepati et al., 2008). The major difference was in the predominance of Opa1 isoform 1 in the nervous system. Because this isoform has been shown to increase the elongation of mitochondria and to prevent cells from apoptosis (Frezza et al., 2006), the authors believe that mutations affecting this isoform may have a strong impact especially on neurons. They also point out that all mutations found in ADOA patients reside in the exons present in the isoform 1 transcript suggesting the link between the level of functional isoform 1 and RGCs survival.

Mitochondrial membrane potential in optic nerve diseases

So far in optic atrophy diseases membrane potential reduction has been associated with oxidative stress. Battisti et al studied the effect of dRib- induced oxidative stress on mitochondrial membrane potential in LHON. The JC-1 test revealed greater depolarization of the mitochondrial membrane potential in lymphocytes from patients, with a percentage of cells emitting green fluorescence being 91.6% in LHON and 75.7% in the control. There was also an increased rate of apoptosis in LHON lymphocytes (Battisti et al., 2004) (*Opa1* +/- embryonic fibroblasts vulnerability to oxidative stress is discussed in Chapter 7). The link between oxidative stress, membrane potential reduction and optic nerve degeneration was also shown in ribozyme-induced SOD2 knockdown mouse. While a mutant mouse showed loss of RGCs and loss of axons and myelin in the optic nerve, infection of NIH/3T3 cells with this ribozyme caused a 64% reduction in mitochondrial membrane potential. (Qi et al., 2003).

Concluding remarks

Opa1 +/- mutant mice show the late onset of the disease that affects their visual performance. The disease is slowly progressive with structural abnormalities developing in the mitochondria from the RGC layer and the optic nerve (Davies et al., 2007; White et al., 2009). This study was carried out on young animals which performed well in visual tests and therefore was aimed at finding early molecular changes in mitochondrial function that could cause the disease. The results suggest that other factors than destabilization of mitochondrial membrane potential may be responsible for the

development of the disease in *Opa1* +/- mutant mice. However it is possible that the measurements of mitochondrial membrane potential should target more specifically mitochondria from the RGC layer and the optic nerve because the change measured in the whole retina is too modest and under the sensitivity threshold of the assay. Mitochondrial membrane potential could be measured in RGCs isolated from the mouse retina by immunopanning or laser cupture microdissection. It would be also interesting to compare this with the study of mitochondrial membrane potential in older *Opa1* +/- mice which develop pathological changes in the structure of their mitochondria.

7. MITOCHONDRIAL MORPHOLOGY AND VULNERABILITY TO OXIDATIVE STRESS IN *OPA1* +/- MOUSE MODEL

7. MITOCHONDRIAL MORPHOLOGY AND VULNERABILITY TO OXIDATIVE STRESS IN *OPA1* +/- MOUSE MODEL

7.1 Introduction

The aim of the experiments described in this Chapter was to seek more evidence that could suggest to what extent *Opa1* mutation in *Opa1* +/- mice could be pathological for the mitochondria and the cell. Opa1 protein is required for mitochondrial fusion, a process that plays an important role in the biology of the cell and a protective role in apoptosis (Frezza et al., 2006). Fusion-defective cells have reduced growth rates, reduced respiration and a mitochondrial population prone to loss of mitochondrial membrane potential (Chen et al., 2005). When fusion is inhibited, unopposed fission leads to mitochondrial fragmentation (Chen et al., 2003). Opa1 is also involved in maintaining cristae structure and Opa1 knockdown by siRNA leads to disorganized cristae (Griparic et al., 2004, Arnoult et al., 2005). It has recently been shown that impaired Opa1 function in mitochondria due to prohibitin deficiency results in an impaired cell proliferation (Merkwirth et al., 2008). Furthermore, an alteration in mitochondrial morphology also accompanies a cellular response to oxidative stress (Jendrach et al., 2008, Koopman et al., 2005).

The appearance of alterations in mitochondrial morphology in *Opa1* +/- mice, cell vitality and resistance to oxidative stress were studied. Gene expression analysis in the retina was performed to cast light on key genes implicated in mitochondrial structure which might be altered in their expression. Imaging of mitochondrial morphology was carried out in *Opa1* +/+ and *Opa1* +/- MEFs. Cell growth was assessed by the population doubling level and the vulnerability of *Opa1*+/- MEFs to oxidative stress was studied with hydrogen peroxide and blue light treatment.

7.2 Expression of selected genes in the retina that regulate mitochondrial morphology is normal in 3 month old *Opa1* +/- mice

7.2.1 Selection of genes for qRT-PCR

Mitochondrial morphology in the retina of *Opa1* +/- mouse was studied by preliminary analysis of the expression of six genes by qRT-PCR (Materials and Methods 2.8.3). The selection of genes was based on two objectives: to explore whether reduction of Opa1 in mitochondria activates other genes that are known to shape the mitochondrial network and second, to learn whether the IMM structure is normal in mutant mice. The list of genes included Spg7, Mfn2 and Dnm1l, which were classified in Gene Ontology to biological process involved in mitochondrial organization (Table 7.1). It has been shown that Spg7 regulates Opa1 processing and Spg7 knockdown induces highly connected mitochondrial network (Ishihara et al., 2006), Mfn2 promotes mitochondrial fusion (Chen et al., 2003), whereas Dnm1l promotes fission. In addition, Dnm1l together with its interacting partner Bik induces cristae remodelling. During apoptosis Bik stimulates opening of the cristae junctions, which mobilizes cytochrome c for the release (Germain et al., 2005). Therefore it has been assumed that the change in the transcription of Dnm1l and/or Bik may conceivably suggest the alteration in cristae organization. Two last genes that were studied: Slc25a4 and Atp5k while being directly involved in energy metabolism (Table 7.1) are also important structural and functional components of the inner mitochondrial membrane. Inhibitors of Slc25a4 have been shown to induce a dramatic change in inner membrane topology in beef heart mitochondria (Scherer et al., 1974). Moreover Slc25a4 (ANT1- adenine nucleotide translocator) regulates the activity of permeability transition pores and through this cell death (Vieira et al., 2000; Kokoszka et al., 2004). Mutations in Slc25a4 are responsible for another eye disease Autosomal Dominant Progressive External Ophthalmoplegia (OMIM 609283). Atp5k (subunit e of ATP synthase) contributes to the correct curvature of the inner membrane (cristae formation) (Paumard et al., 2002; Gavin et al., 2004). Studies on *Saccharomyces cerevisiae* have shown that the stability of subunit e is regulated by Mgm1 (yeast homolog of opa1) (Amutha et al., 2004).

Gene	Go Term (GO ID)
Mfn2	Mitochondrial fusion (0008053)
Spg7	Mitochondrion organization (0007005)
Dnm1l	Mitochondrial membrane organization (0007006)
Bik	Induction of apoptosis (0006917)
Slc25a4	Generation of precursor metabolites and energy (0006091)
Atp5k	ATP synthesis coupled proton transport (0015986)

Table 7.1 Functional classification of genes selected for qPCR by Gene Ontology (http://www.geneontology.org/). Go Category: biological process.

Primers for all experimental genes and the chosen housekeeper gene for data normalization (Hprt) were designed using Primer3 software (Materials and Methods 2.6; 2.6.1). Specificity of the primers to the respective mouse transcripts was verified by determining PCR amplicon sizes in 2% agarose gel electrophoresis (Fig.7.1) and melting curve analysis (Fig.7.2) (Materials and Methods 2.4; 2.6.2). PCR amplification was performed on randomly selected *Opa1* +/+ and *Opa1* +/- retinal samples.

A

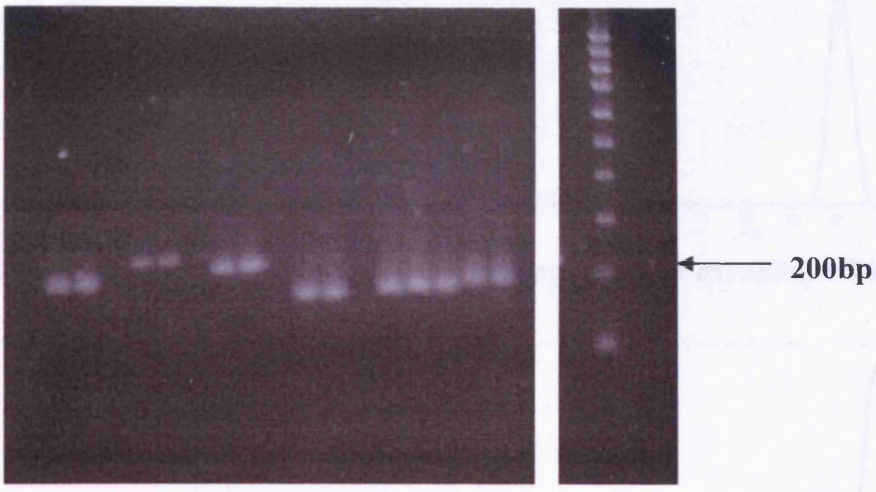

B

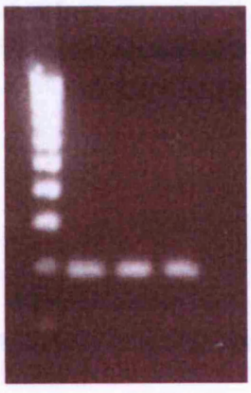

Gene	Length (bp)
Mfn2	219
Dnm1l	238
Bik	229
Atp5k	176
Slc25a4	184
Spg7	194

Fig.7.1 Specificity of the primers verified by analysis of PCR products on 2% agarose gel. Specificity of the primers designed for each gene was verified by comparison of the amplicon sizes separated by 2% agarose gel electrophoresis to the theoretical calculations. There were no non-specific amplification products. (A) Fragments of genes PCR-amplified from mouse retina were stained with Ethidium Bromide and observed under UV light. Bands in the ladder show increasing length every 100bp. (B) Theoretical calculations of all fragments are based on the knowledge of mRNA sequences and primer recognition sites in the mRNAs.

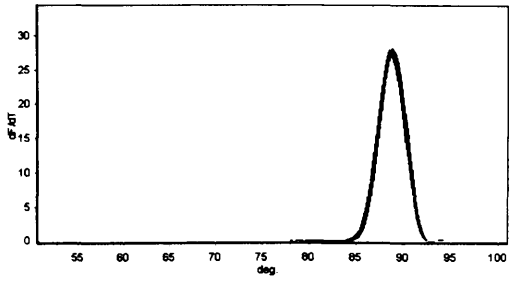

Mfn2-Mitofusin2

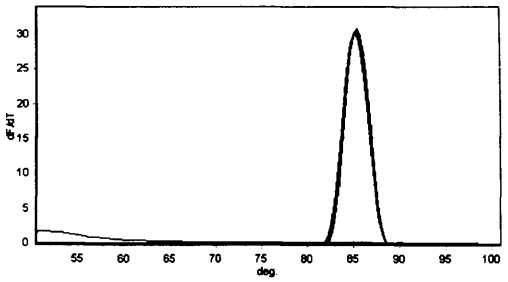

Spg7-Spastic paraplegia 7 homolog

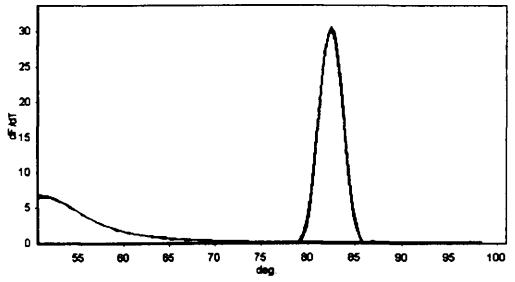

Dnm1l- dynamin 1-like

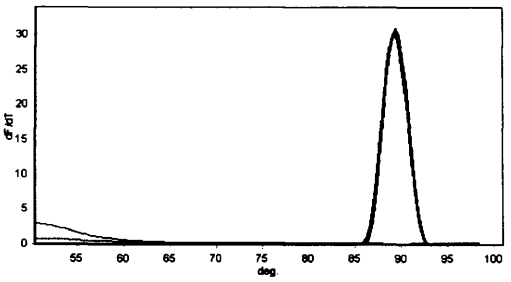

Bik- Bcl2- interacting killer

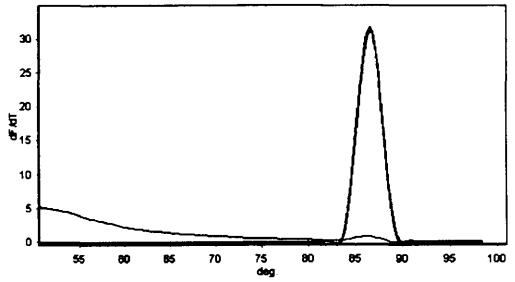

Slc25a4- adenine nucleotide translocator

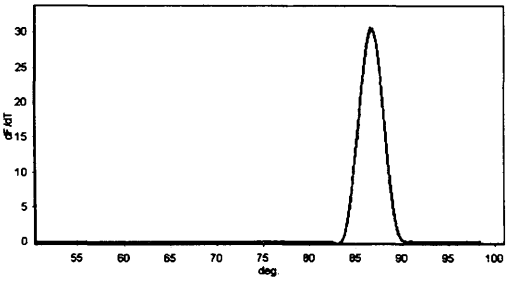

Atp5k- Atp synthase, subunit e

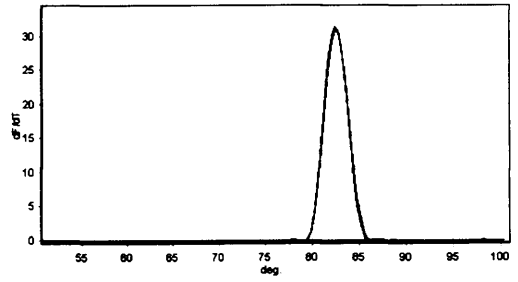

Hprt- Hypoxanthine phosphoribosyltranserase

Fig.7.2 Specificity of the primers verified by melting curve analysis.

Primers were designed for six genes. For each gene 3-4 different cDNA samples run in duplicate were PCR amplified and their melting curves analyzed. Single melting curves indicated purity of the products.

7.2.2 Quantification and quality of RNA samples

RNA was isolated from the retinas of 3 month-old mutant and wild type mice (Materials and Methods 2.7.1) and was quantified by staining with RiboGreen Reagent and reading the fluorescence of RiboGreen bound to RNA (Materials and Methods 2.7.2.2, Appendix 2).

RNA integrity of all retinal samples was assessed by the intensity of specific ribosomal RNA bands: 28S rRNA and 18S rRNA after denaturing agarose gel electrophoresis (Fig.7.3) (Materials and Methods 2.5).

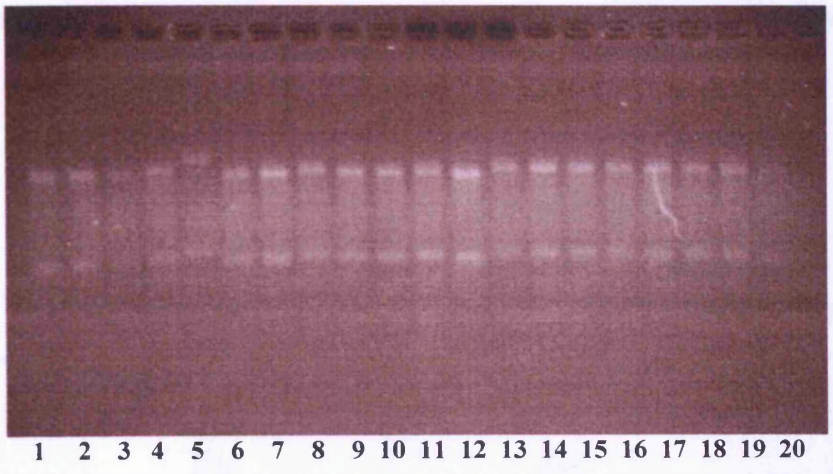

Fig.7.3 Denaturing agarose gel electrophoresis of RNA samples.

To check the integrity of RNA isolated from mouse retina, 20 RNA samples from *Opa1* +/+ and *Opa1* +/- animals (Appendix 2) were separated by denaturing agarose gel electrophoresis. Two distinct bands specific for 28S rRNA and 18S rRNA were detected in all RNA samples.

7.2.3 Analysis of gene expression by two step qRT-PCR

The expression of genes involved in mitochondrial morphology in retina of *Opa1* +/- mice was quantified by the two step relative qRT-PCR method and was compared to the expression levels in *Opa1* +/+ mice. The relative expression of each gene was determined by the $\Delta\Delta C_t$ method (Materials and Methods 2.8.3). The reference gene Hprt was used to control for variation in cDNA amount. (Hprt expression was reported stable in the models of pathological RGC death (Agudo et al., 2008)). Standard curves were run for both the target and reference gene in each assay and the coefficient determination obtained was $R^2 \geq 0.98$ (Fig.7.4). Amplification efficiencies (E) generated from standard dilution curves were compared between the target gene and Hprt. The difference in efficiency was for Spg7, Bik, Slc25a4, Atp5k: $\Delta E \leq 0.04$. For Mfn2 and Dnm1l ΔE was 0.13 and 0.17 respectively.

Mfn2- Mitofusin 2

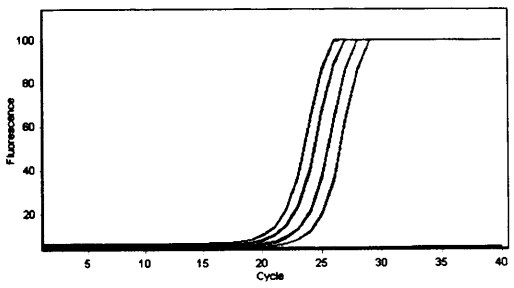

Spg7- spastic paraplegia 7 homolog

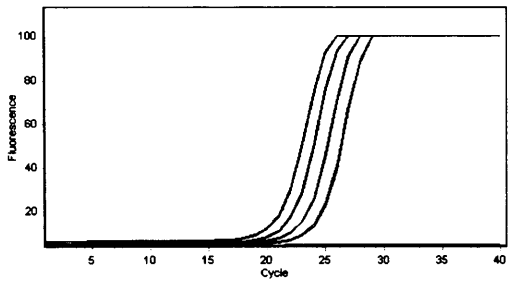

Fig.7.4 Amplification standard curves for all genes (continued on the next page).
Amplification curves were the products of 40 cycles of real-time PCR amplification of cDNA template using gene-specific primers. cDNA template was prepared from randomly selected *Opa1* samples. cDNA samples prepared in four standard dilutions

were run in duplicate for each assay. Conditions for PCR amplifications are described in details in Materials and Methods 2.8.3.

Dnm1l- dynamin 1-like

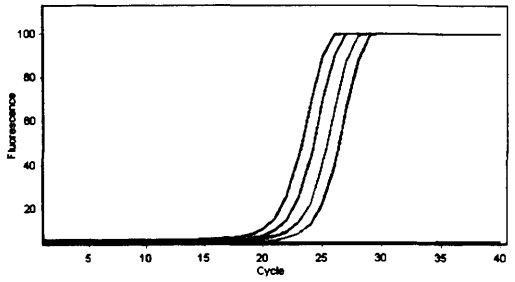

Bik-Bcl2- interacting killer

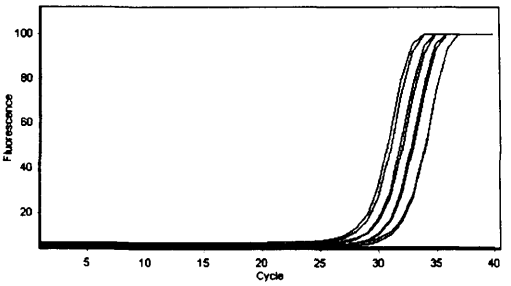

Slc25a4- adenine nucleotide translocator

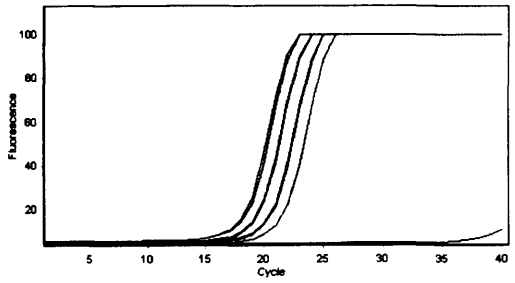

Atp5k- Atp synthase, subunit e

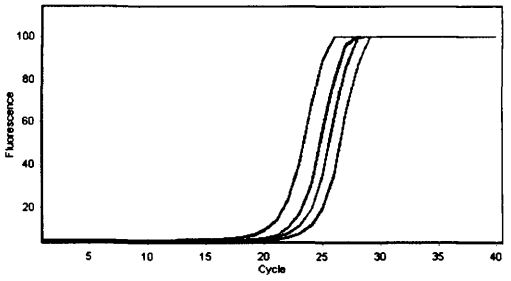

Hprt- Hypoxanthine phosphoribosyltranserase

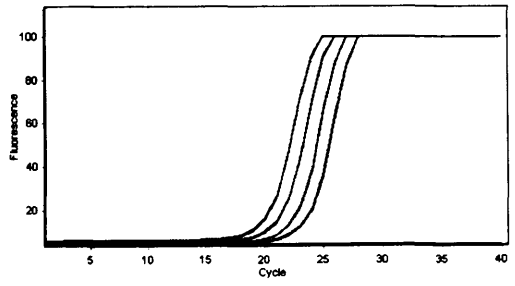

Fig.7.4 Amplification standard curves for all genes (continued from the next page). Amplification curves were the products of 40 cycles real-time PCR amplification of cDNA template using gene-specific primers. cDNA template was prepared from randomly selected *Opa1* samples. cDNA samples prepared in four standard dilutions

were run in duplicate for each assay. Conditions for PCR amplifications are described in details in Materials and Methods 2.8.3.

Statistical analysis of qRT-PCR results from six animals per group was done by T-Test for independent samples. In each assay samples were run in duplicate and the obtained intra-sample variation was SD≤ 0.65%. The difference in the expression of six candidate genes in *Opa1* +/- mouse retina was not found statistically significant when compared to *Opa1* +/+ animals ($p>0.05$) Data represent mean± SD of six animals (Fig.7.5).

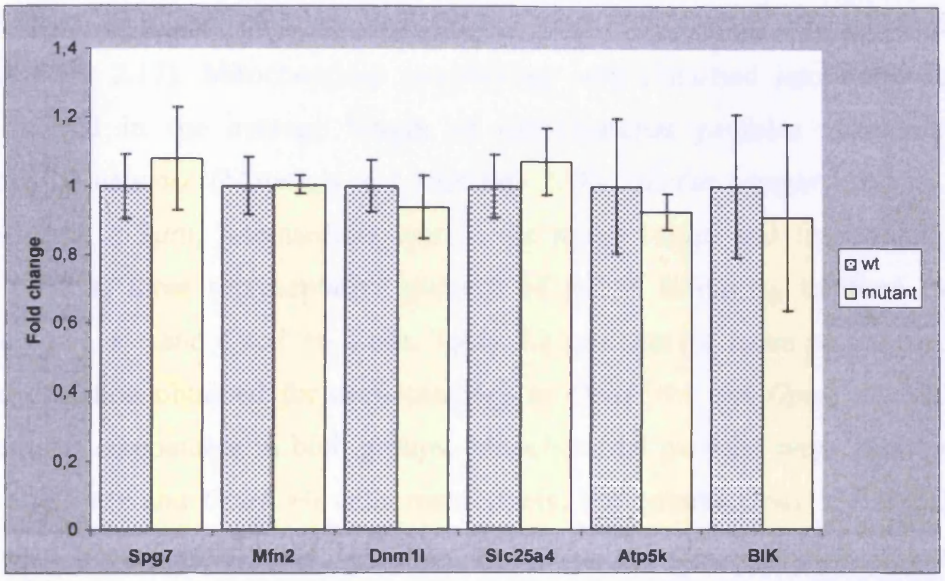

gene	qRT-PCR analysis of gene expression in retina, mean±SD Spg7	Mfn2	Dnm1l	Slc25a4	Atp5k	Bik
***Opa1* +/+**	1±0.09	1±0.08	1±0.07	1±0.09	1± 0.195	1±0.21
***Opa1* +/-**	1.08±0.15	1±0.025	0.94±0.09	1.07±0.10	0.925±0.05	0.91±0.27

Fig.7.5 Expression of genes involved in mitochondrial morphology in retina is not changed in 3 month-old *Opa1* mutant mice

Six candidate genes were studied by qRT-PCR. Results are presented as fold change of average expression level for *Opa1* +/- and *Opa1* +/+ animals ± SD. Statistical significance was determined by unpaired t-test. Mean fold change in the expression of

genes from mutant retina was not significantly different when compared to wild type mice, $p>0.05$.

7.3 Comparative analysis of mitochondrial morphology in *Opa1* +/+ and *Opa1* +/- MEFs

7.3.1 Classification of mitochondrial morphology in MEFs

To compare mitochondrial morphology in *Opa1* +/+ and *Opa1* +/- MEFs, cells were isolated from 13.5 dpc embryos and stained with Mitotracker Red (Materials and Methods 2.16; 2.17). Mitochondrial morphology was classified into three categories which differed in the average length of mitochondrial particles measured in the mitochondrial network (Materials and Methods 2.18): tubular category had an average particle length $\geq$ 2μm, intermediate was in the range 1-2μm and fragmented $\leq$ 1μm. Fig.7.7 presents three representative pictures of MEFs belonging to these categories found in *Opa1* +/+ and *Opa1* +/- lines. Table 7.2 presents the mean particle length and standard deviation obtained for each category in *Opa1* +/+ and *Opa1* +/- MEFs with measurements comparable in both groups. Mitochondrial particles were measured in 73 and 97 *Opa1* +/+ and *Opa1* +/- cells respectively. For control Opa1 +/+ and Opa1 +/- MEFs were treated with 1mM H_2O_2 for 1h, which induced extensive mitochondrial fragmentation in all cells (Fig.7.6). The average length of mitochondrial particles was 0,4 μm, SD =0,01.

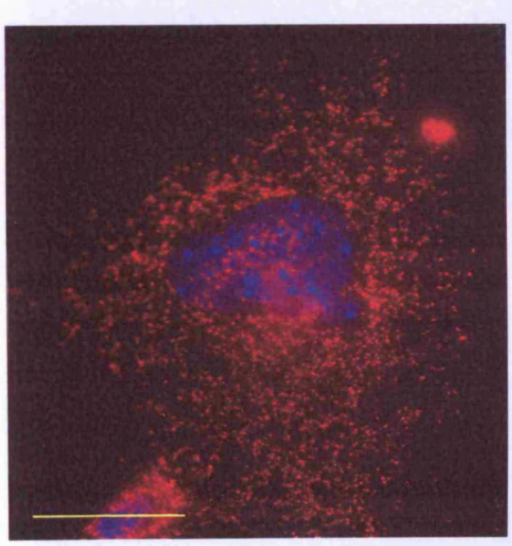

Fig.7.6 The representative fluorescent image of *OPA1* +/+ MEF treated with 1mM H_2O_2 shows fragmentation of mitochondrial network (stained with Mitotracker Red).

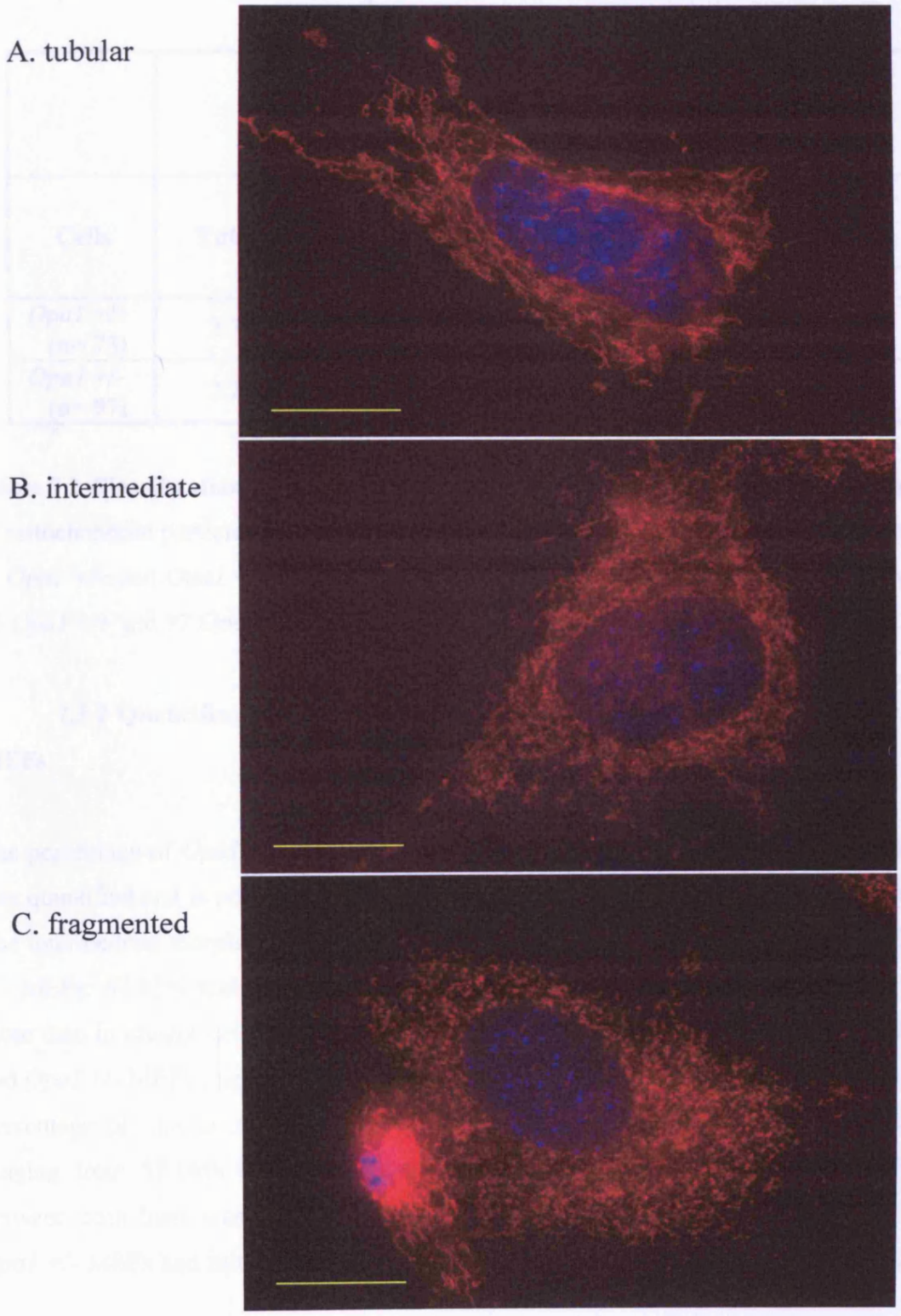

Fig.7.7 Mitochondrial morphology. Fluorescent images of three classes of mitochondrial morphology. Mitochondria were stained with Mitotracker Red and mitochondrial morphology was divided into three categories: tubular (A), intermediate (B) and fragmented (C). Bar =20μm.

	Mitochondrial particles, mean length ±SD [μm]		
Cells	**Tubular**	**Intermediate**	**Fragmented**
***Opa1* +/+ (n= 73)**	2.39±0.27	1.53±0.27	0.93±0.06
***Opa1* +/- (n= 97)**	2.28 ±0.22	1.47±0.25	0.88±0.08

Table 7.2 Classification of mitochondrial morphology in MEFs. The mean length±SD of mitochondrial particles was obtained for tubular, intermediate and fragmented network in *Opa1* +/+ and *Opa1* +/- MEFs. On average 25-50 particles per cell were measured in 73 *Opa1* +/+ and 97 *Opa1* +/- MEFs.

7.3.2 Quantification of mitochondrial morphology in *Opa1* +/+ and *Opa1* +/- MEFs

The percentage of *Opa1* +/+ and *Opa1* +/- cells with selected mitochondrial morphology was quantified and is presented in Fig. 7.8. The results are also summarized in Table 7.3. The intermediate morphology was the most common form found in *Opa1* +/+ and *Opa1* +/- MEFs: 67.42% and 66.97% respectively. There was a tendency in wild type cells more than in mutant cells to acquire tubular morphology: 27.95%, 12.97% for *Opa1* +/+ and *Opa1* +/- MEFs respectively. However *Opa1* +/+ MEFs showed a big variation in the percentage of tubular morphology between three different cultures that were studied ranging from 57.14% to 12%. A statistically significant difference (T-Test, $p<0.05$) between both lines was found in the category with fragmented mitochondria. 20.06% *Opa1* +/- MEFs had mitochondrial particles ≤ 1μm whereas in *Opa1* +/+ MEFs this was

4.63%. These results suggest that a small population of *Opa1* +/- cells (about 15%) may differ from wild type cells in their mitochondrial morphology. More cells with fragmented mitochondria would seem to be the effect of a reduction of the pro-fusion Opa1 protein in these cells.

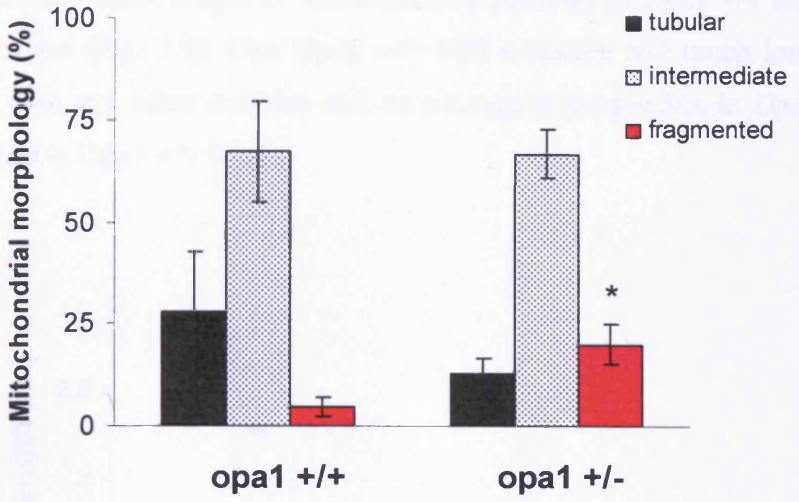

Fig.7.8 Mitochondrial morphology in *Opa1* +/+ and *Opa1* +/- MEFs. Graph bars show the percentage of cells with tubular, intermediate and fragmented mitochondria in both genotypes. Data represent mean± SEM of three different cultures for each genotype. 73 *Opa1* +/+ and 97 *Opa1* +/- cells were scored. (*) P<0.05 versus opa1 +/+ group.

	Mitochondrial morphology [%]		
Cells	**Tubular**	**Intermediate**	**Fragmented**
***Opa1* +/+ (n=73)**	27.95±14.61	67.42±12.28	4.63±2.39
***Opa1* +/- (n=97)**	12.97±3.54	66.97±5.78	20.06±5.05

Table 7.3 The summary of mitochondrial morphology in *Opa1* +/+ and *Opa1* +/- MEFs presented in Fig.7.7. Data represent mean± SEM of three different cultures for each genotype. 73 *Opa1* +/+ and 97 *Opa1* +/- cells were scored.

Additionally an alternative approach to the measurement of mitochondrial morphology was taken. The mean length of mitochondrial particles in *Opa1* +/+ and *Opa1* +/- MEFs was measured (Fig. 7.9). One *Opa1* +/+ MEFs culture had much longer mitochondrial particles than any other cultures and on average mitochondria in *Opa1* +/- MEFs were shorter than in Opa1 +/+ MEFs.

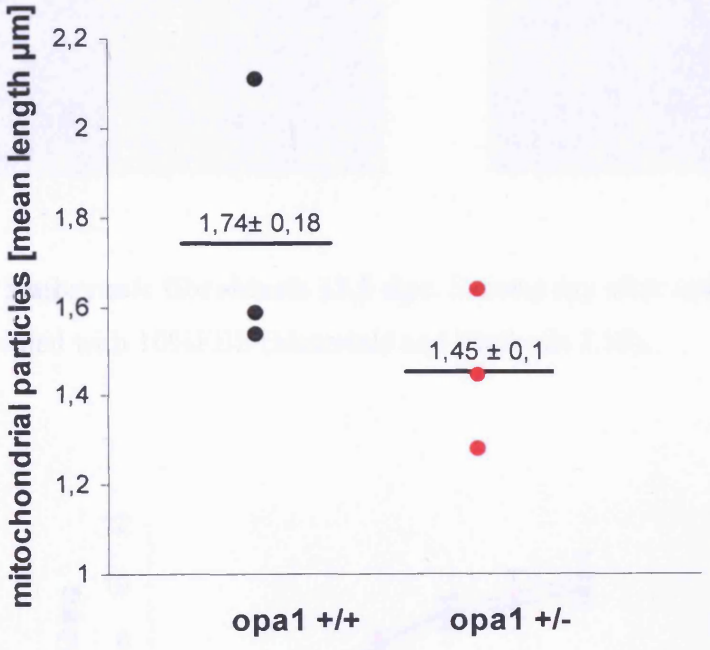

Fig.7.9 Analysis of mitochondrial particles in three *Opa1* +/+ and *Opa1* +/- MEF cultures. Mitochondria were stained with Mitotracker Red and mitochondrial particles were measured in *Opa1* +/+ and Opa1 +/- MEFs. The mean length was obtained for three *Opa1* +/+ and *Opa1* +/- cultures (black and red circles respectively). Horizontal bars show mean± SEM for each genotype (n=3).

7.4 *Opa1* +/- cell growth

Cells (MEFs) were isolated from 13.5dpc *Opa1* +/- and *Opa1* +/+ mouse embryos (Materials and Methods 2.16) (Fig.7.10) and cell growth was assessed by the population doubling level measured for 3 weeks (Materials and Methods 2.19). A similar growth curve was obtained for *Opa1* +/+ and *Opa1* +/- MEFs, as shown in Fig.7.11. After a fast cell growth for about 10 days in both lines there was a significant reduction in their proliferation observed over the last week.

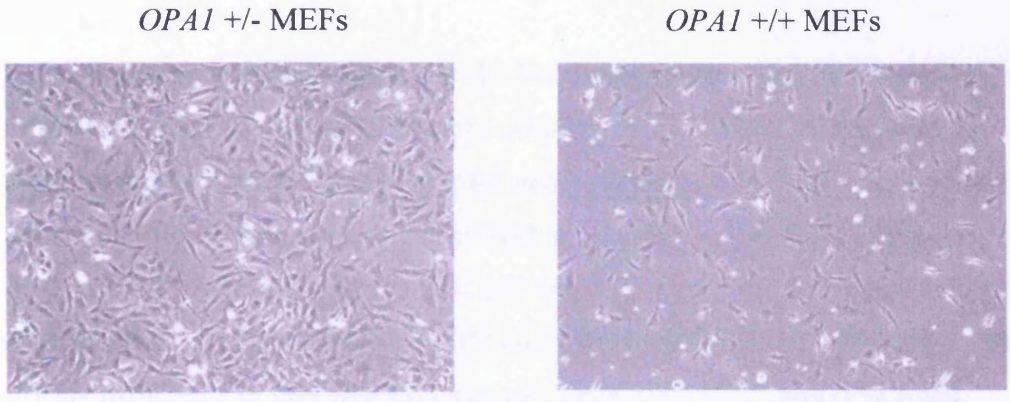

Fig.7.10 Embryonic fibroblasts 13.5 dpc. Second day after isolation cultured in DMEM supplemented with 10%FBS (Materials and Methods 2.16).

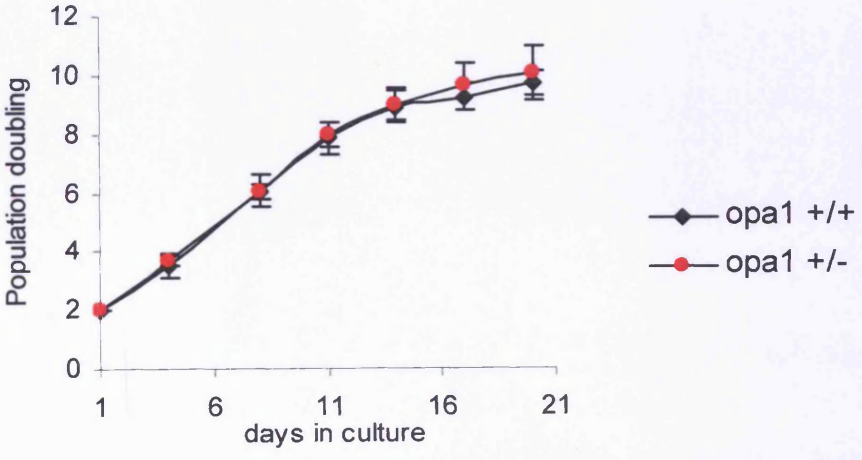

Fig.7.11 Cellular growth of *Opa1*+/- and *Opa1* +/+ MEFs. Population doubling was determined every third day in 3 *Opa1* +/+ and 4 *Opa1* +/- MEFs cultures seeded in duplicate. Data represent mean± SEM.

7.5 Vulnerability to light- and H_2O_2 induced oxidative stress

To assess how *Opa1* +/- MEFs are vulnerable to oxidative stress, *Opa1* +/- and control *Opa1* +/+ cell cultures were exposed to blue light and hydrogen peroxide, which are known to stimulate ROS production and cause apoptosis (Li et al., 2007). The survival of cells after treatment was determined in a MTT assay (Materials and Methods 2.22).

7.5.1 Light treatment of *Opa1* +/+ and *Opa1* +/- MEFs.

Cells were treated with blue-filtered light for a maximum of 24 hours and cell viability was measured after 12, 18 and 24 hours (Godley et al., 2005). For further details about the light treatment protocol see Materials and Methods 2.20. MEFs which were kept in the same conditions but not exposed to light were used as controls. Treatment with light for 12 hours did not cause any evident cell death in *Opa1* +/- and *Opa1*+/+ MEFs. The phototoxic effect was observed after 18 and 24 hours (Fig.7.12), however without any significant difference in this effect on mutant versus wild type cells (Fig.7.13).

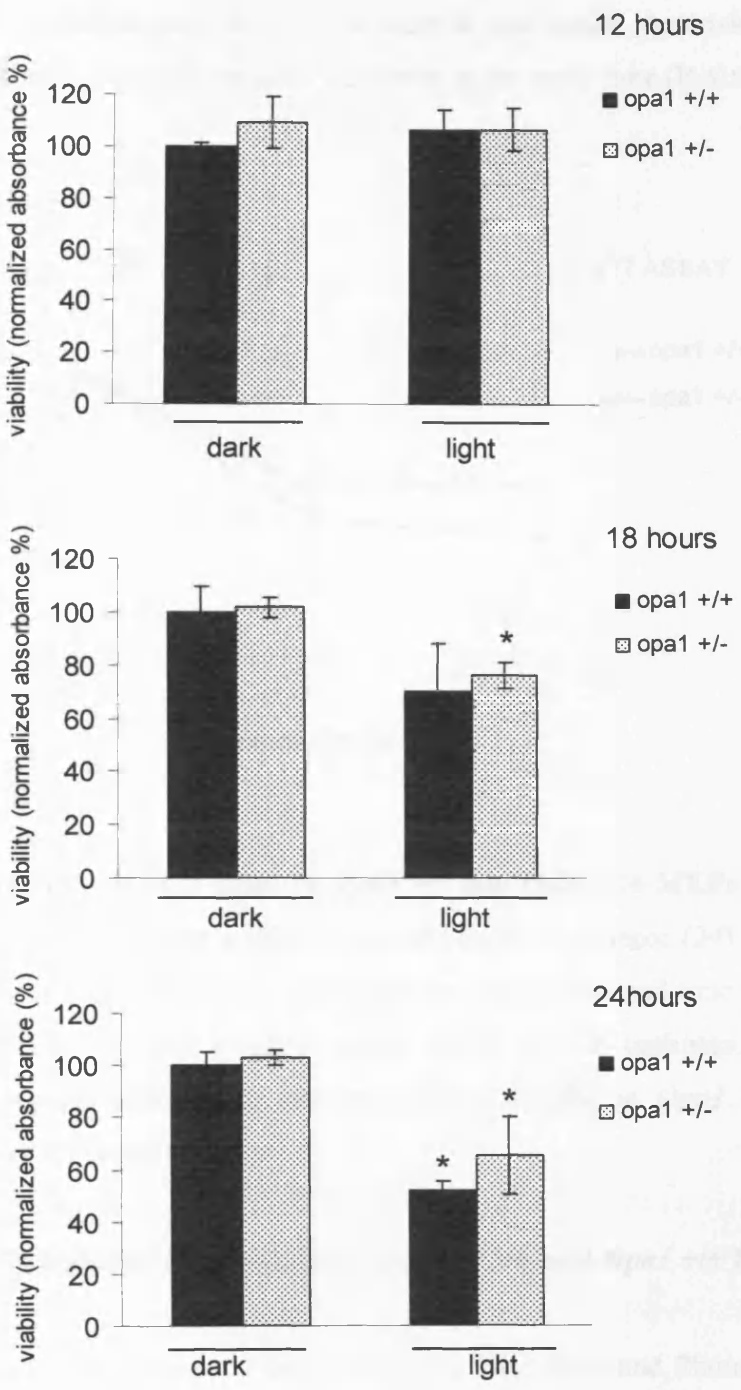

Fig.7.12 Viability of *Opa1* +/- and *Opa1* +/+ MESs treated with blue light for the time indicated. MEFs of respective genotype kept in the same conditions but not exposed to light were used as controls. The number of viable cells was determined in a MTT assay. The values were expressed as percentage of the absorbance value obtained for *Opa1* +/+ MEFs kept in darkness (100% value). Data are the means ± SEM of three (12 and 24 hours) or two (18 hours) independent experiments. At each time point 6-9

individual MEFs cultures were analyzed at least in quadruplet. Asterisk denotes values significantly different from the respective controls at the same time ($P<0.05$).

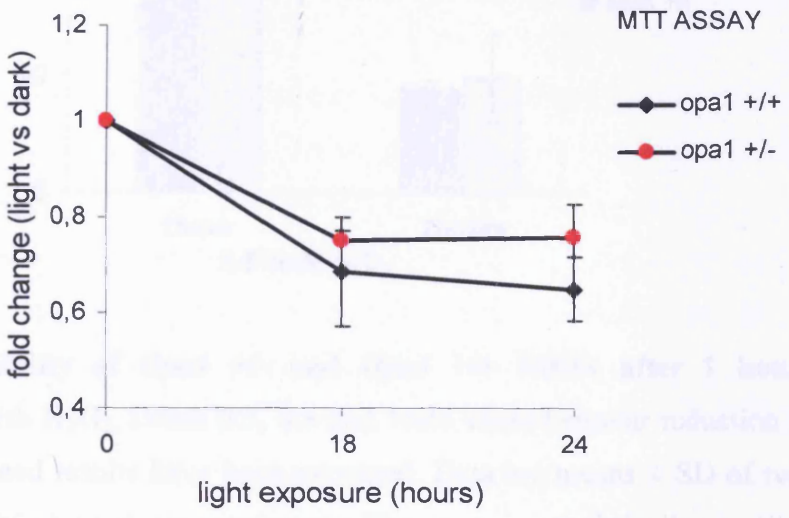

Fig.7.13 Phototoxicity of blue light on *Opa1* +/- and *Opa1* +/+ MEFs after 18 and 24 hrs exposition. Data are means ±SEM of two (18 hours) and three (24) experiments and are expressed as the fold change in a MTT activity at the indicated time point, calculated from the ratio MEFs exposed to light versus MEFs kept in darkness. Student's t-test analysis did not show statistically different effect of light on *Opa1* +/- MEFs when compared to *Opa1* +/+ MEFs.

7.5.2 H_2O_2 induced oxidative stress in *Opa1* +/- and *Opa1* +/+ MEFs

Cells were treated with increasing doses of H_2O_2 for 1 hour and 2hours (Frezza at al., 2006). Doses 0.1-1mM were tested and the toxic effect was induced with 0.5, 0.8 and 1mM H_2O_2 treatment. For further details about the H_2O_2 treatment protocol see Materials and Methods 2.21. MEFs not treated with H_2O_2 were used as controls. Sensitivity to H_2O_2 at the doses 0.5-1mM was similar in *Opa1* +/- and *Opa1* +/+ MEFs. After 2 hours treatment the significant reduction (about 60%) was observed in both cell lines (Fig.7.14).

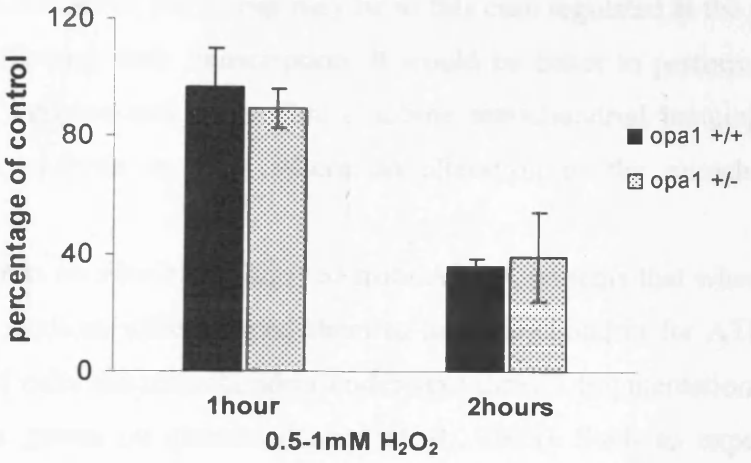

Fig.7.14 Viability of *Opa1* +/- and *Opa1* +/+ MEFs after 1 hour and 2hours treatment with H_2O_2. Doses 0.5, 0.8 and 1mM caused similar reduction in cell viability and the obtained results have been averaged. Data are means ± SD of two (1 hour) and three (2hours) independent experiments. There was no statistically significant increase in vulnerability of *Opa1* +/- MEFs to H_2O_2- induced death at the doses 0.5-1mM.

7.6 Discussion

Mitochondrial morphology in *Opa1* +/- mice

Opa1 plays a significant role in mitochondrial inner membrane fusion and maintaining mitochondrial morphology. It was expected that mitochondrial morphology might be affected in Opa1 mutant mice due to the reduction of Opa1 protein in mutant mitochondria (see Chapter 6).

Mitochondrial morphology was studied in the retina of 3-month-old mutant mice by qRT-PCR analysis of gene expression. The results did not indicate any evident differences in the expression of genes that play an important role in mitochondrial membrane organization and dynamics of mitochondrial inner membrane (Mfn2, Dnm1l, Spg7, Bik, Slc25a4, Atp5k). However analysis of mitochondrial morphology in MEFs isolated from 13.5dpc embryos suggested a higher incidence of fragmented mitochondria in *Opa1* +/- MEFs versus *Opa1* +/+ MEFs. This difference applied to approximately 15% of the cell population. It is difficult to compare these two experiments. First the change in gene expression when measured in the whole retina may be too small to be detected by qRT-PCR. It is also possible that mitochondrial fragmentation can be caused solely by Opa1

protein reduction without causing changes in the expression of other genes (see the paragraph below) or that genes may be in this case regulated at the posttranslational level without affecting their transcription. It would be better to perform both experiments on the same samples and if possible combine mitochondrial imaging with the single-cell qRT-PCR analysis in cells where an alteration in the mitochondrial network was observed.

It was shown on fibroblasts derived from ADOA patients that when cells were grown on galactose medium which forced them to use mitochondria for ATP production, in large number of cells the mitochondria underwent drastic fragmentation, as opposed to when cells were grown on glucose (Zanna et al., 2008). Such an experiment could be also performed on *Opa1* +/- MEFs to find out if the change in mitochondrial morphology will be enhanced in cells grown on galactose.

Mitochondrial morphology in mouse model of glaucoma. Comparison to Opa1 deficiency-induced mitochondrial fragmentation

Recently significant alterations in Opa1 (decrease) and Dnm1 (increase) mRNA expression have been found in the optic nerve head of 10 month-old glaucomatous mice and these changes were accompanied by substantial optic nerve damage (Won Kyu Ju et al., 2008). In glaucomatous mice a bidirectional change was observed: the 'fission gene-*Drp1*' was upregulated whereas the 'fusion gene-*Opa1*' was downregulated. Interestingly in *Opa1*-ablated MEFs where Opa1 levels were ~30% compared with control cells, other mitochondria-shaping proteins such as Drp1, hFis1 and Mfn2 were not affected but still mitochondrial fragmentation was observed (Cipolat et al., 2004). The results were not shown and possibly protein rather than mRNA expression was studied but it seems that the reduction in Opa1 expression alone, without changes in the expression of other genes, as reported in glaucomatous mice, was sufficient to induce an imbalance in the mitochondrial morphology. These two examples suggest the presence of different molecular mechanisms that could lead to mitochondrial fragmentation.

Cell viability and sensitivity to oxidative stress in Opa1 +/- MEFs

The viability of *Opa1* +/- MEFs was studied by observation of cellular growth and an oxidative stress-induced cell death. Cell growth was studied by calculation of population doubling level. Survival after blue light and hydrogen peroxide (0.5-1mM) was measured in a MTT assay. In neither experiments the differences in *Opa1* +/- MEFs behaviour

could be detected, when compared to the control *Opa1* +/+ cells. More such research evaluating the role of oxidative stress in the *Opa1* mouse model is needed. An increased oxidative stress was found to be the hallmark of pathology in the heterozygous Drosophila model of ADOA (Tang et al., 2009). On the other hand Frezza et al. (2006) showed that the onset of H_2O_2-induced apoptosis in cells can be delayed by over-expression of wild-type Opa1 protein (Introduction 1.2.6). Oxidative stress induced in *Opa1* +/- MEFs could be further studied by e.g. the measurement of ROS production and counting cells undergoing apoptosis.

Since RGCs in the retina are exposed to light, it would be interesting to study the effect of increased exposition to light on visual performance and retinal damage in living *Opa1* +/- mutant mice. This would answer the question of whether *Opa1* mutations can make RGCs more vulnerable to light-induced apoptosis.

Limitations concerning the use of fibroblasts for the assessment of light and hydrogen peroxide toxicity

Opa1 +/- MEFs did not demonstrate an increased vulnerability to oxidative stress. Oxidative stress was induced with blue light and hydrogen peroxide and neither factor increased the percentage of the mutant cell death when compared to WT cells. However, this finding cannot be directly translated to the vulnerability of RGCs in our mutant mice. It is not clear whether RGCs would respond to the oxidative stress similarly to MEFs and therefore would not show any increase in sensitivity. Preventing cell death initiated by oxidative stress has been shown to be cell-type specific (Jarrett, et al., 2006). MEFs are actively dividing cells. By contrast, neurons are long-lived, nonproliferative and terminally differentiated postmitotic cells which do not undergo a cell division. Therefore in neurons any oxidant- induced damage to macromolecules and organelles will accumulate, while in fibroblasts this will be continuously diluted during repetitive cell divisions (Terman et al., 2007). It has been also observed that oxidative stress can induce replicative senescence (growth arrest) in fibroblasts (Parrinello et al., 2003). This mechanism cannot occur in neurons which are already at a nonproliferative stage. Furthermore due to their electrical excitability, and structural and synaptic complexity, neurons depend on an enhanced metabolic rate with high levels of O_2 utilization and ATP synthesis. This increases the risk for the generation of elevated levels of ROS. Constant exposition of RGC to light may further enhance oxidative stress in these cells and cause damage to the mitochondrial genome and cell death, particularly in cells with

compromised mitochondrial function (Godley et al., 2005, Lascaratos et al., 2007, Osborne et al., 2008). Thus, in future experiments it would be desirable to evaluate the effect of oxidative stress directly on RGC survival. This would entail the extraction of primary RGCs by an immuno-panning method, or assessment on retinal explants. However, any such method is inherently artificial due to removing RGCs from their host environment and nutritive support, which may play an important role in prevention of cell death. Since it has been shown that light is a risk factor and generator of ROS, another approach would be to study RGC death *in vivo* in mice exposed to light.

Concluding remarks

Imaging of mitochondrial morphology has given an indication that a small population of cells may be affected by Opa1 protein reduction. It is too preliminary to say how this finding represents biological changes occurring in the retina of mutant mice, although it would be very tempting to think that similarly in a subpopulation of retinal ganglion cells mitochondrial morphology abnormalities develop which could explain the late onset and slow progression of the disease observed in *Opa1* +/- mutant mice. More research is needed using sensitive methods to detect probably mild changes. If the defect in mitochondrial fusion is the primary cause of RGCs dysfunction, in order to understand ADOA disease it would be helpful to reconstruct the course of molecular events taking place in RGCs in response to this defect.

8. DISCUSSION

8. DISCUSSION

This work present results from the study of *OPA1*-associated disease in a mouse model B6;C3-Opa1^{Q285STOP}. The main findings and accomplishments are:

- Opa1 heterozygous mice show ~ 50% reduction of Opa1 in their mitochondria from the retinal tissue
- The reduction of Opa1 in the mitochondria results in a higher incidence of mitochondrial fragmentation, as shown in *Opa1* +/- MEFs and compared to *Opa1* +/+ MEFs
- A considerable number of mitochondria in the retina of young mutant mice appear to maintain an intact IMM structure
- Despite degenerative changes in the optic nerve in 24 month old mutant mice (White et al., 2009) significant RGC loss is not observed
- A new, faster and more reliable genotyping method was designed (Chapter 3)
- RT-PCR analysis of *Opa1* transcripts showed three mRNA isoforms present in the retina of mutant and WT mice, with the dominance of mRNA isoform 1 (Davies et al., 2007)
- RT-PCR analysis revealed the presence of exon 4 in all mouse *Opa1* isoforms, which means that alternative splicing occurs only between exons 4b and 5b, which is different from what is found in humans (Chapter 4)

8.1 Opa1 reduction in mitochondria in heterozygous mice

Western blot analysis confirmed the reduction of Opa1 protein in mitochondria in heterozygous *Opa1* mice. When compared to published studies *in vitro* where Opa1 is nearly totally silenced by siRNA (Olichon et al., 2003; Griparic et al., 2004), the presence of Opa1 protein produced from one wild type allele, appears, at least to some extent, to maintain the Opa1 function in mitochondria. It can explain why a relatively mild effect of *OPA1* mutation is observed in tissues obtained from some ADOA patients (Chevrollier et al., 2008). In a heterozygous mutant mouse model, which is characterized by slowly progressive optic neuropathy (Chapter 1.4.2), the impact of mutation on mitochondria was expected to be rather moderate.

8.2 Mitochondrial network fragmentation in *Opa1* +/- MEFs

Mitochondrial morphology was studied in MEFs isolated from 13.5 dpc embryos. At this stage there were no homozygous mutants present, because they died at the earlier stages of embryonic development (Davies et al., 2007). Mitochondrial morphology was compared between *Opa1* +/- and *Opa1* +/+ MEFs. In *Opa1* +/- MEFs mitochondria were more prone to fragmentation, as shown by a higher percentage of cells with an average length of mitochondrial particles below 1μm. Mitochondrial fragmentation has been also observed in fibroblasts from human ADOA patients (Olichon et al., 2007b, Zanna et al., 2008) and in muscle explants from our 3 month old mutant mice. Interestingly, in muscle explants most *Opa1* +/- cells displayed punctuated and completely dispersed mitochondria. This difference in the degree of mitochondrial fragmentation between embryonic fibroblasts and muscle fibroblasts from adult tissue is not understood and could be due to the age, the cell type or the culture conditions. Mitochondrial network fragmentation was also shown in the *Caenorhabditis elegans* model, where mutation was induced in *eat-3* gene, the *OPA1* orthologue (Kanazawa, et al., 2008).

Mitochondrial fragmentation is clearly related to the role of Opa1 in fusion. Decreased fusion may shift the balance toward increased mitochondrial fission. However, the relationship between the defect in mitochondrial fusion and degeneration of the optic nerve is not yet understood. Recently, OPA1 function has been postulated to be important for a mitochondrial quality control, which counteracts and protects mitochondria from accumulation of the damage. Many specific proteases, chaperones and proteins that regulate mitochondrial dynamics and autophagy have been identified in this process (Tatsuta et al., 2008). An increased number of autophagic vesicles observed in the RGCs of 24 month old *Opa*1 mutant mice may suggest " a state of emergency ": an accumulation of mitochondria with reduced fusion competency and low membrane potential, which are targeted for degradation (Twig et al., 2008; White et al., 2009). It is also known that RGCs are highly vulnerable to energetic impairment. A defect in energy production explains another optic neuropathy: LHON in which mutations in mtDNA affect respiratory chain activity (Wallace et al., 1998; Ruiz-Pesini et al., 2007). It is possible that the imbalance in the fusion and fission may severely affect mitochondrial distribution in axons of the optic nerve and the provision of energy. Interestingly, fibroblasts from LHON patients can have a highly interconnected mitochondrial network (Chevrollier et al., 2008), whereas this study further supports the view that in ADOA mitochondria are likely to become fragmented. So far there has been one study that links

the loss of mitochondrial fine positioning in the axons of RGCs to the neurodegeneration in ADOA (Spinazzi et al., 2008). The study by confocal microscopy showed increased mitochondrial fragmentation and uneven distribution in fibroblasts and myotubes from patients with deletion in the GTPase domain of *OPA1*. However, it is worth noticing that this mutation is also associated with severe peripheral neuropathy. Mitochondrial fusion and fission regulate mitochondrial distribution to the synapse. It was demonstrated that the modification in Opa1 level can influence the maintenance of dendritic spines and synapses in hippocampal neurons (Li et al., 2004). Thus, hypothetically, reduced mitochondrial fusion may disorganize mitochondrial distribution to RGC dendrites and axons and ultimately affect function of the synapses.

8.3 IMM functional and structural integrity in the retina of heterozygous mice

OPA1 contributes to the mitochondrial inner membrane (IMM) structure, which implies the need for the study of *OPA1*- associated diseases in the context of structural and functional integrity of the IMM (Zanna et al., 2008). The disruption of elaborate IMM structure composed of cristae, cristae junctions and domains of interaction with OMM is likely to have an impact on respiration and generation of ROS, as well as induction of apoptosis by releasing the cytochrome c from the cristae stores. The experiments carried out on young *Opa1* +/- mice seem to support the view that IMM structure and energy metabolism are normal. Mitochondrial membrane potential across the IMM was measured in mouse retinas and brains at 4-5 months and appeared to be stable in the mutant mice. Consistent with this an increased Opa1 proteolysis in the IMM was not observed. Furthermore qRT-PCR assessment of the expression of genes involved in mitochondrial membrane dynamics in the retina did not find any significant differences in the *Opa1* +/- mice, compared to the control group. Overall in the mutant mice by the age of 5 months most mitochondria are able to cope with the mutation, such that they maintain functional and structural integrity of the IMM. It is important to note that whereas these experiments were performed on mitochondrial population from the whole retina, EM analysis of the optic nerve revealed some mitochondrial structural abnormalities in two *Opa1* mouse models (Alavi et al., 2007; White et al., 2009; Introduction 1.4.2; 1.4.3). The advantage of EM is that it enables the detection of changes at the level of single mitochondrion. Nevertheless, this may further indicate that mitochondria in the optic nerve are particularly vulnerable in *OPA1*- associated disease. In our *Opa1* +/- mice disorganized cristae was observed in older animals at 24 months,

which indicates the age-related development of pathological changes. Interestingly, an increase in the number of opaque mitochondria was also seen by EM in the optic nerve of mutant mice at 6 and 24 months and it was postulated to represent an increase in the density of cristae in order to fulfill the energy requirements of the axon. In fact, these results seem to suggest that in the RGC axons mitochondrial energy metabolism is likely to be affected and that mitochondria develop a compensatory strategy to ensure survival of the cells.

8.4 Lack of evidence on RGC loss in 24 month old heterozygous mice

Signs of optic nerve degeneration were observed by EM in both mouse models. Surprisingly, RGC loss or even a tendency in decreasing the number of RGCs on H&E stained retinal sections was not observed in mutant mice at 24 months. This may suggest that the optic nerve is the primary target of the disease in the mutant mice. However, there is also possibility that the RGC count was not accurate enough. As described in Discussion to Chapter 5, RGC layer is comprised of approximately equal numbers of RGCs and displaced amacrine cells, which could make the observation of a decrease in the number of only RGCs difficult to detect on retinal sections. To circumvent this limitation the different approach could be used e.g. Alavi et al., 2007 studied RGC loss in another *Opa1* +/- model on the whole mount retinal preparations with retrograde labelled RGCs and was able to show a time-dependent RGC loss from the retina.

8.5 Conclusions (Fig.8.1)

Taking all the evidence we have from the B6;C3-*Opa1*^{L122P} mouse, it is possible to postulate some mechanisms and hypotheses regarding the pathophysiology of the ADOA phenotype that we are attempting to model.

Heterozygous *Opa1* mice develop signs of visual dysfunction which first became apparent at the age of 12 months. A significant degenerative process seems to proceed in the RGC axons affecting nerve myelin, yet, so far, without any evidence for the loss of RGC bodies in the retina (Fig.8.1-1). Studying the magnitude of mitochondrial impairment showed partial fragmentation of the mitochondrial network in *Opa1* +/- MEFs, which suggests a defect in mitochondrial fusion (Fig.8.1-2). Many studies have indicated that mitochondria with this defect have aberrant ultrastructure, distribution and electron transport chain activity (Chen et al., 2007) and that their accumulation will have

a severe impact on the cell maintenance and stress response. However, study *in vitro* of *Opa1* +/- MEFs did not find any apparent weakness in these cells: their proliferative life span, and susceptibility to oxidative stress were similar to MEFs derived from WT mouse embryos. The defect in fusion must be subtle and does not culminate in cellular dysfunction of MEFs. So what could be said from this about RGCs? (Fig.8.1-3). In contrast to MEFs, RGCs are postmitotic neuronal cells, cannot divide and their mitochondrial network looks different, the cells have shorter and less connected mitochondria. Also, it has been recently postulated that proteins related to mitochondrial fusion/fission play a direct, more active role in controlling cell survival in neurons and thus neurons are more sensitive to the change in their expression (Uo et al., 2009). Therefore the comparison of MEFs and RGCs in their response to Opa1 deficiency cannot be straightforward.

Next, in the *Opa1* +/- retina there was no indication of any deficiency in the energy metabolism in young animals (Fig.8.1-4). This was mostly concluded from the observations that mitochondria maintained normal membrane potential and that there was normal expression of a few genes associated with mitochondrial activity and IMM ultrastructure. These data, however accurate they are in relation to the whole retina, they may be misleading or not too relevant when trying to link them to the pathological process occurring in the *Opa1* +/- mice (Fig.8.1-5). It may have been using too "bulky" an approach for studying fine mitochondrial aberrations that do occur specifically in the optic nerve as evidenced recently by EM. EM showed distinct morphologic remodeling of mitochondria and increased autophagy, which are likely to accompany deregulation of mitochondrial activity. Another factor that could significantly influence the results obtained on the retina is the age of animals studied. Due to the late onset of the disease, at the preclinical stage (3-5 month old animals) there will be less defective mitochondria and more difficulties to spot them and estimate the magnitude of their dysfunction.

Finally, how does the defect in mitochondrial fusion affect RGC function? At present there is a view which links this to the disruption of specific distribution of mitochondria that occurs in the RGC axons. It may be that mitochondria do not go where their presence is essential. We may see degeneration of the axons which are overloaded with abnormal mitochondria and an increase in the autophagic process. However, sadly we do not know what it all means to the cell. The cellular language has so far been untouched. There has

recently been one significant discovery which showed that cone degeneration in retinitis pigmentosa could be due to the cone starvation induced through the changes in the insulin/mTOR pathway (Punzo et al., 2009). Similar molecular in-sight in ADOA RGCs is awaited with interest (see also 8.6).

8.6 Future research and avenues for therapy

Future study on ADOA carried out on this mouse model could focus on detailed understanding of Opa1- mediated mitochondrial quality control in RGCs, which relates mitochondrial fusion to autophagy and how this process is integrated into cellular signaling pathways that govern RGC functions and apoptosis. Furthermore more experiments to measure mitochondrial morphology and function in RGCs and the optic nerve need to be undertaken. The experiments such as: the measurement of activity of respiratory chain complexes, membrane potential, ATP synthesis and mitochondrial distribution could be performed systematically over longer period of time on younger and aging animals.

In relation to RGC specific vulnerability in ADOA it is important to broaden our understanding of biological differences between different tissues and the possible specific thresholds that set the maximal limit of tissue adaptation to stress and instability. In this work for example the dominance of *Opa1* isoform 1 transcript in the retina was found (another study showed the dominance of isoform 1 protein in neuronal tissues, including the retina (Akepati et al., 2008)). However, it is not known what it means in the context of mitochondrial function in neurons. Tissue specificity also requires more study that takes into account not only the intrinsic properties of the tissue but also its localization, external surrounding and environmental factors, such as light, with regard to RGCs. Since it has been identified that *OPA1* mutations are also associated with multi-systemic mitochondrial disorders, the challenge now is to design treatments that will be beneficial for all patients with *OPA1* mutation. Would it be possible to design one treatment that will be universal for all patients with different ADOA phenotypes? The pharmacological strategies that would enhance energetic metabolism or prevent apoptosis were proposed to have potentially therapeutic effect on optic neuropathies (Amati-Bonneau et al., 2009). Gene therapy aiming at increasing OPA1 expression in the eye could be beneficial for patients with haploinsufficiency. It is not entirely clear yet whether the primary site of injury in ADOA is the RGC axon or body and this information would be useful in finding an effective neuroprotection (Levin, 2007).

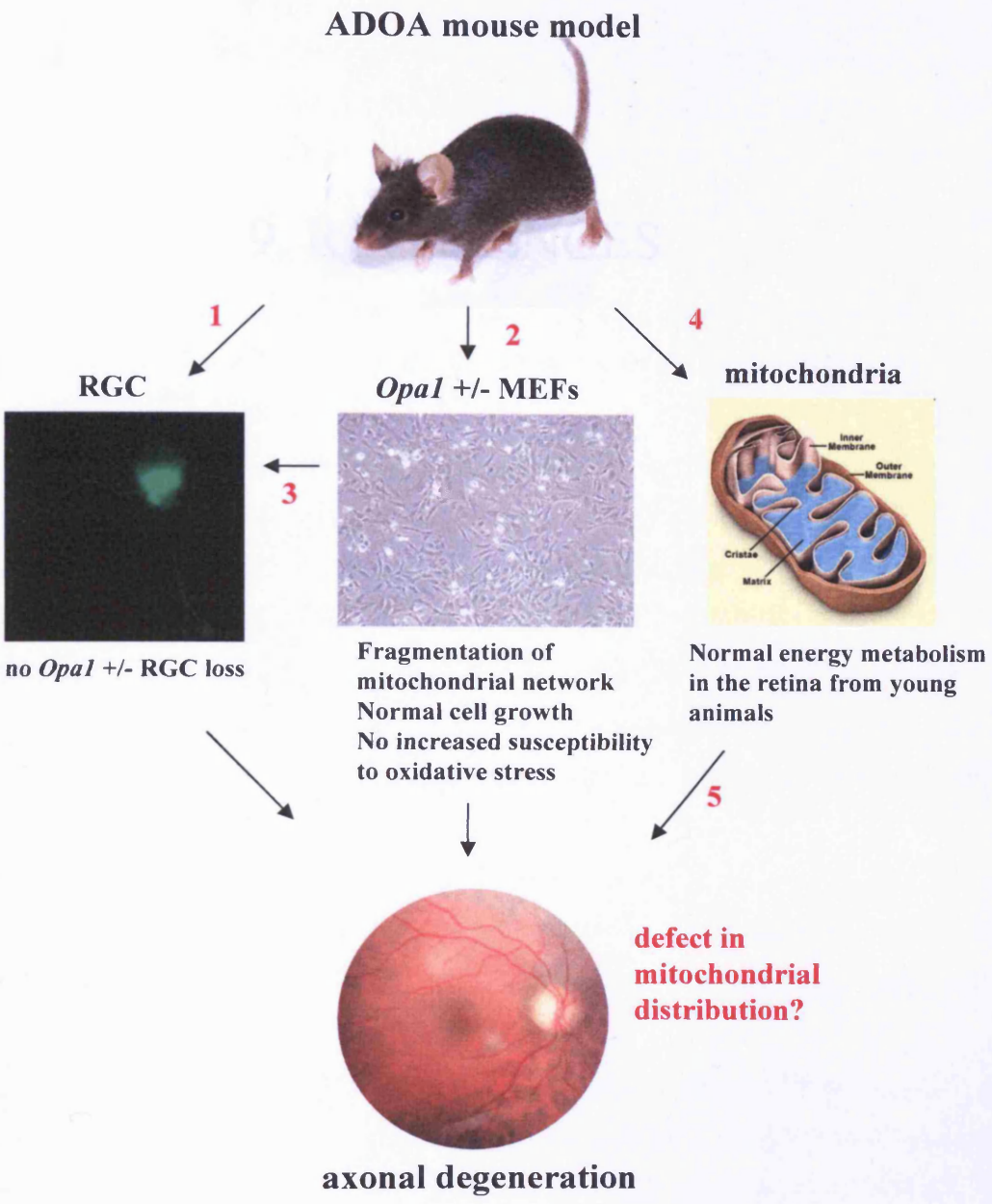

Fig. 8.1 The summary of the results on ADOA mouse model.

In heterozygous mice the defect in mitochondrial fusion can be responsible for mild optic degeneration and visual dysfunction. No RGCs loss in old animals suggests that the primary site of pathology is in RGC axons.

9. REFERENCES

9. REFERENCES

1. Agudo, M., Pérez-Marín, M.C., Sobrado-Calvo, P., Lönngren, U., Salinas-Navarro, M., Cánovas, I., Nadal-Nicolás, F.M., Miralles-Imperial, J., Hallböök, F., Vidal-Sanz, M. (2008) Immediate upregulation of proteins belonging to different branches of the apoptotic cascade in the retina after optic nerve transection and optic nerve crush. Invest Ophthalmol Vis Sci.
2. Akepati, V.R., Müller, E.C., Otto, A., Strauss, H.M., Portwich, M., Alexander, C. (2008). Characterization of OPA1 isoforms isolated from mouse tissues. J. Neurochem. *106*, 372-83.
3. Alavi, M.V., Bette, S., Schimpf, S., Schuettauf, F., Schraermeye, U., Wehrl, H.F., Ruttiger, L., Beck, S.C., Tonagel, F., Pichler, B.J., Knipper, M., Peters, T., Laufs, J., Wissinger, B. (2007). A splice site mutation in the murine Opa1 gene features pathology of autosomal dominant optic atrophy. Brain *130*, 1029-1042.
4. Alexander, C., Votruba, M., Pesch, U. E., Thiselton, D. L., Mayer, S., Moore, A., Rodriguez, M., Kellner, U., Leo-Kottler, B., Auburger, G., *et al.* (2000). OPA1, encoding a dynamin-related GTPase, is mutated in autosomal dominant optic atrophy linked to chromosome 3q28. Nat Genet *26*, 211-215.
5. Amati-Bonneau, P., Odent, S., Derrien, C., Pasquier, L., Malthiéry, Y., Reynier, P., Bonneau, D. (2003). The association of autosomal dominant optic atrophy and moderate deafness may be due to the R445H mutation in the OPA1 gene. Am J Ophthalmol *136*, 1170-1171.
6. Amati-Bonneau, P., Guichet, A., Olichon, A., Chevrollier, A., Viala, F., Miot, S., Ayuso, C., Odent, S., Arrouet, C., Verny, C. *et al.* (2005). OPA1 R445H mutation in optic atrophy associated with sensorineural deafness. Ann Neurol *58*, 958-63.
7. Amati-Bonneau, P., Valentino, M.L., Reynier, P., Gallardo, M.E., Bornstein, B., Boissière, A., Campos, Y., Rivera, H., de la Aleja, J.G., Carroccia, R. *et al.* (2008) OPA1 mutations induce mitochondrial DNA instability and optic atrophy 'plus' phenotypes. Brain *131,* 338-351
8. Amati-Bonneau, P., Milea, D., Bonneau, D., Chevrollier, A., Ferré, M., Guillet, V., Gueguen, N., Loiseau, D., Crescenzo, M.A., Verny, C. *et al.* (2009). OPA1-associated disorders: Phenotypes and pathophysiology. Int J Biochem Cell Biol.
9. Amrani, N., Sachs, M.S., Jacobson, A. (2006). Early nonsense: mRNA decay solves a translational problem. Nat Rev Mol Cell Biol 7, 415-425.

10. Amutha, B., Gordon, D.M., Gu, Y., Pain, D. (2004) A novel role of Mgm1p, a dynamin-related GTPase, in ATP synthase assembly and cristae formation/maintenance. Biochem J *381*, 19-23.
11. Arnold, I., Langer, T. (2002). Membrane protein degradation by AAA proteases in mitochondria. Biochim Biophys Acta *2*, 89-96.
12. Arnoult, D., Grodet, A., Lee, Y. J., Estaquier, J., and Blackstone, C. (2005). Release of OPA1 during apoptosis participates in the rapid and complete release of cytochrome c and subsequent mitochondrial fragmentation. J Biol Chem *280*, 35742-35750.
13. Austin, C. P., Battey, J. F., Bradley, A., Bucan, M., Capecchi, M., Collins, F. S., Dove, W. F., Duyk, G., Dymecki, S., Eppig, J. T., *et al.* (2004). The knockout mouse project. Nat Genet *36*, 921-924.
14. Barbet, F., Hakiki, S., Orssaud, C., Gerber, S., Perrault, I., Hanein, S., Ducroq, D., Dufier, J.L., Munnich, A., Kaplan, J., Rozet, J.M. (2005). A third locus for dominant optic atrophy on chromosome 22q. J Med Genet *42*
15. Baricault, L., Ségui, B., Guégand, L., Olichon, A., Valette, A., Larminat, F., Lenaers, G. (2007). OPA1 cleavage depends on decreased mitochondrial ATP level and bivalent metals. Exp Cell Res *15*, 3800-3808.
16. Battisti, C., Formichi, P., Cardaioli, E., Bianchi, S., Mangiavacchi, P., Tripodi, S.A., Tosi, P., Federico, A. (2004) Cell response to oxidative stress induced apoptosis in patients with Leber's hereditary optic neuropathy. J Neurol Neurosurg Psychiatry *75*, 1731-6.
17. Benard, G., Karbowski, M. (2009). Mitochondrial fusion and division: Regulation and role in cell viability. Semin Cell Dev Biol *20,* 365-374.
18. Benard, G., Rossignol, R. (2008), Ultrastructure of the mitochondrion and its bearing on function and bioenergetics. Antioxid Redox Signal. *10*, 1313-42.
19. Berninger, T. A., Jaeger, W., and Krastel, H. (1991). Electrophysiology and colour perimetry in dominant infantile optic atrophy. Br J Ophthalmol *75*, 49-52.
20. Bleazard, W., McCaffery, J. M., King, E. J., Bale, S., Mozdy, A., Tieu, Q., Nunnari, J., and Shaw, J. M. (1999). The dynamin-related GTPase Dnm1 regulates mitochondrial fission in yeast. Nat Cell Biol *1*, 298-304.
21. Buckingham, B.P., Inman, D.M., Lambert, W., Oglesby, E., Calkins, D.J., Steele, M.R., Vetter, M.L., Marsh-Armstrong, N., Horner, P.J. (2008). Progressive

ganglion cell degeneration precedes neuronal loss in a mouse model of glaucoma. J Neurosci. *28*, 2735-44.

22. Carelli, V., Ross-Cisneros, F. N., and Sadun, A. A. (2004). Mitochondrial dysfunction as a cause of optic neuropathies. Prog Retin Eye Res *23*, 53-89.
23. Carelli, V., La Morgia, C., Iommarini, L., Carroccia, R., Mattiazzi, M., Sangiorgi, S., Farne', S., Maresca, A., Foscarini, B., Lanzi, L. (2007). Mitochondrial optic neuropathies: how two genomes may kill the same cell type? Biosci Rep *27*, 173-84.
24. Chen, H., Detmer, S. A., Ewald, A. J., Griffin, E. E., Fraser, S. E., and Chan, D. C. (2003). Mitofusins Mfn1 and Mfn2 coordinately regulate mitochondrial fusion and are essential for embryonic development. J Cell Biol *160*, 189-200.
25. Chen, H., Chomyn, A., Chan, D.C. (2005). Disruption of fusion results in mitochondrial heterogeneity and dysfunction. J Biol Chem *280*, 26185-92.
26. Chen, H., McCaffery, J.M., Chan, D.C. (2007). Mitochondrial fusion protects against neurodegeneration in the cerebellum. Cell *130*, 548-62.
27. Chevrollier, A., Guillet, V., Loiseau, D., Gueguen, N., de Crescenzo, M.A., Verny, C., Ferre, M., Dollfus, H., Odent, S., Milea, D. (2008). Hereditary optic neuropathies share a common mitochondrial coupling defect. Ann Neurol *63*, 794-8.
28. Cipolat, S., Martins de Brito, O., Dal Zilio, B., and Scorrano, L. (2004). OPA1 requires mitofusin 1 to promote mitochondrial fusion. Proc Natl Acad Sci U S A *101*, 15927-15932.
29. Cipolat, S., Rudka, T., Hartmann, D., Costa, V., Serneels, L., Craessaerts, K., Metzger, K., Frezza, C., Annaert, W., D'Adamio, L., *et al.* (2006). Mitochondrial rhomboid PARL regulates cytochrome c release during apoptosis via OPA1-dependent cristae remodeling. Cell *126*, 163-175.
30. Cornille, K., Milea, D., Amati-Bonneau, P., Procaccio, V., Zazoun, L., Guillet, V, El Achouri, G., Delettre, C., Gueguen, N., Loiseau D *et al.* (2008). Reversible optic neuropathy with OPA1 exon 5b mutation. Ann Neurol *63*, 667-71.
31. Dalke, C., and Graw, J. (2005). Mouse mutants as models for congenital retinal disorders. Exp Eye Res *81*, 503-512.
32. Danino, D., and Hinshaw, J. E. (2001). Dynamin family of mechanoenzymes. Curr Opin Cell Biol *13*, 454-460.

33. Davies, V.J., Hollins, A.J., Piechota, M.J., Yip, W., Davies, J.R., White, K.E., Nicols, P.P., Boulton, M.E., Votruba, M. (2007) Opa1 deficiency in a mouse model of autosomal dominant optic atrophy impairs mitochondrial morphology, optic nerve structure and visual function. Hum Mol Genet *1*, 1307-1318.
34. De Jager, P. L., Harvey, D., Polydorides, A. D., Zuo, J., and Heintz, N. (1998). A high-resolution genetic map of the nervous locus on mouse chromosome 8. Genomics *48*, 346-353.
35. Delettre, C., Lenaers, G., Griffoin, J.M., Gigarel, N., Lorenzo, C., Belenguer, P., Pelloquin, L., Grosgeorge, J., Turc-Carel, C., Perret, E. (2000). Nuclear gene OPA1, encoding a mitochondrial dynamin-related protein, is mutated in dominant optic atrophy. Nat Genet *26*, 207-210.
36. Delettre, C., Griffoin, J.M., Kaplan, J., Dollfus, H., Lorenz, B., Faivre, L., Lenaers, G., Belenguer, P., Hamel, C.P. (2001). Mutation spectrum and splicing variants in the OPA1 gene. Hum Genet *109*, 584-591.
37. Detmer, S.A., Chan, D.C. (2007). Functions and dysfunctions of mitochondrial dynamics. Nat Rev Mol Cell Biol *8*, 870-9.
38. Duvezin-Caubet, S., Jagasia, R., Wagener, J., Hofmann, S., Trifunovic, A., Hansson, A., Chomyn, A., Bauer, M. F., Attardi, G., Larsson, N. G., *et al.* (2006). Proteolytic processing of OPA1 links mitochondrial dysfunction to alterations in mitochondrial morphology. J Biol Chem.
39. Duvezin-Caubet, S., Koppen, M., Wagener, J., Zick, M., Israel, L., Bernacchia, A., Jagasia, R., Rugarli, E.I., Imhof, A., Neupert, W. *et al.* (2007). OPA1 processing reconstituted in yeast depends on the subunit composition of the m-AAA protease in mitochondria. Mol Biol Cell *18*, 3582-3590.
40. Eiberg, H., Kjer, B., Kjer, P., Rosenberg, T. (1994). Dominant optic atrophy (OPA1) mapped to chromosome 3q region. I. Linkage analysis. Hum Mol Genet *3*, 977-980.
41. Eliott, D., Traboulsi, E. I., and Maumenee, I. H. (1993). Visual prognosis in autosomal dominant optic atrophy (Kjer type). Am J Ophthalmol *115*, 360-367.
42. Ferre, M., Amati-Bonneau, P., Tourmen, Y., Malthiery, Y., and Reynier, P. (2005). eOPA1: an online database for OPA1 mutations. Hum Mutat *25*, 423-428.
43. Frank, S., Gaume, B., Bergmann-Leitner, E.S., Leitner, W.W., Robert, E.G., Catez, F., Smith, C.L., Youle, R.J. (2001). The role of dynamin-related protein 1, a mediator of mitochondrial fission, in apoptosis. Dev Cell *1*, 515-25.

44. Frezza, C., Cipolat, S., Martins de Brito, O., Micaroni, M., Beznoussenko, G. V., Rudka, T., Bartoli, D., Polishuck, R. S., Danial, N. N., De Strooper, B., and Scorrano, L. (2006). OPA1 controls apoptotic cristae remodeling independently from mitochondrial fusion. Cell *126*, 177-189.

45. Fuhrmann, N., Alavi, M.V,, Bitoun, P., Woernle, S., Auburger, G., Leo-Kottler, B., Yu-Wai-Man, P., Chinnery, P., Wissinger, B. (2009) Genomic rearrangements in OPA1 are frequent in patients with autosomal dominant optic atrophy. J Med Genet *46*, 136-144.

46. Gavin, P. D., Prescott, M., Luff, S. E., and Devenish, R. J. (2004). Cross-linking ATP synthase complexes in vivo eliminates mitochondrial cristae. J Cell Sci *117*, 2333-2343.

47. Germain, M., Mathai, J. P., McBride, H. M., and Shore, G. C. (2005). Endoplasmic reticulum BIK initiates DRP1-regulated remodelling of mitochondrial cristae during apoptosis. Embo J *24*, 1546-1556.

48. Green, D. R., and Kroemer, G. (2004). The pathophysiology of mitochondrial cell death. Science *305*, 626-629.

49. Griparic, L., van der Wel, N. N., Orozco, I. J., Peters, P. J., and van der Bliek, A. M. (2004). Loss of the intermembrane space protein Mgm1/OPA1 induces swelling and localized constrictions along the lengths of mitochondria. J Biol Chem *279*, 18792-18798.

50. Griparic, L., Kanazawa, T., van der Bliek, A.M. (2007). Regulation of the mitochondrial dynamin-like protein Opa1 by proteolytic cleavage. J Cell Biol *178*, 8757-8764.

51. Guillery, O., Malka, F., Landes, T., Guillou, E., Blackstone, C., Lombès, A., Belenguer, P., Arnoult, D., Rojo, M. (2008). Metalloprotease-mediated OPA1 processing is modulated by the mitochondrial membrane potential. Biol Cell *100*, 315-325.

52. Hales, K. G., and Fuller, M. T. (1997). Developmentally regulated mitochondrial fusion mediated by a conserved, novel, predicted GTPase. Cell *90*, 121-129.

53. Hatten, M. E., and Heintz, N. (2005). Large-scale genomic approaches to brain development and circuitry. Annu Rev Neurosci *28*, 89-108.

54. Herlan, M., Vogel, F., Bornhovd, C., Neupert, W., and Reichert, A. S. (2003). Processing of Mgm1 by the rhomboid-type protease Pcp1 is required for

maintenance of mitochondrial morphology and of mitochondrial DNA. J Biol Chem *278*, 27781-27788.

55. Holder, G. E., Votruba, M., Carter, A. C., Bhattacharya, S. S., Fitzke, F. W., and Moore, A. T. (1998). Electrophysiological findings in dominant optic atrophy (DOA) linking to the OPA1 locus on chromosome 3q 28-qter. Doc Ophthalmol *95*, 217-228.
56. Hollenbeck, P. J. (2005). Mitochondria and neurotransmission: evacuating the synapse. Neuron *47*, 331-333.
57. Huang, T.T., Naeemuddin, M., Elchuri, S., Yamaguchi, M., Kozy, H.M., Carlson, E.J., Epstein, C.J. (2006). Genetic modifiers of the phenotype of mice deficient in mitochondrial superoxide dismutase. Hum Mol Genet *15*, 1187-1194.
58. Ishihara, N., Fujita, Y., Oka, T., and Mihara, K. (2006). Regulation of mitochondrial morphology through proteolytic cleavage of OPA1. Embo J *25*, 2966-2977.
59. Ito, Y., Nakamura, M., Yamakoshi, T., Lin, J., Yatsuya, H., Terasaki, H. (2007). Reduction of inner retinal thickness in patients with autosomal dominant optic atrophy associated with OPA1 mutations. Invest Ophthalmol Vis Sci *48*, 4079-1086
60. Jarrett, S.G., Albon, J., Boulton, M. (2006). The contribution of DNA repair and antioxidants in determining cell type-specific resistance to oxidative stress. Free Radic Res. *40*, 1155-65.
61. Jendrach, M., Mai, S., Pohl, S., Vöth, M., Bereiter-Hahn, J. (2008) Short- and long-term alterations of mitochondrial morphology, dynamics and mtDNA after transient oxidative stress. Mitochondrion. *8*, 293-304
62. Jeon, C.J., Strettoi, E., Masland, R.H. (1998). The major cell populations of the mouse retina. J Neurosci *18*, 8936-46.
63. Jonasdottir, A., Eiberg, H., Kjer, B., Kjer, P., and Rosenberg, T. (1997). Refinement of the dominant optic atrophy locus (OPA1) to a 1.4-cM interval on chromosome 3q28-3q29, within a 3-Mb YAC contig. Hum Genet *99*, 115-120.
64. Jones, B. A., and Fangman, W. L. (1992). Mitochondrial DNA maintenance in yeast requires a protein containing a region related to the GTP-binding domain of dynamin. Genes Dev *6*, 380-389.
65. Ju, W.K., Kim, K.Y., Lindsey, J.D., Angert, M., Duong-Polk, K.X., Scott, R.T., Kim, J.J., Kukhmazov, I., Ellisman, M.H., Perkins, G.A., Weinreb, R.N. (2008).

Intraocular pressure elevation induces mitochondrial fission and triggers OPA1 release in glaucomatous optic nerve. Invest Ophthalmol Vis Sci *49*, 4903-11.

66. Jun, A.S., Brown, M.D., Wallace, D.C. (1994) A mitochondrial DNA mutation at nucleotide pair 14459 of the NADH dehydrogenase subunit 6 gene associated with maternally inherited Leber hereditary optic neuropathy and dystonia. Proc Natl Acad Sci U S A *91*, 6206-6210.
67. Justice, M. J., Noveroske, J. K., Weber, J. S., Zheng, B., and Bradley, A. (1999). Mouse ENU mutagenesis. Hum Mol Genet *8*, 1955-1963.
68. Johnston, P.B., Gaster, R.N., Smith, V.C., Tripathi, R.C. (1979). A clinicopathologic study of autosomal dominant optic atrophy. Am J Ophthalmol *88*, 868-75.
69. Kamei, S., Chen-Kuo-Chang, M., Cazevieille, C., Lenaers, G., Olichon, A., Belenguer, P., Roussignol, G., Renard, N., Eybalin, M., Michelin, A., *et al.* (2005). Expression of the Opa1 mitochondrial protein in retinal ganglion cells: its downregulation causes aggregation of the mitochondrial network. Invest Ophthalmol Vis Sci *46*, 4288-4294.
70. Kanazawa, T., Zappaterra, M.D., Hasegawa, A., Wright, A.P., Newman-Smith, E.D., Buttle, K.F., McDonald, K., Mannella, C.A., van der Bliek, A.M. (2008) The C. elegans Opa1 homologue EAT-3 is essential for resistance to free radicals. PLoS Genet *4*
71. Karbowski, M., and Youle, R. J. (2003). Dynamics of mitochondrial morphology in healthy cells and during apoptosis. Cell Death Differ *10*, 870-880.
72. Kerrison, J. B., Arnould, V. J., Ferraz Sallum, J. M., Vagefi, M. R., Barmada, M. M., Li, Y., Zhu, D., and Maumenee, I. H. (1999). Genetic heterogeneity of dominant optic atrophy, Kjer type: Identification of a second locus on chromosome 18q12.2-12.3. Arch Ophthalmol *117*, 805-810.
73. Kjer, P., Jensen, O.A., Klinken, L. (1983). Histopathology of eye, optic nerve and brain in a case of dominant optic atrophy. Acta Ophthalmol (Copenh) *61*, 300-312.
74. Kokoszka, J.E., Waymire, K.G., Levy, S.E., Sligh, J.E., Cai, J., Jones, D.P., MacGregor, G.R., Wallace, D.C. (2004) The ADP/ATP translocator is not essential for the mitochondrial permeability transition pore *427*, 461-5.
75. Koopman, W.J., Verkaart, S., Visch, H.J., van der Westhuizen, F.H., Murphy, M.P., van den Heuvel, L.W., Smeitink, J.A., Willems, P.H. (2005). Inhibition of

complex I of the electron transport chain causes O2-. -mediated mitochondrial outgrowth. Am J Physiol Cell Physiol. *288*, 1440-50.

76. Lascaratos, G., Ji, D., Wood, J.P., Osborne, N.N. (2007). Visible light affects mitochondrial function and induces neuronal death in retinal cell cultures. Vision Res. *47*, 1191-201.
77. Lenaers, G., Reynier, P., Elachouri, G., Soukkarieh, C., Olichon, A., Belenguer, P., Baricault, L., Ducommun, B., Hamel, C., Delettre, C. (2009). OPA1 functions in mitochondria and dysfunctions in optic nerve. Int J Biochem Cell Biol (Epub ahead of print)
78. Levin, L.A. (2007). Axonal loss and neuroprotection in optic neuropathies. Can J Ophthalmol, *42*, 403-8
79. Li, G.Y., Osborne, N.N. (2007). Oxidative-induced apoptosis to an immortalized ganglion cell line is caspase independent but involves the activation of poly(ADP-ribose)polymerase and apoptosis-inducing factor. Brain Res *10*, 35-43.
80. Li, Z., Okamoto, K., Hayashi, Y., and Sheng, M. (2004). The importance of dendritic mitochondria in the morphogenesis and plasticity of spines and synapses. Cell *119*, 873-887.
81. Liguori, M., La Russa, A., Manna, I., Andreoli, V., Caracciolo, M., Spadafora, P., Cittadella, R., Quattrone, A. (2008). A phenotypic variation of dominant optic atrophy and deafness (ADOAD) due to a novel OPA1 mutation. J Neurol *255*, 127-129
82. Livak, K.J., Schmittgen, T.D. (2001). Analysis of relative gene expression data using real-time quantitative PCR and the 2(-Delta Delta C(T)) Methods *25*, 402-8.
83. Marchbank, N. J., Craig, J. E., Leek, J. P., Toohey, M., Churchill, A. J., Markham, A. F., Mackey, D. A., Toomes, C., and Inglehearn, C. F. (2002). Deletion of the OPA1 gene in a dominant optic atrophy family: evidence that haploinsufficiency is the cause of disease. J Med Genet *39*, e47.
84. Meeusen, S., McCaffery, J.M., Nunnari, J. (2004). Mitochondrial fusion intermediates revealed in vitro. Science *305*, 1747-52.
85. Meire, F., De Laey, J.J., de Bie, S., van Staey, M., Matton, M.T. (1985). Dominant optic nerve atrophy with progressive hearing loss and chronic progressive external ophthalmoplegia (CPEO). Ophthalmic Paediatr Genet. *5*, 91-97.
86. Merkwirth, C., Dargazanli, S., Tatsuta, T., Geimer, S., Löwer, B., Wunderlich, F.T., von Kleist-Retzow, J.C., Waisman, A., Westermann, B., Langer, T. (2008).

Prohibitins control cell proliferation and apoptosis by regulating OPA1-dependent cristae morphogenesis in mitochondria. Genes Dev *22*, 476-88.

87. Misaka, T., Miyashita, T., and Kubo, Y. (2002). Primary structure of a dynamin-related mouse mitochondrial GTPase and its distribution in brain, subcellular localization, and effect on mitochondrial morphology. J Biol Chem *277*, 15834-15842.
88. Molina, A.J., Wikstrom, J.D., Stiles, L., Las, G., Mohamed, H., Elorza, A., Walzer, G., Twig, G., Katz, S., Corkey, B.E., Shirihai, O.S. (2009). Mitochondrial Networking Protects Beta Cells from Nutrient Induced Apoptosis. Diabetes (Epub ahead of print)
89. Newman, N. J. (2005). Hereditary optic neuropathies: from the mitochondria to the optic nerve. Am J Ophthalmol *140*, 517-523.
90. Olichon, A., Baricault, L., Gas, N., Guillou, E., Valette, A., Belenguer, P., and Lenaers, G. (2003). Loss of OPA1 perturbates the mitochondrial inner membrane structure and integrity, leading to cytochrome c release and apoptosis. J Biol Chem *278*, 7743-7746.
91. Olichon, A., Elachouri, G., Baricault, L., Delettre, C., Belenguer, P., and Lenaers, G. (2007a). OPA1 alternate splicing uncouples an evolutionary conserved function in mitochondrial fusion from a vertebrate restricted function in apoptosis. Cell Death Differ.
92. Olichon, A., Emorine, L. J., Descoins, E., Pelloquin, L., Brichese, L., Gas, N., Guillou, E., Delettre, C., Valette, A., Hamel, C. P., *et al.* (2002). The human dynamin-related protein OPA1 is anchored to the mitochondrial inner membrane facing the inter-membrane space. FEBS Lett *523*, 171-176.
93. Olichon, A., Landes, T., Arnauné-Pelloquin, L., Emorine, L.J., Mils, V., Guichet, A., Delettre, C., Hamel, C., Amati-Bonneau, P., Bonneau, D. (2007b) Effects of OPA1 mutations on mitochondrial morphology and apoptosis: relevance to ADOA pathogenesis. J Cell Physiol *211*, 423-430.
94. Osborne, N.N., Li, G.Y., Ji, D., Mortiboys, H.J., Jackson, S. (2008) Light affects mitochondria to cause apoptosis to cultured cells: possible relevance to ganglion cell death in certain optic neuropathies. J Neurochem. *105*, 2013-28.
95. Otsuga, D., Keegan, B. R., Brisch, E., Thatcher, J. W., Hermann, G. J., Bleazard, W., and Shaw, J. M. (1998). The dynamin-related GTPase, Dnm1p, controls mitochondrial morphology in yeast. J Cell Biol *143*, 333-349.

96. Parrinello, S., Samper, E., Krtolica, A., Goldstein, J., Melov, S., Campisi, J. (2003) Oxygen sensitivity severely limits the replicative lifespan of murine fibroblasts. Nat Cell Biol. *5*, 741–747.

97. Paumard, P., Vaillier, J., Coulary, B., Schaeffer, J., Soubannier, V., Mueller, D. M., Brethes, D., di Rago, J. P., and Velours, J. (2002). The ATP synthase is involved in generating mitochondrial cristae morphology. Embo J *21*, 221-230.

98. Payne, M., Yang, Z., Katz, B.J., Warner, J.E., Weight, C.J., Zhao, Y., Pearson, E.D., Treft, R.L., Hillman, T., Kennedy, R.J. *et al.* (2004). Dominant optic atrophy, sensorineural hearing loss, ptosis, and ophthalmoplegia: a syndrome caused by a missense mutation in OPA1. Am J Ophthalmol *138*, 749-55.

99. Pesch, U. E., Leo-Kottler, B., Mayer, S., Jurklies, B., Kellner, U., Apfelstedt-Sylla, E., Zrenner, E., Alexander, C., and Wissinger, B. (2001). OPA1 mutations in patients with autosomal dominant optic atrophy and evidence for semi-dominant inheritance. Hum Mol Genet *10*, 1359-1368.

100. Pittler, S. J., and Baehr, W. (1991). Identification of a nonsense mutation in the rod photoreceptor cGMP phosphodiesterase beta-subunit gene of the rd mouse. Proc Natl Acad Sci U S A *88*, 8322-8326.

101. Punzo, C., Kornacker, K., Cepko, C.L. (2009) Stimulation of the insulin/mTOR pathway delays cone death in a mouse model of retinitis pigmentosa. Nat Neurosci *12*, 44-52.

102. Qi, X., Lewin, A.S., Hauswirth, W.W., Guy, J. (2003). Optic neuropathy induced by reductions in mitochondrial superoxide dismutase. Invest Ophthalmol Vis Sci *44*, 1088-96.

103. Rube, D. A., and van der Bliek, A. M. (2004). Mitochondrial morphology is dynamic and varied. Mol Cell Biochem *256-257*, 331-339.

104. Ruiz-Pesini, E., Lott, M.T., Procaccio, V., Poole, J.C., Brandon, M.C., Mishmar, D., Yi, C., Kreuziger, J., Baldi, P., Wallace, D.C. (2007). An enhanced MITOMAP with a global mtDNA mutational phylogeny. Nucleic Acids Res *35* (Database issue), D823-8.

105. Satoh, M., Hamamoto, T., Seo, N., Kagawa, Y., and Endo, H. (2003). Differential sublocalization of the dynamin-related protein OPA1 isoforms in mitochondria. Biochem Biophys Res Commun *300*, 482-493.

106. Scherer, B., Klingenberg, M. (1974). Demonstration of the relationship between the adenine nucleotide carrier and the structural changes of mitochondria as induced by adenosine 5'-diphosphate. Biochemistry *13*, 161-70.

107. Schimpf, S., Fuhrmann, N., Schaich, S., Wissinger, B. (2008). Comprehensive cDNA study and quantitative transcript analysis of mutant OPA1 transcripts containing premature termination codons. Hum Mutat. *29*, 106-12.

108. Schütt, F., Davies, S., Kopitz, J., Holz, F.G., Boulton, M.E. (2000). Photodamage to human RPE cells by A2-E, a retinoid component of lipofuscin. Invest Ophthalmol Vis Sci *41*, 2303-8.

109. Schwerk, C., and Schulze-Osthoff, K. (2005). Regulation of apoptosis by alternative pre-mRNA splicing. Mol Cell *19*, 1-13.

110. Sesaki, H., Dunn, C. D., Iijima, M., Shepard, K. A., Yaffe, M. P., Machamer, C. E., and Jensen, R. E. (2006). Ups1p, a conserved intermembrane space protein, regulates mitochondrial shape and alternative topogenesis of Mgm1p. J Cell Biol *173*, 651-658

111. Smirnova, E., Griparic, L., Shurland, D. L., and van der Bliek, A. M. (2001). Dynamin-related protein Drp1 is required for mitochondrial division in mammalian cells. Mol Biol Cell *12*, 2245-2256.

112. Smirnova, E., Shurland, D. L., Newman-Smith, E. D., Pishvaee, B., and van der Bliek, A. M. (1999). A model for dynamin self-assembly based on binding between three different protein domains. J Biol Chem *274*, 14942-14947.

113. Smirnova, E., Shurland, D. L., Ryazantsev, S. N., and van der Bliek, A. M. (1998). A human dynamin-related protein controls the distribution of mitochondria. J Cell Biol *143*, 351-358.

114. Song, Z., Chen, H., Fiket, M., Alexander, C., Chan, D.C. (2007) OPA1 processing controls mitochondrial fusion and is regulated by mRNA splicing, membrane potential, and Yme1L. J Cell Biol *178*, 749-55.

115. Song, Z., Ghochani, M., McCaffery, J.M., Frey, T.G., Chan, D.C. (2009). Mitofusins and OPA1 Mediate Sequential Steps in Mitochondrial Membrane Fusion. Mol Biol Cell. 2009 (Epub ahead of print).

116. Spinazzi, M., Cazzola, S., Bortolozzi, M., Baracca, A., Loro, E., Casarin, A., Solaini, G., Sgarbi, G., Casalena, G., Cenacchi, G. *et al.* (2008) A novel deletion in the GTPase domain of OPA1 causes defects in mitochondrial morphology and distribution, but not in function. Hum Mol Genet *17*, 3291-302.

117. Stoilova, D., Child, A., Desai, S. P., and Sarfarazi, M. (1997). Refinement of the locus for autosomal dominant juvenile optic atrophy to a 2 cM region on 3q28. Ophthalmic Genet *18*, 1-6.

118. Tang, S., Le, P.K, Tse, S., Wallace, D.C, Huang, T. (2008). Heterozygous mutation of Opa1 in Drosophila shortens lifespan mediated through increased reactive oxygen species production. PLoS One *4*,e4492.

119. Tatsuta, T., Langer, T. (2008). Quality control of mitochondria: protection against neurodegeneration and ageing. EMBO J *27*, 306-14.

120. Terman, A., Gustafsson, B., Brunk, A.T. (2007) Autophagy, organelles and ageing. J Pathol. *211*, 134-143.

121. Thiselton, D. L., Alexander, C., Morris, A., Brooks, S., Rosenberg, T., Eiberg, H., Kjer, B., Kjer, P., Bhattacharya, S. S., and Votruba, M. (2001). A frameshift mutation in exon 28 of the OPA1 gene explains the high prevalence of dominant optic atrophy in the Danish population: evidence for a founder effect. Hum Genet *109*, 498-502.

122. Thiselton, D. L., Alexander, C., Taanman, J. W., Brooks, S., Rosenberg, T., Eiberg, H., Andreasson, S., Van Regemorter, N., Munier, F. L., Moore, A. T., *et al.* (2002). A comprehensive survey of mutations in the OPA1 gene in patients with autosomal dominant optic atrophy. Invest Ophthalmol Vis Sci *43*, 1715-1724.

123. Tondera, D., Grandemange, S., Jourdain, A., Karbowski, M., Mattenberger, Y., Herzig, S., Da Cruz, S., Clerc, P., Raschke, I., Merkwirth, C. *et al.* (2009). SLP-2 is required for stress-induced mitochondrial hyperfusion. EMBO J. *28*, 1589-600.

124. Toomes, C., Marchbank, N. J., Mackey, D. A., Craig, J. E., Newbury-Ecob, R. A., Bennett, C. P., Vize, C. J., Desai, S. P., Black, G. C., Patel, N., *et al.* (2001). Spectrum, frequency and penetrance of OPA1 mutations in dominant optic atrophy. Hum Mol Genet *10*, 1369-1378.

125. Toye, A.A., Lippiat, J.D., Proks, P., Shimomura, K., Bentley, L., Hugill, A., Mijat, V., Goldsworthy, M., Moir, L., Haynes. *et al.* (2005) A genetic and physiological study of impaired glucose homeostasis control in C57BL/6J mice. Diabetologia *48*, 675-86.

126. Treft, R.L., Sanborn, G.E., Carey, J., Swartz, M., Crisp, D., Wester, D.C., Creel, D. (1984). Dominant optic atrophy, deafness, ptosis, ophthalmoplegia, dystaxia, and myopathy. A new syndrome. Ophthalmology *91*, 908-15.

127. Twig, G., Elorza, A., Molina, A.J., Mohamed, H., Wikstrom, J.D., Walzer, G., Stiles, L., Haigh, S.E., Katz, S., Las, G *et al.* (2008) Fission and selective fusion govern mitochondrial segregation and elimination by autophagy. EMBO J *27*, 433-46.

128. Uo T, Dworzak J, Kinoshita C, Inman DM, Kinoshita Y, Horner PJ, Morrison RS. (2009) Drp1 levels constitutively regulate mitochondrial dynamics and cell survival in cortical neurons. Exp Neurol *218*, 274-85.

129. van der Bliek, A. M. (1999). Functional diversity in the dynamin family. Trends Cell Biol *9*, 96-102.

130. Vicencio, J.M., Galluzzi, L., Tajeddine, N., Ortiz, C., Criollo, A., Tasdemir, E., Morselli, E., Ben Younes, A., Maiuri, M.C., Lavandero, S., Kroemer, G. (2008). Senescence, apoptosis or autophagy? When a damaged cell must decide its path--a mini-review. Gerontology *54*, 92-9

131. Vieira, H. L., Haouzi, D., El Hamel, C., Jacotot, E., Belzacq, A. S., Brenner, C., and Kroemer, G. (2000). Permeabilization of the mitochondrial inner membrane during apoptosis: impact of the adenine nucleotide translocator. Cell Death Differ *7*, 1146-1154.

132. Votruba, M. (2004). Molecular genetic basis of primary inherited optic neuropathies. Eye *18*, 1126-1132.

133. Votruba, M., Leary, S., Losseff, N., Bhattacharya, S. S., Moore, A. T., Miller, D. H., and Moseley, I. F. (2000). MRI of the intraorbital optic nerve in patients with autosomal dominant optic atrophy. Neuroradiology *42*, 180-183.

134. Votruba, M., Moore, A. T., and Bhattacharya, S. S. (1997). Genetic refinement of dominant optic atrophy (OPA1) locus to within a 2 cM interval of chromosome 3q. J Med Genet *34*, 117-121.

135. Votruba, M., Thiselton, D., and Bhattacharya, S. S. (2003). Optic disc morphology of patients with OPA1 autosomal dominant optic atrophy. Br J Ophthalmol *87*, 48-53.

136. Wallace, D.C., Brown, M.D., Melov, S., Graham, B., Lott, M. (1998) Mitochondrial biology, degenerative diseases and aging. Biofactors *7*, 187-90.

137. White, K.E., Davies, V.J., Hogan, V.E., Piechota, M.J., Nichols, P.P., Turnbull, D.M., Votruba, M. (2009). OPA1 deficiency associated with increased autophagy in retinal ganglion cells in a murine model of dominant optic atrophy. Invest Ophthalmol Vis Sci *50*, 2567-2571.

138. Wong, E. D., Wagner, J. A., Gorsich, S. W., McCaffery, J. M., Shaw, J. M., and Nunnari, J. (2000). The dynamin-related GTPase, Mgm1p, is an intermembrane space protein required for maintenance of fusion competent mitochondria. J Cell Biol *151*, 341-352.

139. Yarosh W, Monserrate J, Tong JJ, Tse S, Le PK, Nguyen K, Brachmann CB, Wallace DC, Huang T. (2008). The molecular mechanisms of OPA1-mediated optic atrophy in Drosophila model and prospects for antioxidant treatment. PLoS Genet *4*, e6.

140. Youle, R. J., and Karbowski, M. (2005). Mitochondrial fission in apoptosis. Nat Rev Mol Cell Biol *6*, 657-663.

141. Yu Wai Man, C. Y., Chinnery, P. F., and Griffiths, P. G. (2005). Optic neuropathies--importance of spatial distribution of mitochondria as well as function. Med Hypotheses *65*, 1038-1042.

142. Yu-Wai-Man, P., Griffiths, P.G., Hudson, G., Chinnery, P.F. (2008). Inherited mitochondrial optic neuropathies. J Med Genet Epub 2008

143. Yu-Wai-Man, P., Davies, V.J., Piechota, M.J., Cree, L.M., Votruba, M., Chinnery, P.F. (2009). Secondary mtDNA defects do not cause optic nerve dysfunction in a mouse model of dominant optic atrophy. Invest Ophthalmol Vis Sci *14*.

144. Zanna, C., Ghelli, A., Porcelli, A.M., Karbowski, M., Youle, R.J., Schimpf, S., Wissinger, B., Pinti, M., Cossarizza, A., Vidoni, S. *et al.* (2008). OPA1 mutations associated with dominant optic atrophy impair oxidative phosphorylation and mitochondrial fusion. Brain *131*, 352-367.

APPENDICES

APPENDIX 1

Digestion Solution Master Mix (DNA extraction, Chapter 2.2)

Nuclei Lysis Solution	200µl
0.5M EDTA (pH 8.0)	50µl
Proteinase K, 20mg/ml	20µl
RNase A Solution	5µl

Total Volume 275µl/sample

TBE buffer 5x (Agarose gel electrophoresis, Chapter 2.4)

Tris base	54g
Boric acid	27.5g
0.5M EDTA (pH 8.0)	20ml

Make up to 1L

1.2% Denaturing (formaldehyde) agarose gel (Chapter 2.5)

150ml:

Agarose	1.8g
10x MESA buffer	15ml

Add RNase-free H_2O to 150ml
Heat the mixture to melt agarose, cool to 65^0C
Add 2.7ml of 37% formaldehyde
and 1.5 µl of 10mg/ml ethidium bromide stock solution
Prior to running the gel, equilibrate in 1x FA running buffer for at least 30min

MESA buffer 10x (Chapter 2.5)

200mM MOPS (41.8g in 700ml DEPC treated H_2O) adjust to pH 7.0 with 2NaOH
20ml DEPC treated 1M sodium acetate (1M sodium acetate- 13.6g in 100ml)
20ml of 0.5M EDTA (pH 8.0)
Adjust the volume to 1L with DEPC treated H_2O

Formaldehyde agarose (FA) running buffer (Chapter 2.5)

100ml 10x MESA buffer
20ml 37% formaldehyde
880 ml RNase-free H_2O

TE buffer (Chapter 2.6)

10mM Tris-HCl
1mM EDTA, pH7.5

PBS buffer

NaCl	8g
KCl	0.2g
Na_2HPO_4	14.4g
KH_2PO_4	2.7g

Dissolve in 800ml H_2O. Adjust to pH 7.4 with HCl
Add H_2O to 1 liter.

Sample Loading Buffer 2x (western blotting, Chapter 2.12)

4% SDS	4ml of 10% SDS
20% glycerol	2ml
120mM Tris	2.4ml 0.5M Tris pH 6.8
Water	1.6ml
Bromophenol blue	0.01%

Resolving gel (8%) (Western blotting, Chapter 2.12)

Acrylamide (30%)	2.7ml
MilliQ	4.6ml
1.5M Tris pH 8.8	2.5ml
10% SDS	0.1ml
10% APS	100 µl
TEMED	20 µl

Stacking gel (5%) (Western blotting, Chapter 2.12)

Acrylamide (30%)	1.67ml
MilliQ	5.83ml
0.5M Tris pH 6.	2.5ml
10% SDS	0.1ml
10% APS	50µl
TEMED	10µl

SF10PF medium (light treatment protocol, Chapter 2.19)

50ml:

10x SF10PF	5ml
MilliQ	42.5ml
20mM HEPES	1ml
Sodium bicarbonate	60mg
FBS	1ml
Antibiotic-Antimycotic 100x	0.5ml

APPENDIX 2

I. Concentration of mitochondrial proteins isolated from the retina (with proximal part of optic nerve attached) in *Opa1* +/+ and *Opa1* +/- animals.

Each sample is pooled from 3 animals. Each reading is a mean of three readings.

Total mitochondrial protein concentration from retina [mg/ml]		
sample	***Opa1* +/+ mean± SD**	***Opa1* +/- mean± SD**
1.	11.95± 0.86	10.50± 0.07
2.	11.11± 1.03	11.87± 0.79
3.	12.06± 0.81	11.91± 0.84

II. Concentration of mitochondrial proteins from brain in three *Opa1* +/+ and *Opa1* +/- animals. Each reading is a mean of three readings.

Total mitochondrial protein concentration from brain [mg/ml]		
Sample	***Opa1* +/+ mean± SD**	***Opa1* +/- mean ± SD**
1.	10.35± 0.11	9.30± 0.11
2.	13.00± 0.08	10.94± 0.18
3.	8.00± 0.14	9.90± 0.43

III. RNA concentration obtained from retina of WT *Opa1* +/+ and mutant *Opa1* +/- mice (*Opa1* +/- samples are labelled red).

RNA QUANTIFICATION [µg/ml]										
animal	1	2	3	4	5	6	7	8	9	10
RNA	51.95	48.55	23.85	47.65	86.05	59.85	73.95	76.65	78.65	65.55
animal	11	12	13	14	15	16	17	18	19	20
RNA	80.95	87.75	59.75	91.65	72.55	67.15	72.05	52.95	59.55	45.05

APPENDIX 3

PUBLICATIONS

1. Yu-Wai-Man, P., Davies, V.J., Piechota, M.J., Cree, L.M., Votruba, M., Chinnery, P.F. (2009). Secondary mtDNA defects do not cause optic nerve dysfunction in a mouse model of dominant optic atrophy. Invest Ophthalmol Vis Sci [Epub ahead of print]
2. White, K.E., Davies, V., Hogan, V., Piechota, M., Nichols, P., Turnbull, D.M., Votruba, M. (2009). OPA1 deficiency is associated with increased autophagy in retinal ganglion cells in a murine model of dominant optic atrophy. Invest Ophthalmol Vis Sci. *21*
3. Davies, V.J., Powell, K.A., White, K.E., Yip W., Hogan, V., Hollins, A.J., Davies, J.R., Piechota, M., Brownstein, D.G., Moat, S.J., Nichols, P.P., Wride, M.A., Boulton, M.E., Votruba, M. (2008). A missense mutation in the murine Opa3 gene models human Costeff syndrome. Brain *131,* 368-80.
4. Davies, V.J., Hollins, A.J., Piechota, M.J., Yip W., Davies, J.R., White, K.E., Nicols, P.P., Boulton, M.E., Votruba, M. (2007). Opa1 deficiency in a mouse model of autosomal dominant optic atrophy impairs mitochondrial morphology, optic nerve structure and visual function. Hum Mol Genet *16,* 1307-18.